2014-07-29

Kinetics of Asphaltene Precipitation and Flocculation from Diluted Bitumen

Shafiee Neistanak, Mahdieh

UNIVERSITY OF CALGARY

Kinetics of Asphaltene Precipitation and Flocculation from Diluted Bitumen

by

Mahdieh Shafiee Neistanak

A THESIS

SUBMITTED TO THE FACULTY OF GRADUATE STUDIES

IN PARTIAL FULFILMENT OF THE REQUIREMENTS FOR THE

DEGREE OF MASTER OF SCIENCE

GRADUATE PROGRAM IN CHEMICAL AND PETROLEUM ENGINEERING

DEPARTMENT

CALGARY, ALBERTA

July, 2014

Abstract

The kinetics of the precipitation and flocculation of asphaltenes can impact the operation of solvent deasphalting processes such as paraffinic froth treatment as well as the potential for deposition from destabilized crude oil. It has also been reported that the solvent content at which asphaltenes precipitate (the onset condition) is a time dependent property and may be far lower than reported because the precipitation kinetics are slow. However, it is possible that the slow kinetics are caused by oxidation or oxygen catalyzed polymerization.

The objectives of this thesis are to: 1) assess the role of oxygen in asphaltene precipitation kinetics; 2) determine the kinetics of asphaltene precipitation from diluted bitumen near the onset of precipitation, and; 3) investigate the kinetics of asphaltene flocculation near the onset of precipitation. The data were collected from a Western Canadian bitumen diluted with *n*-heptane at 23^{o}C. The *n*-heptane content at the onset of precipitation was determined using a combination of optical microscopy and gravimetric analysis. Asphaltene precipitate yields were measured over time gravimetrically, and asphaltene flocculation was investigated using a Lasentec particle size analyzer.

The onset of asphaltene precipitation (defined as the first appearance of 0.5 μm asphaltene particles) in *n*-heptane diluted bitumen occurred at 57.5 wt% heptane. When heptane was added above the onset amount, precipitation yields increased at an exponentially decaying rate over 48 hours. In air, the yields increased and the onset *n*-heptane content decreased at a slow rate for at least a month. In nitrogen, the yields reached a plateau and there was no change in the onset

condition after 48 hours. Once oxygen related artifacts were eliminated, the precipitation kinetics could be described with first order kinetics requiring an ultimate yield and a rate constant. The steady state yield is a function of the solvent content and has been modeled with regular solution theory. A single rate constant was found to apply to all of the data.

The effects of heptane content and shear rate on the kinetics of asphaltene flocculation were investigated and modeled using a population balance based model adopted from Rastegari *et al.* (2004) and Daneshvar (2005). Unfortunately, the particle size analyzer could not detect the particle size distribution in unadulterated bitumen near the onset. Therefore, data was collected at dilutions well above the onset and the possibility of extrapolating the model to near onset conditions investigated.

The main parameters governing flocculation are the particle concentration, the fractal dimension, and the magnitude and ratio of the flocculation and shattering rates, k_f/k_s. The fractal dimension of settled flocs was found to be 2.3 ±0.1 (with a slight dependence on the *n*-heptane content) and this value was assumed to apply for suspended flocs. At the dilutions considered in this thesis, adding *n*-heptane decreased the individual particle concentration and therefore decreased flocculation. An increase in the shear rate resulted in a decrease in the asphaltene volume mean diameter, while the total number of asphaltene flocs in the mixture remained relatively constant. This observation indicates that asphaltene flocs likely become more compact at higher shear rates.

The flocculation model was fitted the data at different dilutions. A constant value of the shattering rate was sufficient to fit the data. Both the fractal dimension and the reaction rate ratio could be

correlated to the mass fraction of *n*-heptane. The effect of shear rate on the k_f/k_s ratio at various heptane contents was investigated for two different bitumen samples. The k_f/k_s ratio appears to decrease with increasing Reynolds number up to 12000, above which the ratio becomes constant. The decrease in the ratio corresponds to the transition zone, while the plateau corresponds to the establishment of a turbulent zone.

While the model parameters could be correlated to n-heptane content, a long extrapolation with a significant a change in parameter values is required to estimate the behavior near the onset condition. Hence, the flocculation rates near the onset conditions cannot be determined from the available data with any confidence. It is recommended that data be collected for toluene-bitumen feedstocks where the onset occurs at higher n-heptane contents so that a more reliable extrapolation can be performed. If successful, both precipitation and flocculation rates can be predicted and used to guide process design and operation.

Acknowledgements

I would like to express my deepest and profound gratitude to my supervisor, Dr. Harvey Yarranton for his constant support and encouragement throughout the course of this study. This work would not have been possible without his guidance and support. It was an honour and a privilege to be part of his research group and work under his supervision toward my master degree.

I am particularly grateful to Florian Schoeggl, our PVT lab manager, for his constant support and assistance throughout the experimental work of my study. I would like to acknowledge his contribution in teaching me the experimental work of my study. He was very patient with me in the lab.

I am thankful to the Department of Chemical and Petroleum Engineering, Faculty of Graduate Studies at the University of Calgary, for providing wonderful facilities and a great educational ambience. I am also grateful to NSERC for their financial support throughout my Master program.

I am also thankful to Elaine Baydak and Hamed Reza Motahhari for their assistance and great help during my master's thesis. I am grateful to have worked with the members of the Asphaltene and Emulsion Research Group and fellow graduate students.

Finally I am profoundly indebted to my parents, for their constant support, dedications and continuous inspiration throughout all stages of my life. I express my gratitude to my dear brothers and caring sister and my lovely friend, Niloufar Hojati, for their continues support and encouragements during the course of my Master study.

Dedication

To my parents, Mohammad Ebrahim and Soraya

To my brothers, Mojtaba and Mohammad

To my sister, Maryam

Table of Contents

List of Tables

List of Figures and Illustrations

List of Symbols, Abbreviations and Nomenclature

Symbol	Definition
A	Area
C_k	Mass concentration of particle *k*
C_i	Mass concentration of particle i
C_j	Mass concentration of particle j
P	Perimeter
D_f	Fractal Dimension
D(i,j)	Disintegration reaction kernel (number of reactions per unit volume per unit time)
D	dimension
d_i	Measured diameter of floc *i*
d_{floc}	Measured diameter of a floc
d_m	Spherical mean diameter of a floc
d_p	Diameter of an individual particle
D_f	Fractal dimension
D_i	Disintegration reaction kernel
f_i	Number frequency of floc *i*
$F_{i,j}$	Flocculation reaction constant (number of reactions per unit volume per unit time)
k	Particle *k*
K	Boltzmann Constant
K_s	non-dimensional constant
k_f	Flocculation reaction constant in terms of number of individual particles in flocs
k_f / k_s	Ratio of flocculation and disintegration reaction constant
k_d	Disintegration reaction constant in terms of number of individual particles in flocs
$k¢_f$	Flocculation reaction constant in terms of mass of flocs
m_A	Mass of precipitated asphaltene
m_i	mass of i_{th} floc
M_k	Mass of particle of particle *k*
Mj	Mass of particle of particle *j*
Mi	Mass of particle of particle *i*
F(i,j)	flocculation reaction rate (number of reactions per unit volume per unit time)
F(i,k)	flocculation reaction rate (number of reactions per unit volume per unit time)
N	Number of particles in a cluster

N	Mixing Speed (min-1) used in Equation 3. 1
n_{bin}	Number of asphaltene bins with sizes between approximately 18 and 396 microns
n_f	Number of individual (primary) particles in a floc
n_i	Number of particles in the floc i
n_j	Number of particles in the floc j
n_{min}	Number of individual particles in the smallest asphaltene bin
n_{max}	Number of individual particles in the biggest asphaltene bin
n_1	Number of individual particles in an asphaltene bin size of 18 microns
d_{imp}	impeller diameter (inch
n_2	Number of individual particles in an asphaltene bin size of 396 microns
N_f	Total number of flocs
N_{re}	Reynolds number
N_t	Total number of individual particles in the solution
R_g	Radius of gyration
R_i	Radius of a floc
R_{i+j}	Radius of floc I an j
s	Sample variance
Y	yield (w/w)
Y_{eq}	equilibrium yield (w/w)
S_f	Scaling factor
t	Time
T	Absolute temperature
v_i	Volume of particle *i*
v_j	Volume of particle j
V_{actual}	Actual volume of a floc
V_{app}	Apparent volume of a floc
V_{total}	The total apparent volume of a distribution of flocs
MB_{err}	material balance error at each time step

Greek Symbol	**Definition**
ϒ	Shear rate (s-1)
α	= 1 – (%conf/100)
β	Disintegration exponent
λ	Flocculation exponent
ρ_A	Density of pure asphaltene
ρm	Mixture density (g/cc)
μ	Viscosity of medium (mPa.s)

CHAPTER ONE: INTRODUCTION

1.1 Background

Mineable oil sands compose a significant proportion, as much as 30%, of the world's known oil reserves (Atkins and MacFadyen, 2008). An average grade oil sand contains approximately 10 wt% bitumen, 1-2 wt% water, and 88 wt% solids of which 3 to 30% are fine solids (Romanova *et al.,* 2006). Commercial bitumen processes recover this relatively small fraction of bitumen from the oil sands using two steps: water based extraction and solvent based froth treatment.

Water based extraction was developed by Clark and Pasternack (1932) and involves mixing the oil sand with hot water and, if necessary, sodium hydroxide to separate bitumen from the sand matrix (Chalaturnuk and Scott, 2004). The hot water and hydroxide release natural surfactants from the oil sand which promote detachment of bitumen from the sand and attachment of the bitumen to air bubbles. The mixture is aerated and tumbled to produce a froth containing approximately 65 wt% bitumen, 25% water, and 10 wt% sands and clays (Sanford and Seyer, 1979; Kotlyar *et al.*, 1998). The froth must be treated separately to separate the bitumen from the remaining water and solids.

There are two commercial froth treatment processes, one based on naphtha and one based on a paraffinic solvent. In the naphtha based process, used by Syncrude and Suncor, the froth is diluted with naphtha to reduce the density and viscosity of the bitumen and the remaining water and solids are removed by centrifugation. In the paraffinic process, used by Albian, a paraffinic

solvent is added and the water and solids are removed by gravity settling. The paraffinic solvent not only reduces the density and viscosity of the bitumen but also precipitates some of the asphaltenes (the heaviest, most aromatic oil constituents) and promotes flocculation of the emulsified water and suspended solids (Long *et al*., 2002; Romanova e*t al.,* 2006). The paraffinic process has a lower bitumen recovery than the naphthenic process because the precipitated asphaltenes are rejected to the tailings stream along with the water and solids. On the other hand, the naphthenic process produces more coke during upgrading because the asphaltenes remain in the bitumen.

Some problems associated with water based extractions are their low energy efficiency, high water usage, and the creation of a tailings stream with poor consolidation properties (Chalaturnuk and Scott, 2004). An alternative is solvent based oil sands extraction, which substantially reduces water consumption and eliminates the need for froth treatment and tailings ponds. However, there are still some unresolved issues in solvent based extraction, such as the optimization of bitumen recovery for the target upgrading process, the production of a clean bitumen product, and the removal of solvent from rejected sand and water tailings (Yarranton, 2012). Imperial Oil has recently patented several non-aqueous process options, which address most of these issues (Adeyinka et al., 2010). The proposed processes involve sequential separations and fine agglomeration. Reportedly, the processes give high bitumen recovery, a bitumen product that meets pipeline specifications, and efficient solvent recovery. Nonetheless, approximately 1 wt% fine solids remain in the bitumen product (Mayer, 2011). There may also be room to optimize the solvent-to-bitumen (S/B) ratios used in different process variations.

One method to remove the fine solids is to use a high dilution of a paraffinic solvent to precipitate asphaltenes and induce flocculation and settling, as is done in paraffinic froth treatment. This method would provide a clean bitumen product, much like paraffinic froth treatment. However, high dilutions are economically disadvantageous. A potential alternative is to design this stage of the process to operate near the onset of asphaltene precipitation in order to minimize both solvent requirements and asphaltene rejection. Also, precipitated asphaltenes contain some solvent, which can be very difficult to recover (George *et al.*, 2009). Hence, minimizing precipitation may also minimize ultimate solvent losses. For this process to work, the suspended solids must still be flocculated and settled in a practical time frame.

Two factors make the process conceptually feasible. First, asphaltenes are often adsorbed on the surface of solids (Yan *et al*., 2001); and therefore, these particles tend to flocculate in solvents that are incompatible with asphaltenes (Saadatmand *et al.*, 2009). Second, the kinetics of asphaltene precipitation are slow near the onset condition (Maqbool *et al*., 2009); hence, there is an operating window to flocculate the solids before a significant amount of asphaltenes come out of solution. In theory, the bitumen product could then be separated before asphaltenes drop out. To complete the process, the product bitumen could be stabilized by evaporating some solvent or adding clean bitumen, a method dependent on asphaltene solubilisation kinetics. To determine the practicality of this concept, it is necessary to assess the kinetics of asphaltene precipitation as well as the kinetics of flocculation near the onset of asphaltene precipitation.

Asphaltene Precipitation Kinetics

At ambient conditions, asphaltenes precipitate as glassy particles, approximately 1 µm in diameter. It is debated whether precipitation is a result of colloidal aggregation (Leontaritis and Mansoori, 1987) or a conventional liquid-solid or liquid-liquid phase transition (Hirschberg *et al.*, 1984). Recent observations with a high pressure microscope have demonstrated that asphaltenes form a liquid phase at higher temperatures, consistent with a phase transition rather than colloidal aggregation (Agrawal *et al.*, 2012). Also, the most successful models for asphaltene precipitation treat it as a phase transition. Note, these models apply at thermodynamic equilibrium and do not consider the kinetics of the precipitation process.

The onset of asphaltene precipitation has been investigated with gravimetric methods (Burke *et al.*, 1990; Beck *et al.*, 2005; Maqbool *et al.*, 2009), optical microscopy (Angle *et al.*, 2006; Maqbool *et al.*, 2009), refractive index (Buckley, 1999; Wattana *et al.*, 2003; Castillo *et al.*, 2010), UV-vis spectrophotometry (Browarzik *et al.*, 1999; Kraiwattanawong *et al.*, 2007), and interfacial tension (Kim *et al.*, 1990; Mousavi-Dehghani *et al.*, 2004). Asphaltene precipitation yields have been measured using gravimetric methods (Beck *et al.*, 2005; Maqbool *et al.*, 2009; Speight 2006; Wiehe *et al.*, 2005). Typically, a poor solvent is added to a solution containing asphaltenes (such as a crude oil or an asphaltene-toluene solution) and the solvent content at which the asphaltenes precipitate (precipitation onset point) or yield of asphaltene precipitate at a given solvent content are determined. Data are usually collected after approximately 24 hours of equilibration and little attention is paid to the kinetics of the precipitation.

Two studies have focussed on precipitation kinetics. Beck *et al.* (2005) measured asphaltene precipitation over time for various heptane contents. They showed that most of the precipitation happened within 24 hours in both air and nitrogen atmospheres. After 24 hours, gradual precipitation continued at a reduced rate for as long as the experiments were conducted in air, but reached a steady state plateau after 24 hours in a nitrogen environment.

Maqbool *et al*. (2009) used optical microscopy and centrifugation-based separation to demonstrate that the time required for precipitating asphaltenes using *n*-heptane as the precipitant varied from a few minutes to several months. Their results indicated that near the onset the kinetics of asphaltene precipitation was very slow. Above the onset point, the precipitation kinetics was fast and precipitation reached a plateau within a short time frame. The long term results from Maqbool *et al.*, differ from those of Beck *et al*., but were carried out in air and may include oxygen related artifacts such as oxygen catalyzed polymerization (Wilson and Watkinson, 1996).

Asphaltene Flocculation Kinetics

Once precipitated, asphaltenes tend to flocculate into aggregates that are 10 to hundreds of micrometers in diameter. Ferworn *et al.* (1993) investigated the kinetics of asphaltene particle growth of crude oils diluted with *n*-heptane. The type of diluent and the ratio of diluent to bitumen both found to have an impact on the size of asphaltene particles. Rastegari *et al.* (2004) measured the asphaltenes particle size distribution in *n*-heptane-toluene mixtures and found that asphaltene floc size increased as the asphaltene concentration, and *n*-heptane content, increased. Daneshvar (2005) studied the asphaltene flocculation well above the onset in diluted bitumen

systems with *n*-heptane and *n*-pentane. However, flocculation kinetics near the onset of precipitation have not been investigated because little material precipitates and measurement is challenging.

1.2 Research Objectives

The objectives of this thesis are:

- to assess the role of oxygen in asphaltene precipitation kinetics
- to determine the kinetics of asphaltene precipitation from diluted bitumen near the onset of precipitation
- to determine the kinetics of asphaltene flocculation near the onset of precipitation

The first stage of this study focuses on the onset and kinetics of asphaltene precipitation from bitumen diluted with *n*-heptane. The onset of precipitation is determined in two ways: 1) extrapolating the yield after 24 hours of equilibration at different solvent contents to zero; and 2) examining micrographs of samples of solution taken at different solvent contents near the onset of precipitation. The yields are measured over time in air (following the procedures of Maqbool *et al.* (2009) and Beck *et al.* (2005)) and nitrogen (following the procedure by *Beck et al.* (2005)). The data are used to assess the impact of oxidation on yields and to assess the kinetics of precipitation.

The second stage of the study focuses on the flocculation rates of asphaltene particles precipitated from *n*-heptane diluted bitumen. Floc size distribution is measured using a Lasentec Model D600S FBRM particle size analyzer. The effect of heptane content, mixing schemes, and

shear rate on the kinetics of asphaltene flocculation is investigated. In addition, the fractal dimension of the flocculated asphaltenes will be determined. Finally, the flocculation data will be modeled using a population balance based model adopted from Rastegari *et al.* (2004) and Daneshvar (2005).

The opacity of the fluid is a critical issue in these measurements. The solvent must provide an onset condition at a dilution that reduces viscosity sufficiently for a good separation and creates a solution sufficiently transparent for microscopy and particle size analysis. Solvent other than *n*-heptane are examined as are methods to extrapolate high dilution measurements to the onset condition.

1.3 Brief Overview of Chapters

This thesis is comprised of seven chapters. Chapter 2 is a literature review and is divided into three main sections. First, the chemistry of asphaltenes and the different steps of asphaltene deposition are presented. Second, the nature of asphaltene precipitation kinetics is introduced and previous research on asphaltene precipitation in air and nitrogen atmosphere is discussed. Third, asphaltene flocculation mechanisms and models are explained and previous research on asphaltene flocculation in *n*-alkane diluted bitumen mixtures is reviewed.

In Chapter 3, the experimental procedures used to measure the kinetics of asphaltene precipitation and flocculation of diluted bitumen systems are described in detail. In Chapter 4 the results from the onset of precipitation and kinetics of asphaltene precipitation in air and nitrogen atmosphere will be discussed. In Chapter 5, the asphaltene flocculation model developed to

predict the kinetics of asphaltene particle growth, and description of the fractal dimension geometry is presented. In Chapter 6, the asphaltene flocculation data, as well as the performance of the proposed modified flocculation model is discussed. Chapter 7 summarizes the findings of this thesis and provides recommendations for future work.

CHAPTER TWO: LITERATURE REVIEW

This chapter explains basic concepts related to asphaltene chemistry including asphaltene self-association. Asphaltene precipitation is reviewed including its kinetics. Finally, asphaltene flocculation mechanisms, models, and previous work on asphaltene flocculation in *n*-alkane diluted bitumen mixtures are discussed.

2.1 Asphaltene Chemistry

Heavy oils and bitumens are often characterized in terms of SARA fractions (saturates, aromatics, resins, and asphaltenes). These classes differ based on polarity, solubility, and adsorptive characteristic as shown in Figure 2.1. Saturates are nonpolar compounds which include paraffins and cycloparaffins or naphthenes. Aromatics, resins, and asphaltenes are polyaromatic compounds with heteroatomic species such as nitrogen, oxygen, and sulphur in their structure. The ring systems in the aromatics vary from mono-aromatics to tri-aromatics. Resins and asphaltenes contain larger ring systems and are progressively higher in molecular weight, aromaticity, polarity, and hetero-compound content.

Asphaltenes are by far the most studied and yet the least understood class of crude oil. Asphaltenes are dark, sticky solids that are defined as the fraction of the oil that is insoluble in normal alkane solvents, such as *n*-heptane or *n*-pentane, but soluble in aromatic solvents such as toluene or benzene (Yen and Chilingarian, 2000). Asphaltenes self-associate into

macromolecular or colloidal structures and are prone to precipitate and flocculate during the course of heavy-oil processing (Rastegari *et al.*, 2004; Rahmani *et al.*, 2005; Daneshvar, 2005).

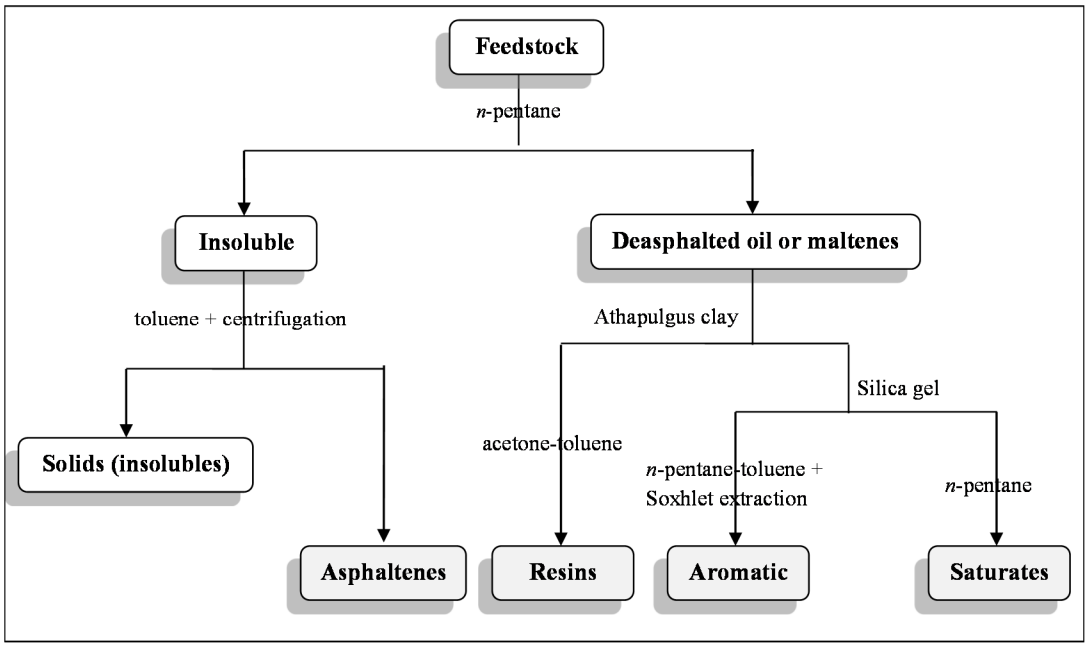

Figure 2.1: ASTM D2007 SARA fractionation procedure.

2.1.1 Asphaltene Molecular Structure

Asphaltenes are mixtures of thousands of structural types and are complex mixtures of high molar mass polynuclear aromatics containing heteroatoms such as nitrogen, oxygen, and sulphur as well as organometallic constituents such as nickel (Yen *et al.*, 1961; Speight, 2006). The elemental constituents of asphaltenes differ in various types of crude oil. Asphaltenes from different source oils have similar hydrogen to carbon atomic ratio (H/C), typically varying between 1.1 to 1.2 (Speight, 2006). Asphaltenes from Western Canadian bitumens are slightly above this range, Table 2.1. More variation is observed in the heteroatom composition where

nitrogen content varies from 0.6 to 3.3 wt%, oxygen content varies from 0.3 to 4.9 wt% and sulphur content varies from 0.3 to 10.3 wt% (Speight, 2006).

Table 2.1: The elemental composition of asphaltenes from various Canadian regions, (Speight, 2006).

Source	Atomic Ratio (wt%)			
	H/C	N/C	O/C	S/C
Athabasca	1.26	0.013	0.018	0.037
Peace River	1.23	0.011	0.017	0.036
Cold Lake	1.23	0.012	0.024	0.033

2.1.2 Asphaltene Self-Association

As discussed, asphaltenes are not a pure component, but consist of tens of thousands (Yen and Chilingarian, 2000) or even millions (McKenna et al., 2013) of molecular species. They have a strong tendency to self-associate and tend to form molecular aggregates of colloidal dimension (Yarranton, 2013). Association has been observed with many methods including molecular weights from vapour pressure osmometry (Speight, 2001; Yarranton *et al.*, 2000), surface and interfacial tensions (Sheu *et al.*, 2007), small angle X-ray scattering, and small angle neutron scattering (Yen *et al.*, 1961; Speight, 1994; Andersen, 2008). The precise fundamental understanding of the self-association mechanism is still lacking (Speight 2006). Association has been attributed to aromatic π-π bond interactions (stacking) (Ravey *et al.*, 1988;), hydrogen bonding (Andersen, 2008), van der Waals forces (Rogel, 2000), or a combination of the different mechanisms (Speight, 2006; *Gray et al.*, 2011).

There are two main concepts of asphaltene nano-aggregates: colloids (Mullins *et al.,* 2012) and macromolecules (Agrawala and Yarranton, 2001). The colloidal theory postulates that asphaltene molecules are primarily continental structures each consisting of primarily of a condensed aromatic sheet. It is hypothesized that these sheets form colloidal stacks held together by π-π bonds. The stacks are expected to aggregate strongly if exposed but are stabilized as suspended colloids by resins adsorbed on the surface of the colloid (Yen *et al.,* 1967; Mullins *et al.,* 2007). A short range intermolecular repulsive force between resins is believed to prevent flocculation of asphaltene particles. Any change in composition, pressure and temperature can disturb the equilibrium of the colloidal system leading to desorption of resins and consequently causing asphaltene precipitation (Mullins *et al.,* 2012). For example, addition of an *n*-alkane to a crude oil can desorb resins and re-established equilibrium can be achieved by reduction in the free surface energy of asphaltene by flocculation (Hemmami *et al.,* 2007). The colloidal model accounts for asphaltene self-association through the limited aggregation of colloidal particles upon partial desorption of the resins. The colloidal model is quite complex and requires a large number of parameters, and cannot explain the effect of solvents like toluene on asphaltene association and precipitation. The colloidal model predicts that asphaltene precipitation is irreversible while other studies have proven reversibility of asphaltene precipitations (Hammami *et al.,* 1999; Hirschberg *et al.,* 1984).

Recent Vapor Pressure Osmometry measurements of asphaltenes in toluene or *o*-dichlorobenzene show that asphaltene self-association increases with asphaltene concentration until a limiting value is reached (Yarranton *et al.,* 2000). The limiting value depends on solvent, temperature, and pressure. This step-wise aggregation resembles polymerization reactions and

therefore asphaltene self-association was modeled analogously to linear polymerization (Agrawala and Yarranton 2001; Murgich *et al*., 2002; Merino-Garcia 2004). In this model resins are not considered a peptizing agent adsorbed on the surface of asphaltene, but are assumed to be part of polymer-like aggregates, which consist of asphaltene and resin molecules. Aggregates are held together by dispersion forces rather than covalent forces and behave like macromolecules. Note, the most successful models for asphaltene association are thermodynamic models which treat asphaltenes as any other component in a solution. In other words, asphaltenes are implicitly treated as macromolecules rather than colloids in phase behavior modeling.

2.2 Asphaltene Precipitation

According to field experience (De Boer *et al.*, 1995; Kokal and Sayegh, 1995) and experimental observations (Fotland *et al.*, 1997; Hammami *et al.*, 2000; Thomas *et al.*, 1992), asphaltenes can precipitate with a change in conditions, such as the composition, pressure, and temperature of the crude oil. The most common occurrences of asphaltene precipitation are from depressurized live conventional oils and from heavy oils diluted with a paraffinic solvent. The effect of composition and pressure on asphaltene precipitation from conventional oil is generally believed to be stronger than the effect of temperature. The effect of composition is usually the dominant factor in precipitation from heavy oil.

At temperatures below approximately 120°C, asphaltenes precipitate as glassy particles of approximately 1 microns in diameter (Johnston, 2013). These particles tend to flocculate rapidly into structures up to hundreds of microns in diameter, Figure 2.2. At higher temperatures, they

come out of solution as liquid droplets which tend to coalesce into a continuous liquid phase (Gray *et al.,* 2004; Agrawal *et al.,* 2012; Johnston, 2013).

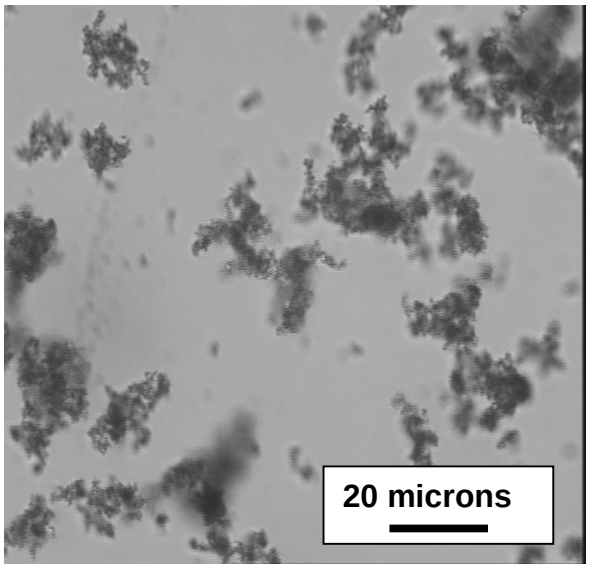

Figure 2.2: Micrograph of asphaltenes precipitated from a solution of asphaltenes in toluene and *n*-heptane (adapted from Rastegari *et al.*, 2004).

This thesis is concerned with the lower temperature behaviour near the onset of precipitation. The data of interest are: the onset of precipitation (the composition, pressure, and temperature at which the particles first appear); the yield (the mass of precipitate divided by the mass of the crude oil), and the size distribution of the flocculated particles. Figure 2.3 shows the gravimetrically determined onset and yield curve from a typical dilution of a bitumen with a paraffinic solvent.

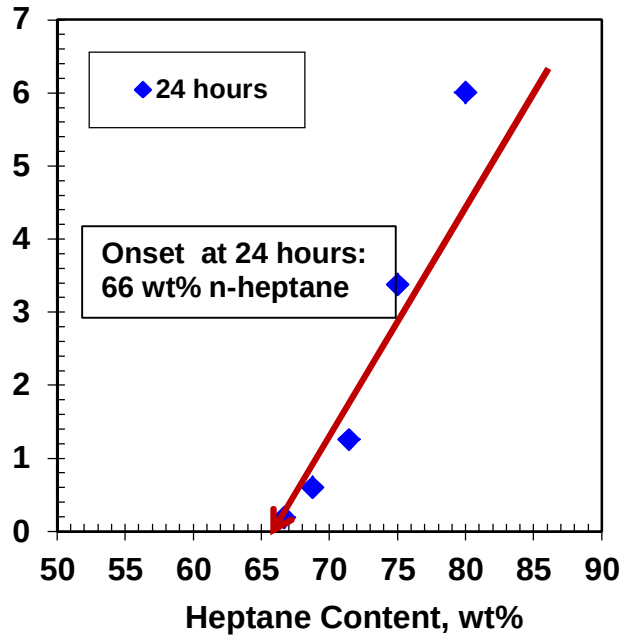

Figure 2.3: The gravimetrically determined onset and yield of asphaltene precipitation from *n*-heptane diluted with Athabasca bitumen at 24 hours at 23°C (adapted from *Beck et al.*, 2005).

A variety of methods have been used to detect the onset of asphaltene precipitation from oils diluted with a poor solvent including: gravimetric measurements interpolated or extrapolated to zero yield (Leontaritis and Mansoori, 1988; Hirschberg *et al.*, 1984; Burke *et al.*, 1990; ; Anderson and Birdi, 1991; Rassamdana *et al.*, 1996; Yarranton and Masliyah, 1996); change in slope from viscosity measurements (Escobedo *et al.*, 1995; Joel and Mansoori, 1995); change in slope of refractive index (Buckley, 1999; Wang *et al.*, 2003; Wattana *et al.*, 2003; Castillo *et al.* (2010); Browarzik *et al.*, 1999); change in slope of interfacial tension (Kim *et al.* 1990; Mousavi-Dehghani *et al.*, 2004). Near infrared and gravimetric methods have been used to detect the onset of precipitation when depressurizing live oils (Hammami *et al.*, 1999). In many cases, the onsets were verified with microscopic observations.

Caution is required for titration based methods because precipitation does not necessarily reach detectable levels immediately upon the onset of precipitation. If the solvent injection rate or depressurization rate is too rapid, more solvent may be injected or lower pressure may be reached before the onset is detected. Hence, the onset will be reported at too high a solvent content or too low a pressure. Anderson (1999) recommended a titration rate of 30 mL/30 seconds to avoid overshoot. Similarly, Kraiwattanawong *et al.* (2007) found that the minimum light absorbance was did not reflect the true onset and instead use the first deviation in slope in a plot of absorbance versus volume fraction of solvent to determine the onset point.

For solvent titrations, the solvent content at the onset of precipitation increases with better solvents because more solvent is required to force precipitation. For *n*-alkanes, the onset increases with increasing carbon number up to a carbon number of 10 to 12 and decreases again higher carbon numbers (Wiehe *et al*., 2005). Data for the effect of temperature are contradictory but more show onsets increase with temperature up to 100°C and either reach a plateau or decreases at higher temperatures (Ali and Al-Ghannam, 1981; Andersen and Birdi, 1990; Hu and Guo, 1991; Kokal *et al*., 1992; Andersen, 1994; Andersen *et al.*, 1998; Buenrostro-Gonzalez *et al*., 2004; Akbarzadeh *et al*., 2005). The onset increases slightly with increasing pressure (Akbarzadeh *et al*., 2005). For live oils, asphaltenes are more soluble at higher pressure. Lower onset pressures were observed at higher temperatures indicating that asphaltenes were more soluble at higher temperatures (Leontaritis and Mansoori, 1988; Hirschberg *et al.*, 1984; Burke *et al.*, 1990).

The same authors show that yield data follow the same trends as the onsets; that is, yields increase in poorer solvents, decrease with temperature increasing up to 100°C and then stabilize at higher temperature, and decrease with increasing pressure. With live oils, yield decreases with increasing pressure above the bubble point. However, below the bubble point, yields decrease with decreasing pressure as the solution gas evolves from the oil (Tharanivasan *et al.,* 2010).

2.2.1 Asphaltene Precipitation Kinetics

In most of the work presented so far, asphaltenes precipitation was induced by adding the paraffinic solvent all at once into the crude oil and precipitation data were mostly collected after approximately 24 hours of equilibration. Relatively little has been reported on the kinetics of asphaltene precipitation. In general, particle formation involves two kinetic aspects, nucleation and growth. Nucleation is the formation of a critical nucleus of molecules from a supersaturated fluid where the free energy minimized by forming a new phase overcomes the cost of forming a new solid/fluid interface. Once the nucleus is formed, it grows to a larger nano-scale size which can then coagulate with pre-existing and newly created particles (Zhang *et al.*, 2011). The growth rate depends on diffusion and adsorption from the medium to the nuclei. Hence, time is required to reach equilibrium, at least several hours for asphaltenes (Speight, 2006).

Beck *et al.* (2005) measured asphaltene precipitation over time for various heptane contents above the onset of precipitation in both air and nitrogen environments. They showed that most of the precipitation happened within 24 hours in both air and nitrogen atmospheres. After 24 hours, gradual precipitation continued at a reduced rate for as long as the experiments were conducted in air, but reached a steady state plateau after 24 hours in a nitrogen environment. The gradual

increase in yield after 24 hours in air environment was likely caused by oxidation or oxygen-catalyzed polymerization. As part of their sample preparation, they aerated their bitumen samples.

Angle et al. (2006) used optical microscopy to show that onset of asphaltene precipitation as a function of time and precipitant concentration. They concluded that the onset of asphaltene precipitation was slow and could take a few hours. They observed a decrease in the lag time prior to precipitation with an increasing dilution ratio. The appearance of precipitation was sequenced as spots, strings, clusters and large flocs. However, in their experiments, crude oil was diluted with 90% toluene. Therefore delay in the precipitation could also be due to the high amount of toluene added.

Maqbool *et al.* (2009) studied the onset of asphaltene precipitation of two crude oils using *n*-heptane as the precipitant in an air atmosphere. They detected the onset of precipitation using optical microscopy. Precipitation onset time was defined as the time required for the first appearance of asphaltene particles. They concluded that the onset of precipitation was a function of time, varied from a few minutes to several months depending on the precipitant concentration. Further, no single concentration could be identified as the critical precipitant concentration for asphaltene precipitation. Near the onset condition, the kinetics of asphaltene precipitation were very slow but above the onset point, the kinetics were fast and precipitation reached a plateau within a short time frame.

The same authors also investigated the effect of temperature on the kinetics of asphaltene precipitation upon addition of *n*-heptane. At higher temperatures, the precipitation onset time was shorter at a given dilution and the solubility of asphaltenes (Hu and Guo, 2001) was higher. They speculated that the reduced viscosity and greater diffusivity at higher temperatures led to a higher aggregation rate and shorter onset time. They remarked that expansion of hydrocarbons, oxidation of crude oil, and the loss of light hydrocarbons due to evaporation at elevated temperatures had very little effect on the asphaltene precipitation kinetics. However, they did not verify their results in an anaerobic environment.

Oxygen can have a significant effect on asphaltene precipitation. Taylor and Frankenfeld (1978) investigated the effect of oxygen and nitrogen on deposit formation from deoxygenated hydrocarbons. They proposed that free radical chain reactions involving molecular oxygen created high molar mass hydrocarbons that fall into the asphaltene solubility class. Watkins *et al.* (1996) demonstrated that oxygen dissolved in a liquid hydrocarbon formed polymeric peroxides through autocatalytic reactions. The peroxides underwent subsequent decomposition reactions and free radical reactions with hydrocarbons. This reaction led to new asphaltene formation and contributed to organic fouling. Beck *et al.* (2002) examined the effect of pre-treatment of bitumen samples with oxygen over a range of heptane to bitumen ratios at three temperatures. They observed no increase in yield at 23^{o}C between the treated and untreated samples, mainly due to the high viscosity of the bitumen samples which prevented effective aeration. However a significant increase in yield was observed after aeration at 40 and 70^{o}C.

2.3 Asphaltene Flocculation

As noted previously, there are two views on asphaltene precipitation: 1) colloidally dispersed asphaltene nano-aggregates destabilize and form larger and larger aggregates that eventually physically separate; 2) asphaltenes chemically separate (precipitate) as micrometer-scale particles. Measurements below the onset of asphaltene precipitation in heptane-toluene mixtures have been interpreted as slow aggregation from nanometer to micrometer scale (Angle *et al.*, 2006; Maqbool *et al.*, 2009). Similarly, Mason and Lin (2003) used time-resolved small angle neutron scattering to investigate the kinetics of asphaltene nanoparticle aggregation in an asphaltene rich crude oil mixed with a paraffinic British crude oil. Their results indicated an initial particle diameter in the nanometre scale with growth to the micrometre range over a period of 11 days. They used a diffusion limited aggregation model to define a "characteristic time" to show when the asphaltene flocs first appeared. However, there are no conclusive observations of particles in the intermediate size range between nanometer-scale colloids/macromolecules and micrometer scale particles. In most cases, once a supersaturation condition is reached, the transition from nanometer to micrometer scale appears to be instantaneous. It is more likely that asphaltenes precipitate as micrometer-scale particles and these authors are observing the outcome of a nucleation and growth process (possibly with oxygen artifacts) rather than an aggregation process.

There are many examples of instantaneous particle formation. Ferworn *et al.* (1993) concluded that asphaltene particle growth and flocculation from *n*-heptane crude oils is an instantaneous process; that is the agglomerates reached a critical size within a few seconds and the asphaltene particles size distribution remained constant over time. Ostlund *et al.* (2002) used nuclear

magnetic resonance to study the kinetics of flocculation of asphaltene. They also found a dramatic increase in flocculation above a certain "threshold concentration," which could be referred as the onset point of the precipitation. Rastegari *et al.* (2004) and Daneshvar (2005) also observed instantaneous particle formation at the onset of precipitation. This review will focus on the asphaltene flocculation from micrometer-scale primary particles.

2.3.1 Floc Structure and Fractal Dimension

The shape and structure of asphaltene flocs in various solvents have been investigated using a variety of techniques including small-angle neutron and X-ray scattering (Savvidis *et al.,* 2001; Mason and Lin, 2003; Headen *et al.,* 2009; Eyssautier, 2011), a combination of viscosimetric and neutron scattering measurement (Sheu, 1998; Fenistein *et al.,*199; Hoepfner *et al.*, 2013), optical microscopy (Rahmani *et al.,* 2005), and particle size analyzer (Rastegari *et al.,* 2004; Daneshvar 2005). These investigations have concluded that precipitated asphaltenes form fractal clusters. The nature of fractals will be discussed later.

Savvidis *et al.* (2001) found that the precipitated and dried asphaltenes appeared as dense spherical structures with diameters ranging from nanometers to micrometers. However, asphaltene particles still suspended in solvent form loose fractal-like structures. Sheu (1998) determined the fractal dimension based on a series of time dependent viscosity measurements of asphaltene flocs in the mixture of 75 wt% heptane to 25 wt% toluene (with no agitation). He assumed that the asphaltene flocs were hydrodynamically spherical and were influenced by diffusion-limited aggregation. He found that the fractal dimension of the asphaltene flocs varied from 1.49 to 1.8 for different asphaltenes and concentrations. The asphaltene fractal dimension

decreased as the concentration increased. A restructuring effect was also observed when the flocculated asphaltenes were shaken for one minute; the fractal dimension increased from 1.53 to 1.8, resulting in a denser structure.

Rastegari *et al.* (2004) and Daneshvar (2005) found that asphaltene flocs were loose fractal-like structures rather than spherical aggregates. They determined fractal dimension by image analysis and indirectly from calculation of the mass of precipitated asphaltenes measured by particle size analysis and then compared it to the fraction precipitated gravimetrically. Rastegari *et al.* (2004) estimated a fractal value of 1.6 for asphaltenes flocs in a mixture of 60:40 *n*-heptane:toluene. Daneshvar (2005) calculated volume fractions occupied by flocs assuming fractal dimensions for bitumen diluted with heptane at 93.5 wt% *n*-heptane. Based on visual observations of settled asphaltenes at high dilution ratios, he concluded that the flocculated asphaltenes occupied no more than 30 to 40 vol% of the solution volume and that the fractal dimension must be larger than 2.0. He used a fractal dimension of 2.05 for his modeling.

Rahmani *et al.* (2005) employed a photographic technique coupled with image analysis to measure the size and fractal dimension of asphaltene aggregates formed in *n*-heptane–toluene mixtures. They determined terminal settling velocities and characteristic aggregate lengths to estimate the two- and three-dimensional fractal dimensions, estimated to be 1.06 to 1.40 depending on the shear rate and asphaltene concentration in heptane-toluene solvent mixtures. These small fractal dimensions showed that asphaltene flocs loose, highly porous structures.

2.3.2 Factors Affecting Asphaltene Flocculation

Asphaltene floc size distributions and fractal behaviour have been investigated as a function of composition, temperature, pressure, and shear using a variety of techniques including laser particle size analysis (Ferworn *et al.*, 1993; Rastegari *et al.*, 2004; Daneshvar, 2005), small-angle neutron and X-ray scattering (Savvidis *et al.*, 2001; Mason and Lin, 2003; Headen *et al.*, 2009; Eyssautier, 2011), and optical microscopy and image analysis (Rahmani *et al.*, 2005).

Composition

Composition is an important parameter in determining the size and rate of asphaltene flocculation. Ferworn *et al.* (1993) used a particle size analyzer to investigate asphaltene floc growth over 24 hours for six different crude oils diluted with *n*-heptane and in some cases with *n*-hexadecane and *n*-pentane. They observed lognormal distributions in all cases with floc sizes ranging from tens to hundreds of micrometers. The mean floc size increased as the diluent to bitumen ratio increased (making the medium a poorer solvent) and as the carbon number of the n-alkane decreased (lower carbon number n-alkanes are poorer solvents). They also investigated the effect of oxygen on the particle size and performed tests under a nitrogen blanket. They observed no measurable differences between the asphaltenes mean floc sizes in air versus nitrogen.

Nielsen *et al.* (1994) used a similar technique, and found the mean size of asphaltene flocs ranged from 266 to 495 μm for different oils diluted with *n*-pentane. They observed bimodal size distributions of asphaltene flocs. However, most other investigators have observed only unimodal distributions.

Rastegari *et al.* (2004) used a particle size analyzer to measure the asphaltenes particle size distribution in a series of *n*-heptane-toluene mixtures. The particle size distributions were observed to be lognormal. The volume mean diameters ranged up to 400 μm with an individual particle diameter of approximately 1 μm. They found that asphaltene floc size increased as the asphaltene concentration and *n*-heptane content increased. Higher concentration is expected to cause more particle collisions and therefore greater flocculation rate. Adding *n*-heptane makes the medium a poorer solvent for asphaltenes increasing the driving force for flocculation. According to their experiments, asphaltene flocs reached a steady-state size distribution indicating that flocculation does not continue indefinitely. To achieve a steady-state condition, flocculation must eventually be balanced by disintegration. Hence, asphaltene flocculation appears to be a reversible process.

Daneshvar (2005) studied the asphaltene flocculation in diluted bitumen systems with *n*-heptane and *n*-pentane using a particle size analyzer. He observed that the volume mean diameter increased as the dilution ratio increased from 75 to 93.5 wt% *n*-heptane in bitumen but remained constant at higher dilutions. At low to moderate heptane content, they observed an increase in the number and size of the asphaltene flocs, resulting in higher flocculation rate as the heptane content increased. At higher heptane content, further dilution had little effect on floc size, and the number concentration of the flocs decreased as the system becomes more dilute. He also found that the type of diluent such as *n*-pentane led to significantly more flocculation both initially and at steady state. The steady state volume mean diameter was approximately 290 μm in *n*-pentane compared to 100 μm in *n*-heptane. Maqbool *et al.* (2011) also observed larger mean diameters at higher n-heptane contents. Maqbool *et al.* (2011) found that as the heptane concentration

increased, the particle size distribution of asphaltene aggregates shifted more quickly to larger diameters.

Kraiwattanawong *et al.* (2009) investigated the effect of asphaltene dispersants on aggregate size distribution using a paraffinic solvent like *n*-heptane. Their study showed that large asphaltene particles are in fact aggregates consisting of very small (sub-micrometer) size asphaltene particles. Their result showed a bimodal distribution, indicating that two types of asphaltenes exist. The asphaltenes in the size range of 0.1-1 μm were called "stabilized asphaltenes. Once asphaltenes are destabilized, they form an intermediate phase called colloidal asphaltenes, which grow to a size of about 1-30 μm in diluted mixture. These asphaltenes with the size greater than 1 μm were called flocculated asphaltene.

Najafi *et al.* (2011) studied the kinetics of asphaltene flocculation of several crude oil samples exposed to ultrasonic waves at different time intervals and used confocal microscopy to observe the size distribution in a mixture of *n*-pentane and toluene. The size distribution of asphaltene flocs ranged from 1 to 10 μm after 120 minutes, showing a multimodal distribution. They concluded that ultrasound reduced the formation of macrostructure aggregates.

Pressure and Temperature

The effect of pressure or temperature on asphaltene floc size distribution has been investigated by Nielsen *et al.* (1994) and Daneshvar (2005). Nielsen *et al.* (1994) studied the effect of pressure and temperature of crude oil diluted with *n*-pentane. They found that the mean floc size

increased slightly as pressure increased and the temperature had negligible effect on asphaltene flocculation.

Daneshvar (2005) investigated the effect of temperature on the volume mean diameter and number count rate for *n*-heptane dilution of 93.5 wt%, at three different mixing speeds. At the slowest mixing speed of 195 rpm, the volume mean diameter did not notably change as temperature increased, but the number count rate decreased. At the higher mixing speeds, the volume mean diameter and number count rate reached a maximum at a temperature of approximately 45°C. The observations were surprising because, in the temperature range of these experiments, asphaltene yield decreases as temperature increases and; therefore, the number of individual particles decreases at a given dilution ratio. The number of flocs and mean floc size are both expected to decrease as the number of particles decreases in contrast to the observations. Daneshvar speculated that the increase in volume mean diameter as temperature increased up to 40°C was due to the stickiness of asphaltene flocs. The decrease in volume means diameter and number count at higher temperatures could be result of deposition on the mixer and beaker walls or of the formation of more compact flocs with higher fractal dimension.

Shear

Rastegari *et al.* (2004) and Daneshvar (2005) both investigated the effect of mixing rate on the asphaltene floc size. They found that asphaltene flocculation is reversible. At higher mixing rates, asphaltene flocs disintegrated and steady state particle size distributions were reached faster. The shape of the sheared particle size distributions indicated that shattering is the dominant disintegration mechanism.

2.4 Asphaltene Flocculation Modeling

2.4.1 Flocculation Models in General

As noted previously, asphaltenes precipitate as micron sized particles that flocculate into structures up to hundreds of micron in diameter. In this thesis, it is assumed that the micron diameter particles are the final product of a phase change. Note, some other models assume flocculation begins with nano-aggregates possibly with a second level of aggregation occurring once micron scale flocs form (Mullins *et al.*, 2012; Maqbool *et al.*, 2011).

Flocculation refers to the formation of clusters in colloidal suspension systems. Individual particles dispersed in the liquid phase will stick to each other and form irregular particle clusters, flocs, or aggregates. Research in flocculation has spanned many fields, such as biomedicine, biotechnology, polymer physics, and surface chemistry. In processes concerned with fine particles, it is often the floc that is the important unit rather than an individual particle, and the size and the shape of the flocs control the behaviour of the systems. One method that attempts to describe the geometry of the flocs is by simulating the random aggregation and to date two mechanisms have been presented as a basis for such simulations; particle-cluster and cluster-cluster flocculation.

In *particle-cluster* flocculation, the floc is formed through successive addition of single particles of unit radius which approach along a linear trajectory, randomly distributed in space while the particle is being rigidly fixed at their first point of contact. In *cluster-cluster* flocculation, the collisions between small clusters are included. Each collision is calculated by randomly rotating the colliding clusters and moving one along a randomly chosen linear trajectory until collision

occurs. The clusters are considered rigidly-fixed at their first point of contact (Sutherland, 1967; Sutherland and Goodarz-Nia, 1971).

In either case, the asphaltene flocculation is modeled based on a population balance of the individual particles. The choice of the population balance equation depends on whether the flocculation is irreversible or reversible of which both will be discussed in the next sections. Many models only consider irreversible asphaltene flocculation and are not applicable for the systems in which asphaltene disintegration occurs. Asphaltene flocculation systems are shear sensitive and reversible. The reaction kernels for cluster-cluster flocculation are only considered in this thesis. The approach is the same for particle-cluster flocculation except that the interacting species must be a single particle. The population balance equations are reviewed below.

2.4.2 Irreversible Flocculation

Irreversible flocculation refers to the collision of particles i and j that stick together to form a larger cluster, k, and no allowance is made for break-up of aggregates as follows:

$$M_i + M_j \xrightarrow{F(i,j)} M_k \qquad i+j=k \tag{2.2}$$

where $F_{i,j}$ represents the flocculation reaction rate between M_i and M_j. This reaction kernel depends on a number of factors such as particle size and transport mechanism. M_i, and M_j are clusters containing i and j elementary units. Smoluchowski assumed that the particle collisions were binary, the fluctuations in density were relatively small, and only random collisions occurred. The classical irreversible Smoluchowski (1916) population balance equation represents

the rate of change of concentration of k^{th} aggregates and is given by:

$$\frac{dC_k}{dt} = \frac{1}{2}\sum_{\substack{i+j\to k \\ i=1}}^{i=k-1} F_{ij}C_i\,C_j - C_k\sum_{k=1}^{\bowtie} F_{ik}C_i \qquad (2.3)$$

where $F_{i,j}$, and F_{ik} are the reaction kernels representing the number of reactions per unit volume per unit time which result in flocculation. C_i and C_j are concentrations of species i and j, and t is time. The first term on the right hand side represents the rate of formation of k aggregates by collision of any pair of aggregates, i and j forming $i+j=k$. Because of the summation, each collision is counted twice; therefore the factor ½ is included. The second term accounts for the loss of k aggregates by collision and aggregation with any other aggregates (Elimelech *et al.*, 1998).

The rate of collision between particles is determined by transport mechanisms such as Brownian diffusion and inter-particle interactions such as London dispersion forces. For two particles to aggregate, these two particles must first be brought into close proximity by a transport mechanism. Transport mechanisms give neighboring particles different velocities and cause collisions. Whether or not the particles are attached to each other after a collision depends on the net inter-particle forces. The differences in the velocities of neighboring particles may result from Brownian motion, spatial velocity variations within the fluid (i.e., fluid shear), and sedimentation (i.e., differential settling). Brownian motion is usually important when the particles are of submicron size. However, as the particles grow larger, Brownian aggregation becomes less important and differential settling becomes the dominant mechanism.

The Smoluchowski (1916) population balance equation was initially derived assuming Brownian motion was the only transport mechanism, and particle diffusion coefficients were constants. Assuming the Stokes-Einstein relation holds for the diffusion coefficient, $F_{i,j}$, Brownian coagulation was expressed as shown in Equation 2.4 (Higashitani *et al.*,1992):

$$F_{i,j} = \frac{2KT}{3\mu}\left[v_i^{1/3} + v_j^{1/3}\right]\left[\frac{1}{v_i^{1/3}} + \frac{1}{v_j^{1/3}}\right] \tag{2.4}$$

where K is Boltzmann's constant, T is the absolute temperature, μ is the viscosity of the suspending fluid, and v_i and v_j are the volumes of particles i and j.

The origin of these forces is the attraction between a temporary dipole and the corresponding induced dipoles (London theory) between the particles. Higashitani *et al.* (1979) proposed a modified Smoluchowski equation. The modification considered the hydrodynamic interactions and the van der Waals potential as follows (Higashitani and Matsuno, 1979; Friedlander, 2000):

$$F_{i,j} = \frac{2KT}{3\mu\delta_{i,j}}\left[v_i^{1/3} + v_j^{1/3}\right]\left[\frac{1}{v_i^{1/3}} + \frac{1}{v_j^{1/3}}\right] \tag{2.5}$$

This model was consistent with the experimental data from the flocculation of polystyrene latex particles (Higashitani *et al.*, 1992) .

Ball *et al.* (1987) modeled the Smoluchowski equations using reaction-limited cluster aggregation theory. They determined the reaction kernel by cluster fractal geometry:

$$F_{i,j} \sim M^{\lambda/D_f}, \qquad \text{for } M_i \approx M_j = M \tag{2.7.a.}$$

$$F_{i,j} \sim M_i^{1/D_f} M_j^{\lambda/D_f}, \qquad \text{for } M_i >> M_j \tag{2.7.b}$$

where λ is the adjustable parameter and D_f is the fractal dimension. Equation 2.7 was developed for low concentrations where three-cluster effects could be ignored.

Rastegari *et al.* (2004) modified this reaction-limited cluster-cluster aggregation reaction kernel to obtain the following general equation:

$$\boldsymbol{F}_{i,j} = \boldsymbol{k}'_f \left(\frac{\boldsymbol{M}_j}{\boldsymbol{M}_i + \boldsymbol{M}_j} \boldsymbol{M}_i^{1/\boldsymbol{D}_f} + \frac{\boldsymbol{M}_i}{\boldsymbol{M}_i + \boldsymbol{M}_j} \boldsymbol{M}_j^{1/\boldsymbol{D}_f} \right)^{\lambda} \tag{2.8}$$

where k'_f is the reaction constant, D_f is the fractal dimension of the flocs. Since the mass of a floc is directly proportional to the number of particles in the floc, Daneshvar (2005) modified it as follows:

$$\boldsymbol{F}_{i,j} = \boldsymbol{k}_f \left(\frac{\boldsymbol{n}_j}{\boldsymbol{n}_i + \boldsymbol{n}_j} \boldsymbol{n}_i^{1/\boldsymbol{D}_f} + \frac{\boldsymbol{n}_i}{\boldsymbol{n}_i + \boldsymbol{n}_j} \boldsymbol{n}_j^{1/\boldsymbol{D}_f} \right)^{\lambda} \tag{2.9}$$

Equation 2.9 is the flocculation rate term that will be used in this thesis.

2.4.3 Reversible Flocculation

Reversible flocculation refers primarily to the flocculation and separation of flocs under shear. Reversible flocculation happens mostly for flocs that are held together by van der Waals forces. In these systems, flocculation and disintegration both affect the floc distributions. The flocculation rate decreases the number of clusters while the disintegration rate increases it and steady state particle size distribution is observed. The Smoluchowski population balance

equation for the k^{th} species, including flocs, up to the order of N for irreversible flocculation (Family *et al.*, 1986) is given by:

$$M_i + M_j \underset{D(i,j)}{\overset{F(i,j)}{\rightleftharpoons}} M_{i+j} \tag{2.11}$$

$$\frac{dC_k}{dt} = \frac{1}{2}\sum_{\substack{i+j=k \\ i=1}}^{k-1}\left(F_{i,j}C_iC_j - D_{i+j}C_{i+j}\right) - \sum_{j=1}^{N-k}\left(F_{k,j}C_kC_j - D_{i+j}C_{i+j}\right) \tag{2.12}$$

where *D(i,j)* is the disintegration reaction term representing the number of reactions per unit volume per unit time. Disintegration involves large particles breaking into a number of smaller particles through grinding or shattering. The disintegration reaction term is a function of the particle diameter and is usually represented as a power law. Welt *et al.* (1977), and Rastegari *et al.* (2004) employed the following disintegration reaction term for a floc of radius R_i:

$$D_i = K_d(R_i)^{\beta} \tag{2.13}$$

where K_d is the disintegration reaction constant and the power of β varies within the range of 0 to 3.

Rastegari *et al.* (2004) expanded Equation 2.13 to represent the mass of a floc of size R_{i+j} that breaks into flocs of size R_i and R_j, as follows:

$$D(i,j) = K_d R_{i+j}^{\beta} = K_d\left(M_i^{1/D_f} + M_j^{1/D_f}\right)^{\beta} \tag{2.14}$$

where *i* and *j* represent the two flocs formed when a larger floc breaks up, K_d is the disintegration reaction constant, R_i, R_j, are the radii of the flocs, D_f is the mass (number) fractal dimension of the flocs, and the disintegration reaction exponent β is a number from 0 to 3. Equation 2.14 was

developed for low concentrations. Since the mass of a floc is directly proportional to the number of particles in the floc, Daneshvar (2005) modified Equation 2.14 as follows:

$$\boldsymbol{D}_{i+j} = \boldsymbol{k}_{\boldsymbol{d}} \left(\boldsymbol{n}_{\boldsymbol{i}}^{1/\boldsymbol{D}_f} + \boldsymbol{n}_{\boldsymbol{j}}^{1/\boldsymbol{D}_f} \right)^{\beta} \tag{2.15}$$

Equation 2.15 is the disintegration reaction term that will be used in this thesis.

2.4.4 Asphaltene Flocculation Models

Most researchers have worked with well mixed systems and therefore have considered asphaltene flocculation as a reaction controlled (low probability of sticking after collision) rather than diffusion controlled (low probability of collision) process. The kinetics of asphaltene flocculation based on the viscosity of asphaltene flocs with time in a heptane/toluene mixture was investigated by Sheu (1998). He observed that initially the viscosity decreased and then stayed constant. After 90 minutes, the viscosity started increasing as a result of asphaltene flocculation. The flocculation rate was very slow initially but increased exponentially as the floc size increased. He interpreted the trends as reaction limited flocculation, where the flocculation rate increased as the size of the flocs increased.

Najafi *et al.* (2011) studied the kinetics of asphaltene flocculation of several crude oil samples for different time intervals from the addition of *n*-pentane to crude oil in toluene. They showed that in the first 90 minutes, the size of the aggregates increased rapidly, matching well with a reaction-limited aggregation model. After 90 minutes, the size of the aggregate continued to increase at a reduced rate.

Rastegari *et al.* (2004) studied the kinetics of asphaltene particle growth in model systems of asphaltenes, *n*-heptane, and toluene using a particle size analyzer. Asphaltene flocs reached a steady-state size distribution, indicating that flocculation does not continue indefinitely but is balanced by disintegration. They developed a reversible reaction limited flocculation model that successfully fit the particle-size distributions and growth in mean volume diameter over time. They examined disintegration through erosion and shattering mechanisms. Erosion is the removal of individual or primary particles from flocs through grinding or shear. Shattering is the fragmentation of flocs into smaller flocs of any size less than the original floc. They concluded that shattering was the dominant disintegration mechanism.

In a similar way, Rahmani *et al*. (2004) developed a mathematical model based on population balance to analyze reversible experimental data for asphaltene floc size distribution for a solution of asphaltene in n-heptane-toluene mixture as the solvent. The aggregation behavior of asphaltenes was investigated by monitoring the size distribution of flocs for various shear rates, n-heptane to toluene ratios, and asphaltene concentrations. They found that steady-state condition was reached when the fragmentation rate balances the aggregation rate and the floc size distribution no longer changes with time. In their modeling, they included collision efficiency, collision frequency, fragmentation rate, breakup distribution function, and porosity instead of fractal dimension. Collision frequency solely due to the fluid shear was employed in their modeling. Furthermore, it was assumed that the collision efficiency is equal to one. They used a simple correlation to estimate the breakup rate as a function of floc apparent volume and shear rate. They found a correlation between porosity, as an adjustable parameter, and shear rate.

Daneshvar (2005) developed a flocculation model based on population balance to analyze reversible experimental data for asphaltene floc size distribution in diluted bitumen systems. To minimize the computational time, his population balance was based on clusters of particles rather than individual particles. He investigated the effect of shear rate, dilution ratio and temperature on the model parameters. The effect of changing the dilution ratio was matched by adjusting only the reaction rate constants. The effect of shear rate was matched by adjusting the fractal dimension. The volume mean diameters were well matched; however the predicted trends for the number mean diameter and number counts versus time were far from the experimental data. They used a fractal dimension of 2.05. In this case, the apparent volume of the asphaltene flocs in the mixture was 33% of the total volume.

CHAPTER THREE: EXPERIMENTAL METHODS

In this chapter, the experimental procedures used to measure the kinetics of asphaltene precipitation and flocculation of diluted bitumen systems are described in detail including asphaltene extraction, asphaltene precipitation yield and onset measurements, flocculation experiments, and particle size analysis.

3.1 Materials

A Western Canadian bitumen (WC_B2), already treated to remove water and solids, such as sand and clays, was supplied by Shell Canada Ltd. The residual water content was measured by Karl Fischer analysis and was less than 1 wt%. Toluene and *n*-heptane were obtained from VWR International LLC. and were 99% pure. Nitrogen was 99.99% pure and was purchased through Praxair.

The saturate, aromatic, resin, and asphaltene composition of the bitumen was determined elsewhere (Okafor, 2014) using the ASTM D2007M procedure, Table 3.1. The SARA procedure used *n*-pentane to precipitate the asphaltenes. However, in this thesis, most experiments were conducted with *n*-heptane (*n*-C_7) precipitated asphaltenes. Asphaltenes precipitated with *n*-pentane and *n*-heptane are termed "C5-asphaltenes" and "C7-asphaltenes", respectively. Both values are reported in Table 3.1. The density of the bitumen used in this study was also measured by Okafor with an Anton Paar density meter and was 1153.5 kg/m^3 at 20°C. The viscosity of the

bitumen was collected by Motahhari *et al.* (2013) using capillary viscometer and was reported to be 120,252 mPa.s at 20^{o}C.

Table 3.1: SARA composition of WCB2 bitumen.

Fraction	Composition, wt%
Saturates	17.1
Aromatics	44.0
Resins	19.4
***n*-C_5 Asphaltenes**	19.4
***n*-C_7 Asphaltenes**	17.3
Solids	2.2

3.2 Precipitation Measurements

Asphaltene precipitation kinetics was investigated in bitumen diluted with a poor solvent such as *n*-heptane or *n*-pentane. The onset of asphaltene precipitation is defined as the minimum amount of added solvent at which asphaltenes first precipitate. Asphaltene yield is defined as the mass of precipitated asphaltenes divided by the initial mass of bitumen.

3.2.1 Asphaltene Yield Measurement

Yield experiments were performed for 54.5, 57.5, 59.5, 61.5 and 64.5 wt% *n*-heptane in bitumen in air and nitrogen atmospheres at 21°C and atmospheric pressure. A small number of experiments were also performed with *n*-pentane diluent. The size of samples varied from 9 to 28 mL. The procedures for air and nitrogen atmospheres differ and each is explained below.

Air Atmosphere

Diluted bitumen samples were prepared by adding a known mass of bitumen to a clean 30 mL centrifuge tube. A specified mass of *n*-heptane was then added to achieve the desired weight percent of solvent. The *n*-heptane was added at a rate of approximately 1 mL/minute while keeping the mixture well stirred using a magnetic bar and stirrer. The mixtures were then sonicated for 50 minutes and left to settle for the desired time. Then, the samples were centrifuged using a Hettich Model EBA 12 centrifuge for five minutes at 4000 rpm. The supernatant was decanted and filtered through a glass microfiber filter with VWR grade of 696. The remaining sediment (precipitated asphaltenes and entrained continuous phase) were washed with 20 mL of *n*-heptane and the mixture was sonicated for 15 minutes and centrifuged for five minutes at 4000 rpm. The washing step was repeated for a total of two washings. The precipitated material was dried in a Thermo Scientific Labline vacuum oven at 60^{o}C at -70 kPA until no further change in the mass was detected. Note, time zero is defined as the time at which the last drop of solvent was added to the bitumen.

The precipitate contains both asphaltenes and inorganic solids which co-precipitate with the asphaltenes. To obtain the solids content, the precipitate was dissolved in toluene and sonicated for one hour and centrifuged at 3500 rpm for six minutes. The supernatant was decanted. This procedure was repeated until the toluene solution was colorless. The remaining solids were dried and weighed. Asphaltene precipitation yields were calculated as the mass of precipitate less the mass of solids all divided by the initial mass of bitumen; that is, the asphaltene yields were all determined on a solids-free basis. The repeatability of the yields was ±6%.

Nitrogen Atmosphere

The nitrogen atmosphere experiments were conducted in an inflatable glove box, Figure 3.1. The glove box was first placed under vacuum to remove air and was then filled with nitrogen. This cycle was repeated three to four times to ensure an oxygen-free environment. To prepare oxygen-free bitumen samples, the bitumen was placed in a flask in a vacuum oven at 70^{o}C for three days. Then, the flask was connected to a nitrogen supply inlet and a vacuum outlet and placed in a 50°C water bath. Nitrogen was bubbled through the bitumen for five days. After removal from the water bath, the bitumen was continuously purged with nitrogen for another two days. The solvent, *n*-heptane, was also purged with nitrogen in the same manner for three hours before it was added to the bitumen.

Apart from the nitrogen purging, the same procedures were followed as described for precipitation measurements in an air atmosphere. Note, any potential evaporation of light components from the bitumen during purging was not monitored because this dead bitumen sample had previously been shown to only release volatiles at temperatures above 120^{o}C (Sanchez, 2013).

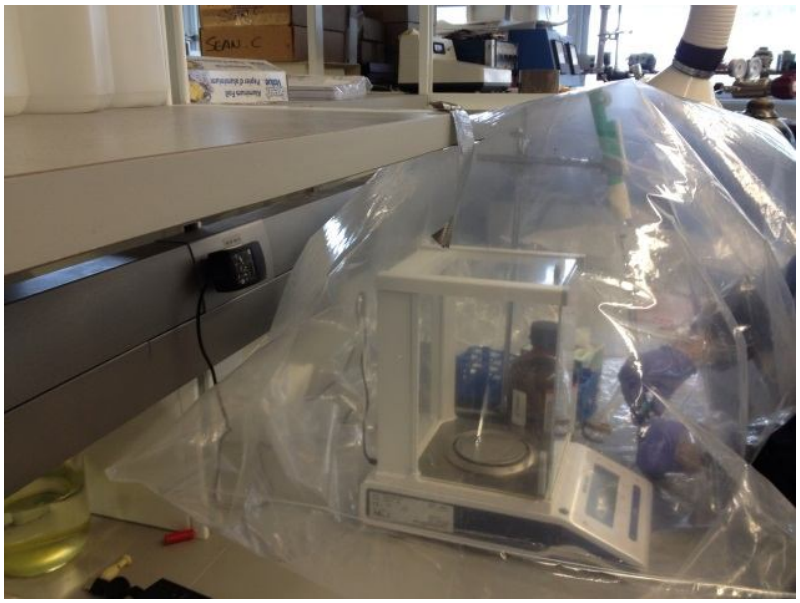

Figure 3.1: Photograph of the nitrogen atmosphere inflatable glove box.

3.2.2 Onset of Precipitation – Gravimetric Method

To determine the onset gravimetrically, a series of yields were measured at the same settling time but with different solvent contents. The onset for that settling time was then determined by extrapolating the yield data to zero yield, Figure 3.2. Based on the scatter in the yield data, the precision of the extrapolated yields was ±1 wt%.

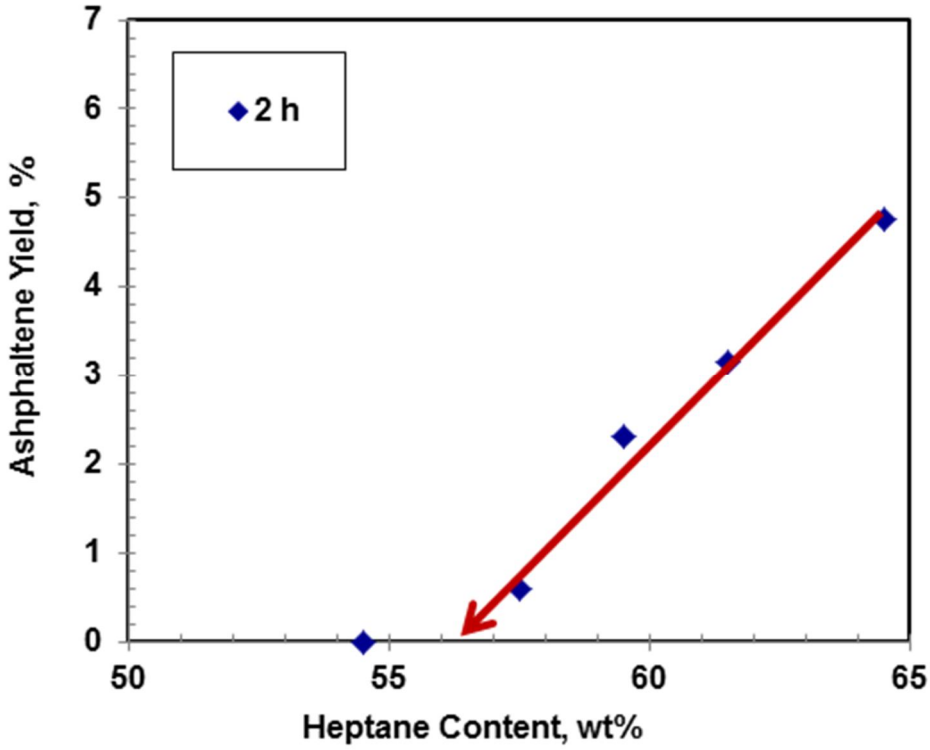

Figure 3.2: Gravimetric determination of the onset of asphaltene precipitation from n-heptane diluted bitumen at 2 hours by extrapolation of asphaltene yield data to zero yield.

3.2.3 Onset of Precipitation – Microscopy Method

To determine the onset using microscopy, a series of diluted bitumen samples were prepared at the same settling time but with different *n*-heptane contents (50.5 - 61.5 wt% in bitumen). A few drops of each mixture were placed on glass convex shaped slides covered with a coverslip and a micrograph was prepared. A Carl Zeiss Axiovert S100 optical microscope equipped with an Axiocam videocamera was used to capture images and Axiovision software was used for image analysis. The onset of asphaltene precipitation was determined as the lowest mass fraction of *n*-heptane at which precipitated asphaltene particles were observed. The same procedure was followed to determine the onset using *n*-pentane.

If the bitumen contains inorganic solids, the onset of precipitation can be obscured by the presence of these particles. Therefore, the bitumen used for these experiments was filtered through Sterlitech silver membrane filters to remove fine solids and water. The bitumen was first passed through a 5 micron filter and then through a 2.5 micron filter. Then the filtered bitumen samples were diluted with a specific mass ratio of *n*-heptane as described in Section 3.2.1 except that the dilute mixtures were not sonicated so that the measurements could begin immediately after the last drop of solvent was added.

3.3 Flocculation Measurements

3.3.1 Particle Size Analyzer

A Lasentec Model D600 (Mettler Toledo, U.S.A.) particle size analyzer was used to measure the particle size distribution of flocculated asphaltenes using a focused beam reflectance measurement (FBRM). The instrument provides an *in-situ* particle chord length distribution over a wide range of suspension concentrations.

The instrument directs a laser of wavelength 780 nm through a lens rotating at 4500 rpm, giving a beam of light highly focused at a point near the instrument window. When the moving laser beam intersects the particle path, some of the light is reflected back to the detector. Since the tangential velocity of the beam is known to be ~1.9 m/s, (Heath *et al.*, 2002), the duration of the reflected light pulse is directly proportional to the width of the particle intersected. This optical signal is processed by the software and the corresponding chord length, *s*, is calculated as the product of measured crossing time Δt and the beam velocity v_b (Mangold, 2012; Kempkes *et al.*, 2008; De Clercq *et al.*, 2004). It is unlikely that the laser beam will pass directly across the

center of the particle (*i.e.*, its diameter), therefore the chord length is measured. Thousands of chords are measured which results in producing a robust chord length distribution. The chord length distribution represents the particle population of the system (Sathe *et al*., 2010).

The particle size analyzer also records the number of counts per second. Total particle number is helpful for mass balances and estimating the aggregate porosity (or fractal dimension). However, the total focused beam reflectance measurement count does not correlate well with the actual number of flocs or the precipitate fraction in the mixture (Heath *et al*. 2002; Barrett and Glennon 1999). The instrument can only count one particle or floc at a time. In other words, between particles or flocs, the reflected time must return to zero for a short time period, therefore, the dead time will be larger in comparison to the time spent traversing the particles. Hence at relatively high particle concentration, the instrument dead-time increases and the chances of particles overlapping in the viewing zone likely increases as well. In addition, the precipitated asphaltenes are prone to adhere onto the probe window and the impeller, which results in an erroneous increase in the count rate. The number and volume *frequency* plots are assumed to be correct because they deal with the relative number of flocs with specific sizes or volumes.

Instrument Preparation, Calibration and Accuracy Check

Some adjustments, such as discrimination electronics (fine vs. coarse electronics), measurement duration, and channelling configuration must be set in the FBRM Control Interface (Version 6) software before any measurements are made.

The instrument data processing is adjusted to use either F-(fine) or C-(coarse) discrimination electronics. The differences are in the interpretation of the backscattered signals. The F-electronics are used in detecting smaller particles travelling closely together, provides sharper resolution and higher sensitivity to fine chords. Whereas C-electronics track larger loosely packed flocs and aggregated particles. For the purpose of this research, the coarse electronic was selected prior to data collection.

The total measurement duration determines how long data are collected before both the current statistics and chord-length distribution can be updated. A single measurement (*i.e.*, the data from total measurement duration) is saved to a data file in the form of a record. To produce robust statistics, the measurement duration should be as long as possible, while still maintaining resolution to change in the process over time. There is a trade-off between measurement precision and time resolution. The more precise a measurement is, the greater its sensitivity to change will be. The measurement duration for all the experiments was set to 15 seconds, which was small enough to capture the flocculation dynamics. Below the 15 second measurement duration, the statistical robustness of the data was reduced and significant spikes were observed in the measurements.

The particle size analyzer also allows various user-defined channel groupings. The particle size analyzer measures flocs or particles of about 1 to 1080 μm diameter. In this study, distributions were categorized using 90 log-intervals over a channel range of 1 to 1080 μm to ensure wide range coverage.

Prior to measurements, the gap between the impeller and probe window was set to 3 mm to ensure optimal distribution. The probe window was cleaned thoroughly until zero counts per second were observed. The particle size analyzer was calibrated using 8.33 wt% polyvinyl chloride (PVC) suspended solids in water as reference sample. This assured instrument repeatability as well as instrument-to-instrument reproducibility. The particle size analyzer parameters were set up as follows:

- Mixing speed: 400 rpm
- Fine vs. Coarse: Fine electronics
- Run Time: 10 minutes

The volume frequency distribution of particle diameters for a calibration reference sample is shown in Figure 3.3. The results are in a good agreement with the volume frequency distribution supplied by the manufacturer, with an average of the error of 8.3 % of volume mean diameter confirming a good calibration.

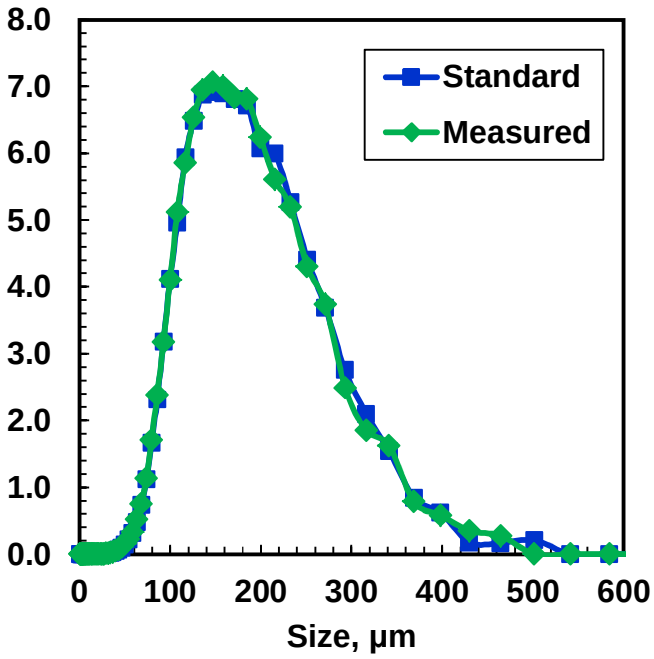

Figure 3.3: Comparison between measured and given volume frequency distribution of a standard sample of 8.33 wt/wt% PVC particles suspended in water at 400 rpm and 23°C.

Detection Limit

The particle size analyzer detection limit was tested using asphaltenes in heptane-toluene (heptol) and diluted bitumen mixtures. For asphaltene concentration above 10 kg/m^3, repeatable approximately log-normal distributions were observed. Below 10 kg/m^3, the distributions became irregular and non-repeatable. For diluted bitumen systems above 75 wt% *n*-heptane, repeatable approximately log-normal distributions were also observed. Below 75 wt% *n*-heptane, measurements suddenly dropped to a volume mean diameter of 10 to 40 µm and particle count of 2 to 4 counts per second, Figure 3.4 a. The transition is well above the onset of asphaltene precipitation and does not correspond to a significant change in asphaltene yield. Possible causes are: 1) the mixture becomes too opaque at lower dilution; 2) asphaltene particles stick to the probe window and impellers. In this work, particle size analyzer measurements were only

analyzed at high dilutions, above 75 wt% *n*-heptane. The detection limit is discussed in more detail in Chapter 6.

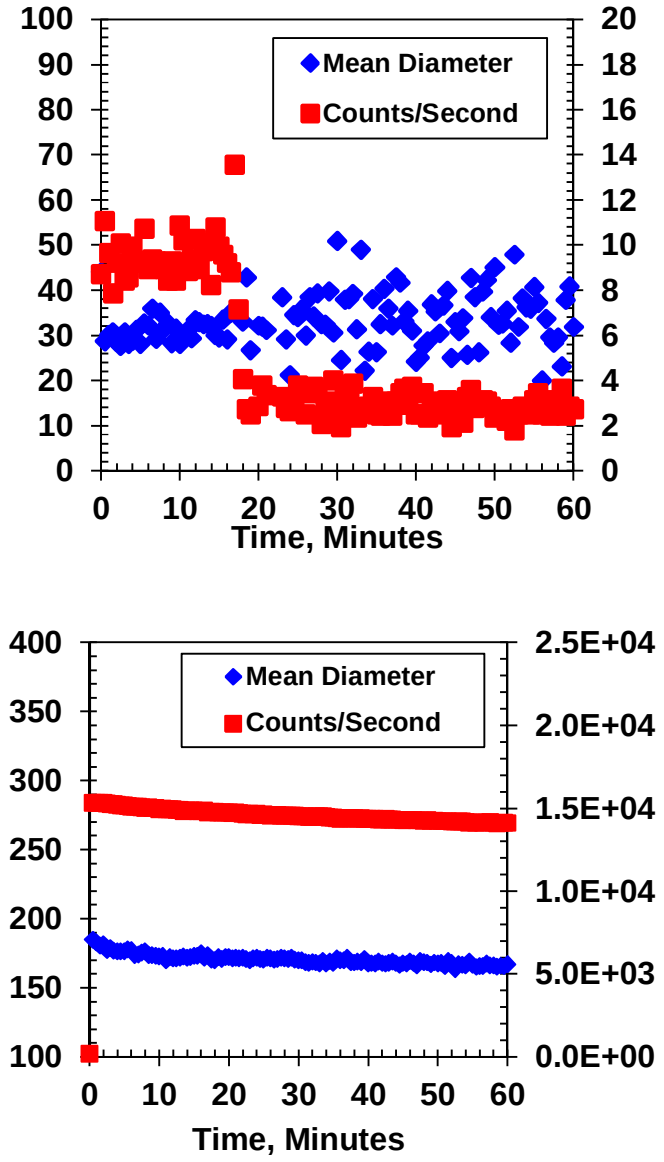

Figure 3.4: Measured volume mean diameter and particle count distribution for a) low dilution of 62 wt%, and b) high dilution of 87.5 wt% *n*-heptane, at 195 rpm and 23°C.

3.3.2 Flocculation Experiments

The flocculation experiments were carried out in a beaker with an internal diameter of 7.4 cm and a height 12.6 cm. The beaker is equipped with a four-angle blade impeller with a diameter of 50 mm as shown in Figure 3.5.

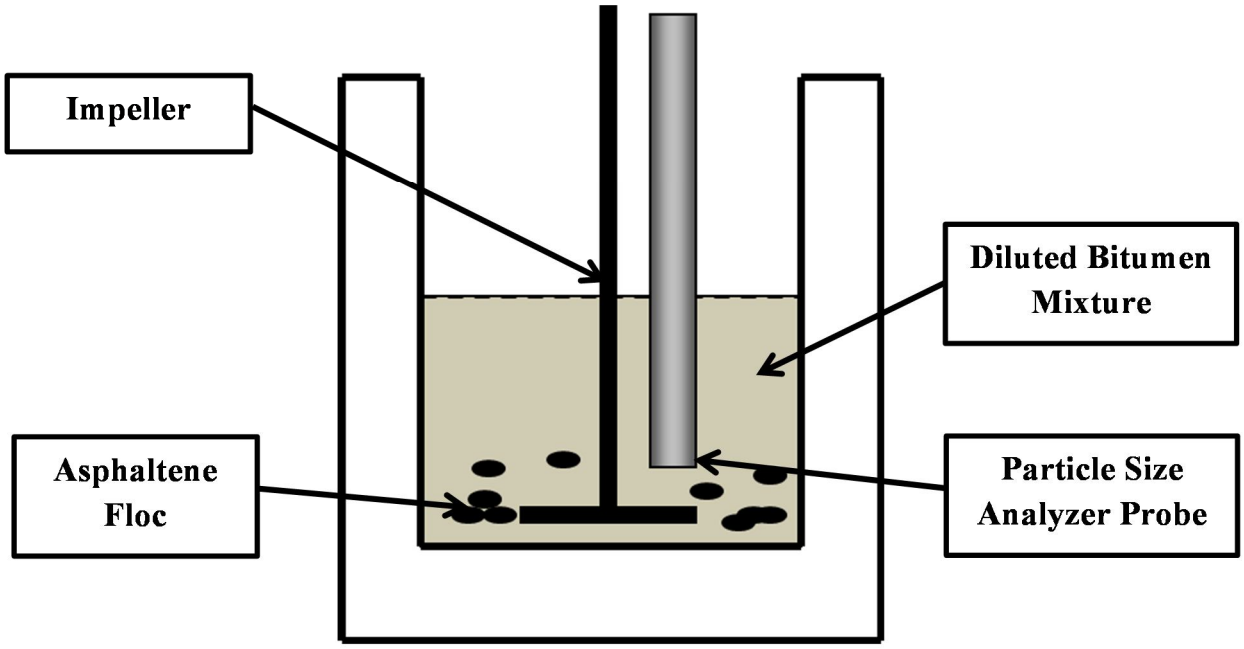

Figure 3.5: Diagram of the beaker with mixer and the probe.

Two different schemes were used to add the diluent: one-stage and two-stage mixing. Most experiments were conducted with two-stage mixing. To conduct a flocculation experiment with two-stage mixing, the bitumen was premixed with solvent to a solvent content below the onset of asphaltene precipitation but sufficient to reduce the viscosity to allow for rapid mixing (50 wt% *n*-heptane). A known weight of bitumen to the beaker and solvent was added to the bitumen at a rate of approximately 1 mL/minute while stirring the mixture with a magnetic stirrer. Then, the

mixture was sonicated in an ultrasonic bath for 50 minutes. If solvent evaporation was observed, more solvent was added to maintain a constant mass. At this stage, the viscosity of bitumen was reduced and no asphaltene precipitation was detected. Then, the remainder of the diluent was added all at once to reach the final desired concentration of *n*-heptane. The stirrer on the particle size analyzer was turned on and the size measurements were started.

For one-stage mixing, all the diluent was added to the bitumen all at once and then the stirrer was turned on and the particle size measurement started. One-stage mixing was used for 87.5 and 90.5 wt% *n*-heptane. To minimize evaporation, the beaker was covered with a cap. The total volume of the mixture was set to be 200 mL.

Mixing Speed, Shear Rate, and Reynolds Number

Below 195 rpm, settling of asphaltene aggregates occurred and at speeds greater than 330 rpm large vortexes and air entrainment was observed. Therefore, only mixing speed between 195 and 330 rpm were investigated.

The relevant measures for comparing data at different mixing speeds are shear rate or Reynolds number. Therefore, the shear rate and Reynolds number were determined for the mixing speeds used in this thesis. The fluid motion in the vicinity of the impeller is characterized by relating shear rate to the impeller speed (Wu *et al.*, 2006), Equation 3.1. a. Shear rate at an impeller is directly proportional to the impeller speed. The shear rate in a beaker with a 45^{o} pitch-bladed impeller is given by Equation 3.1.b (Uhl and Gray, 1986; Wu *et al.*, 2006).

$$\gamma = K_s N \tag{3.1.a}$$

$$\gamma = 11.5\, N \tag{3.1.b}$$

where and γ is the shear rate (s^{-1}), K_s is a non-dimensional constant, dependent on impeller geometry and N is the mixing speed (min^{-1}). The Reynolds number for this geometry is given by (Brawn 2003),

$$N_{Re} = \frac{10.75 N d_{imp}^2 \rho_m}{\mu} \tag{3.2}$$

where N_{Re} is the Reynolds number, d_{imp} is the impeller diameter (inch), and ρ_m is the mixture density (g/cc). The mixture density was determined from Saryazdi *et al.* (2013) correlation based on the Mixing Rule. μ is the fluid viscosity (mPa.s). The viscosity of the mixture was calculated from the known bitumen and solvent viscosities using the Expanded Fluid viscosity correlation (Motahhari *et al.*, 2013). Table 3.2 summarizes the Reynolds number corresponding to each dilution ratio and mixing speed.

Table 3.2: Summary of Reynolds number corresponding to each dilution ratio and mixing speed at 23°C.

Solvent wt%	Mixing Speed rpm	Shear Rate s-1	Viscosity mPa.s	Density kg/m³	Reynolds Number
91.5	195	37	0.50	698	11500
93.5	195	37	0.53	703	10700
95.5	195	37	0.57	708	10000
87.5	195	37	0.68	719	8600
87.5	275	53	0.68	719	12100
87.5	330	63	0.68	719	14500

Repeatability

The repeatability of the particle size distributions was evaluated by repeating, three times each, the measurement of the asphaltene particle size distribution at 87.5 and 91.5 wt% *n*-heptane. The repeated number and volume frequency distributions for 87.5 wt% *n*-heptane are shown in

Figures 3.6a and 3.6b, respectively. The mean diameters were repeatable to within 3.0%. Details of the repeatability analysis are provided in Appendix A.

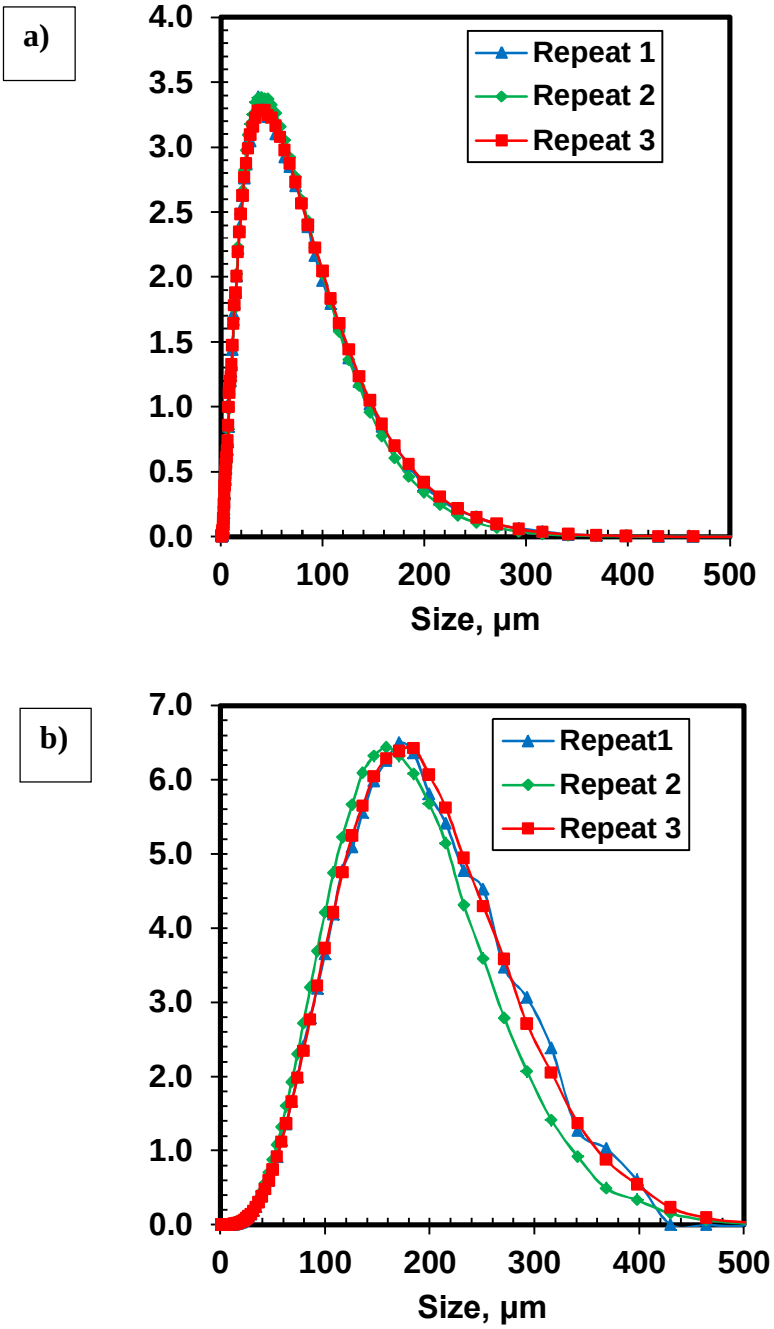

Figure 3.6: a) Number frequency distribution, and b) volume frequency distribution of asphaltene flocs for three different runs after 10 minutes for 87.5 wt% *n*-heptane, at 195 rpm, and 23^{o}C.

CHAPTER FOUR: : KINETICS OF ASPHALTENE PRECIPITATION

This chapter focuses on determining the onset and kinetics of asphaltene precipitation from a Western Canadian bitumen diluted with *n*-heptane at 23^{o}C, in both air and nitrogen atmospheres. The data are used to assess the impact of oxidation on asphaltene yield and precipitation kinetics. The steady state yield in nitrogen is then modeled using a regular solution approach. The effect of the type of solvent on the kinetics of asphaltene precipitation is also investigated briefly.

4.1 Onset of Asphaltene Precipitation in n-Heptane Diluted Bitumen

The first step is to identify the onset of precipitation; that is, the solvent content at which precipitation is first detectable as approximately 0.5 μm asphaltene particles. The onset of precipitation was determined in two ways: by microscopic observation and gravimetrically. Both methods were described in Chapter 3.

4.1.1 Onsets from Microscopic Method

Figure 4.1 shows the micrographs for the experimental runs with 56.5, 57, and 57.5 wt% *n*-heptane at various times in an air atmosphere. The first appearance of particles is a haze that is challenging to capture with a micrograph. This haze appears after 70, 40, and less than 1 minute at 56.5, 57.0, and 57.5 wt%, *n*-heptane, respectively. After the haze is observed, clearly defined particles and flocculation appear gradually over tens of minutes, Figures 4.1a to 4.1c, respectively. Therefore, the appearance of the haze is interpreted as the onset of precipitation. Figure 4.1 demonstrates that the onset of precipitation at time zero (immediately after mixing the

solvent in the bitumen) is 57.5 ± 0.5 wt% *n*-heptane. The onsets shift to lower *n*-heptane contents with longer contact times, as summarized in Table 1. The shift to lower onsets and the gradual growth in the number of particles over time confirm that asphaltene precipitation in air is time dependent.

Table 4.1: Onset of asphaltene precipitation in *n*-heptane and *n*-pentane diluted WC_B2 bitumen at 23°C and 1 atm.

Solvent	Contact Time (min)	Microscopic Onset (wt% solvent)	Gravimetric Onset (wt% solvent)
n-heptane	< 1	57.5 ±0.5	-
n-heptane	40	57.0 ±0.5	-
n-heptane	70	56.5 ±0.5	-
n-heptane	120	-	56.5 ±1
n-pentane	< 1	49.0 ±0.5	-

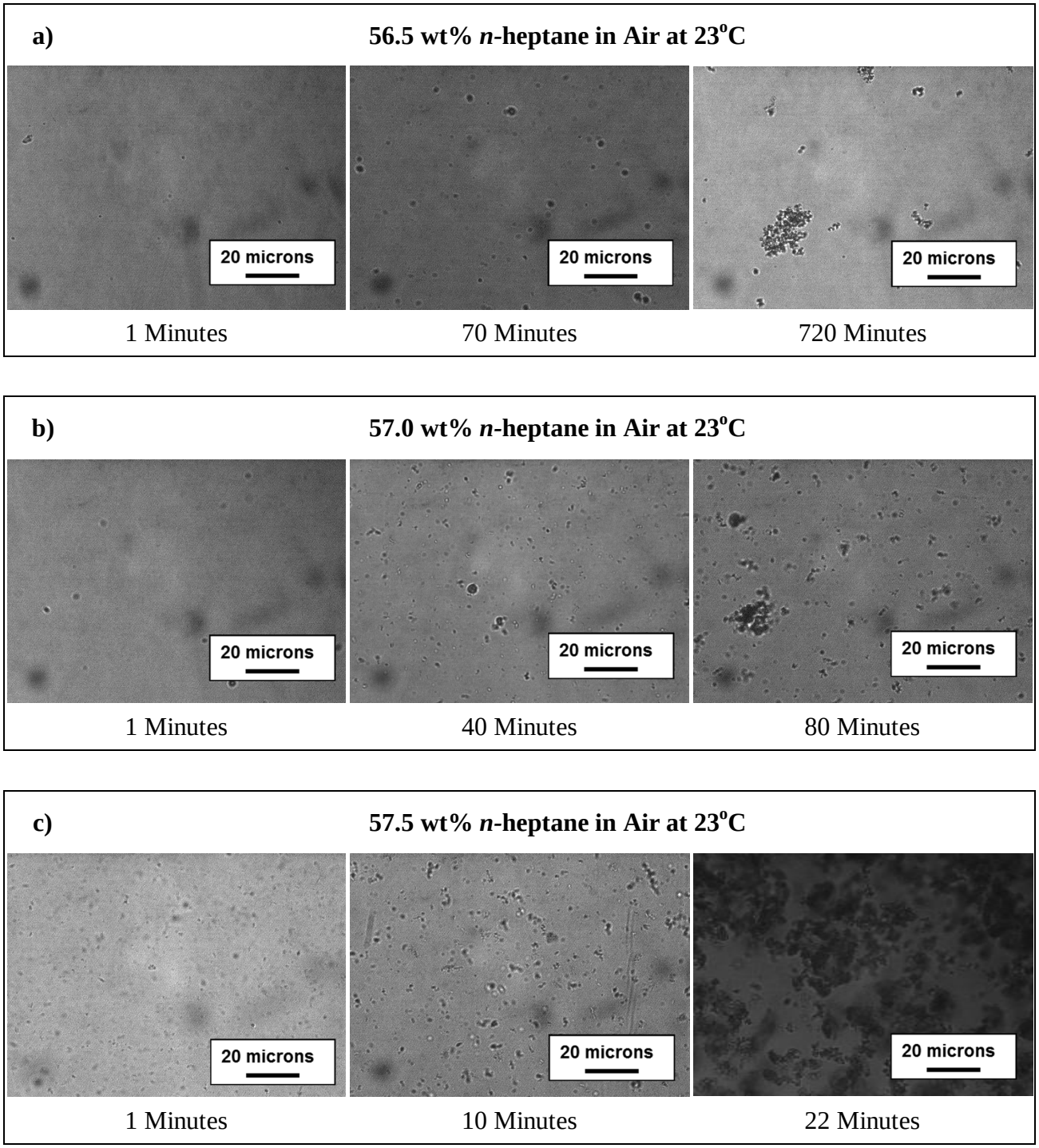

Figure 4.1: Micrographs showing the onset of asphaltene precipitation from *n*-heptane diluted WC_B2 bitumen at a) 56.5 wt%, b) 57.0 wt%, and c) 57.5 wt% *n*-heptane in air at 23°C.

4.1.2 **Gravimetric Observations**

Figure 4.2 shows the amount of precipitation plot versus the mass fraction of *n*-heptane in the diluted bitumen for two hours at 23°C in air. The onset at two hours was found to be approximately ±56.5 wt% *n*-heptane in good agreement with the microscopic observations, Table 1. Figure 4.3 shows that the onsets continue to shift to lower n-heptane content over 48 hours for two bitumen samples from the same source reservoir, WC_B2 and WC_B3, again consistent with the microscopic observations. This trend continued to a lesser extent over times up to 2 months (not shown in Figure 4.3). Note, the WC_B3 bitumen was used to examine onsets and yields in *n*-pentane as will be discussed later.

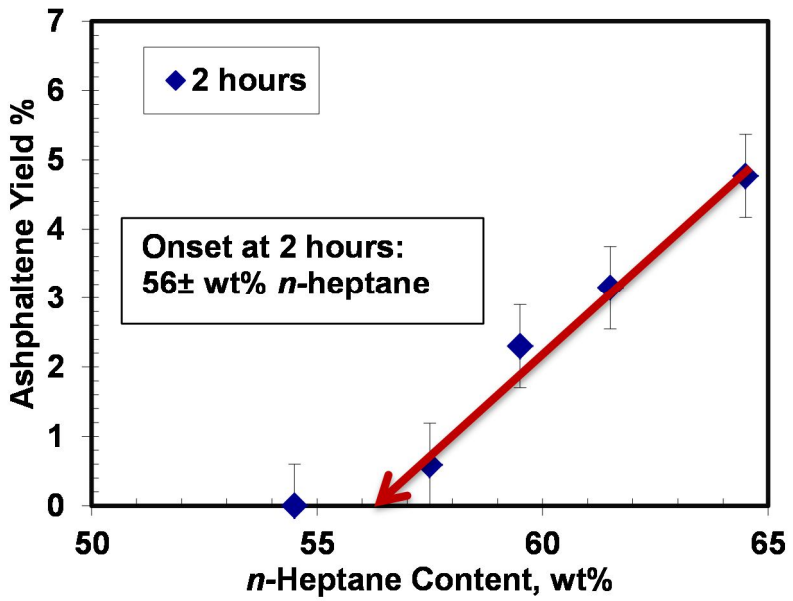

Figure 4.2: Gravimetric determination of the onset of asphaltene precipitation from *n*-heptane diluted WC_B2 bitumen at 2 hours by extrapolation of asphaltene yield data to zero yield at 23°C.

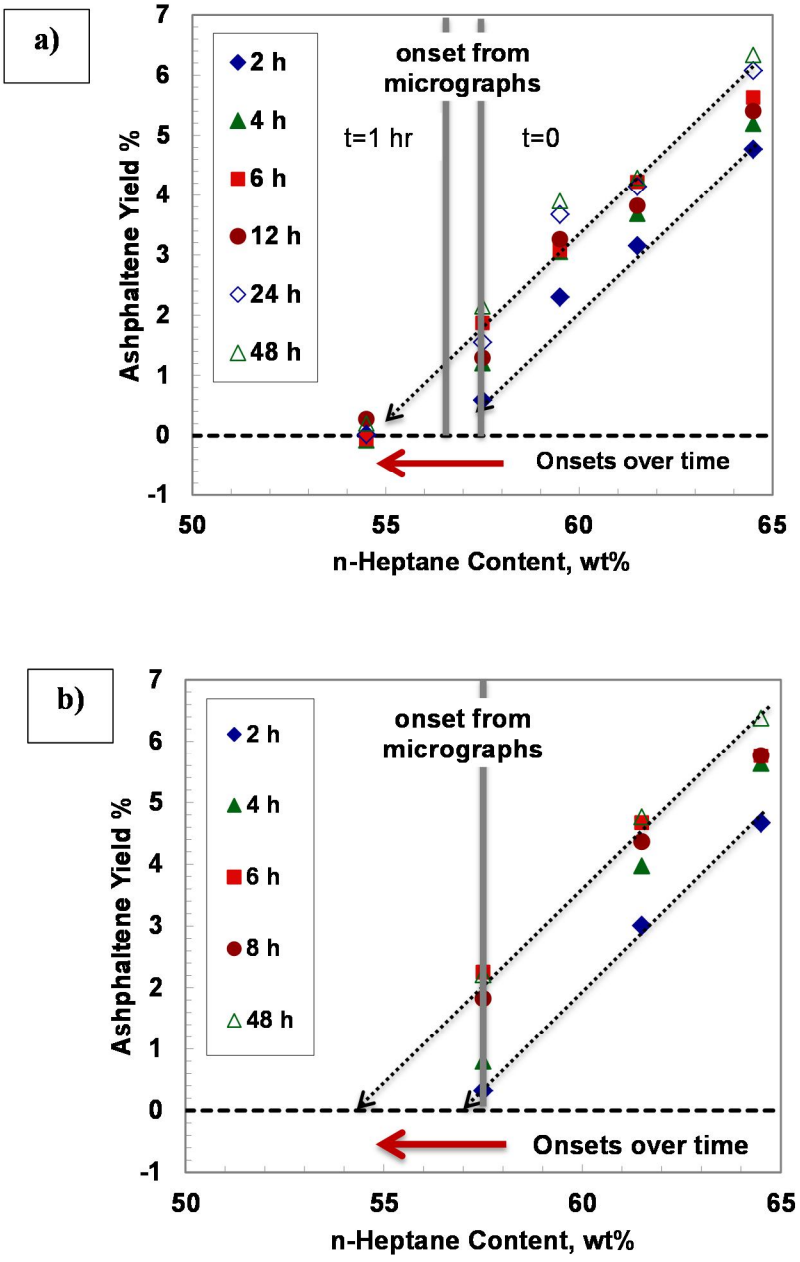

Figure 4.3: Comparison of gravimetric and microscopic precipitation onsets up to 48 hours in *n*-heptane diluted a) WC_B2 (Shafiee, 2014) and b) WC_B3 (Motahhari, 2013) bitumen in air at 23°C and 1 atm. Error bars in yield of ±0.61 wt% are not shown to avoid clutter.

The yield data at each time were extrapolated to determine the onset condition as was shown in Figure 4.3. The onsets are plotted over time in Figure 4.4 and are compared with similar data collected by Maqbool *et al.* (2009) over time for a different crude oil. Both datasets show a steep decrease in the onset wt% of *n*-heptane over 2 days followed by a gradual decrease over more than a month. At first glance, it appears that Maqbool *et al.* (2009) are correct in concluding that the onset of asphaltenes precipitation migrates to lower and lower solvent content over months and perhaps years. However, onset data collected in a nitrogen atmosphere tell a different story. Figure 4.6 shows that the gravimetric onsets observed over time in nitrogen atmospheres are identical to the results in air for the first 48 hours but then reach a plateau. It appears that the long term kinetics observed in air is a result of a separate process such as oxidation or oxygen catalyzed polymerization (Wilson and Watkinson, 1996). Nonetheless, the shift in onset over the first 48 hours is not an oxygen related artefact and is consistent with a nucleation and growth process before reaching equilibrium.

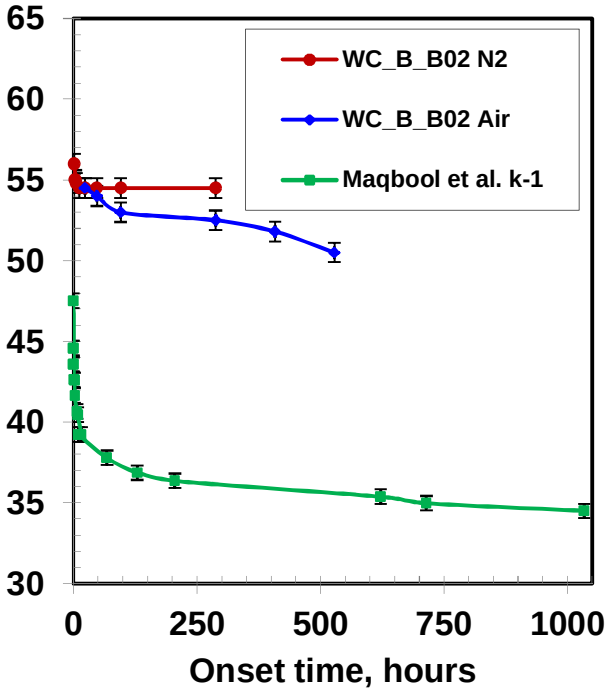

Figure 4.4: Gravimetric precipitation onsets in *n*-heptane diluted WC_B2 bitumen in air and nitrogen (Shafiee, 2014), and *n*-heptane diluted k-1 crude oil (Maqbool *et al.* 2009) at 23°C and 1 atm.

4.2 Asphaltene Yields over Time in *n*-Heptane Diluted Bitumen

Yields in air over time from this thesis are compared with those reported by Maqbool *et al.* (2009) in Figure 4.5 and with data from Beck *et al.*, (2005) in Figure 4.6. Since different oils were used in each study the amount of solvent to obtain a given yield is different in each case. Although different experimental methods and intensity of aeration were employed, the change in yield over time is remarkably similar in all cases.

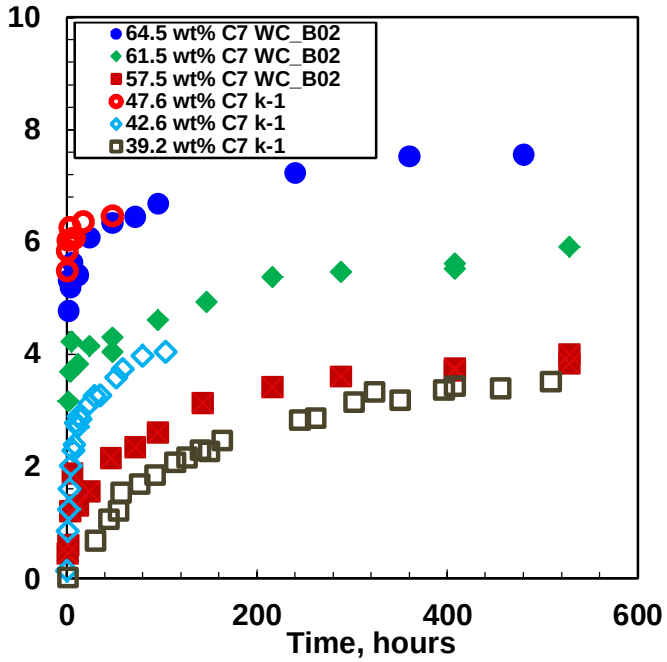

Figure 4.5: Comparison of asphaltene kinetics from WC_B2 bitumen (Shafiee, 2014) and k-1 crude oil (Maqbool *et al.*, 2009), both diluted with *n*-heptane in air at 23°C and 1 atm. Error bars in yield of ±0.61 wt% (Shafiee, 2014), and ±0.41 wt% (Maqbool *et al.*, 2009) are not shown to avoid clutter.

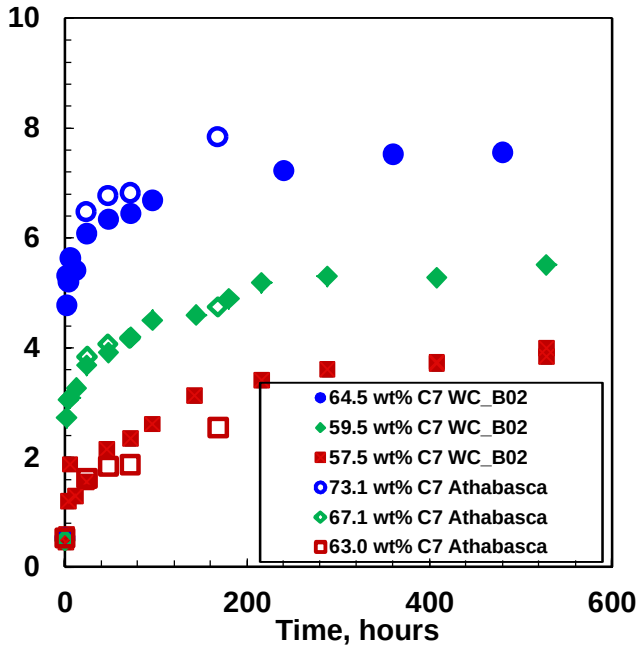

Figure 4.6: Comparison of asphaltene kinetics from WC_B2 bitumen (Shafiee, 2014) and Athabasca bitumen (Beck *et al.*, 2005) both diluted with *n*-heptane in air at 23°C and 1 atm. Error bars in yield of ±0.61 wt% (Shafiee, 2014), and ±0.75 wt% (Beck *et al.*, 2005) are not shown to avoid clutter.

Yields in nitrogen over time from this work are compared with data from Beck *et al*. (2005) in Figure 4.7. The change in yield over time in nitrogen are the same within the scatter of the measurements. For both datasets, it takes 48 hours to reach a plateau. Considering both the air and nitrogen atmosphere datasets, it appears that the kinetics of asphaltene precipitation is similar for different crude oils.

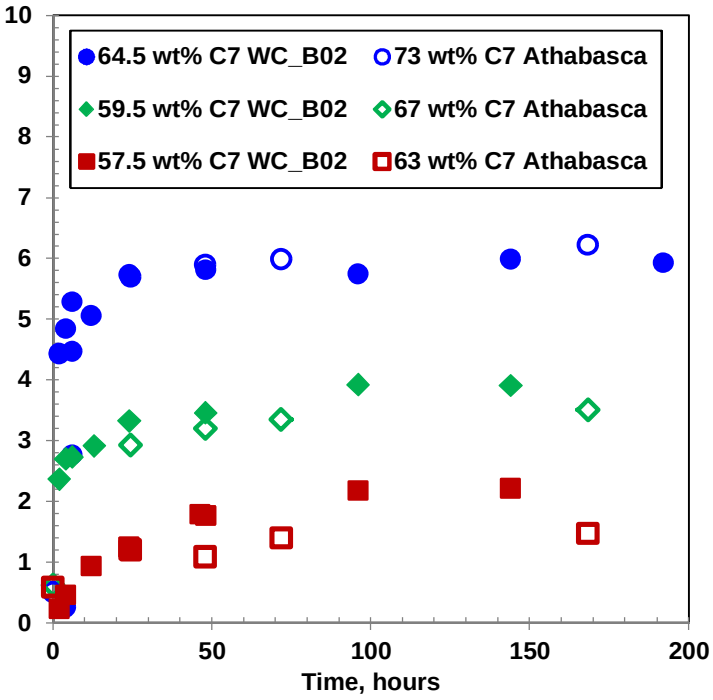

Figure 4.7: Comparison of asphaltene kinetics from WC_B2 bitumen (Shafiee, 2014) and Athabasca bitumen (Beck *et al.*, 2005) both diluted with *n*-heptane in Nitrogen at 23°C and 1 atm. Error bars in yield of ±0.61 wt% (Shafiee, 2014), and ±0.75 wt% (Beck *et al.*, 2005) are not shown to avoid clutter.

A comparison of yield data in air and nitrogen over time, Figure 4.8, reveals the same trends as observed for the onset data. Yields in air and nitrogen atmospheres are similar for the first 24 hours, but deviate after 48 hours. The yields in air increase gradually over time while the yields in nitrogen reach a plateau. The effect of air continues for even longer contact times, Figure 4.9.

It appears that the yield continues to increase for as long as the experiments are conducted; that is, for more than 1000 hours. Again, the long term changes in yield observed in air appear to be caused by oxidation or oxygen catalyzed polymerization. Hence, the yields in nitrogen must be used to determine the kinetics of asphaltene precipitation in non-aerobic conditions.

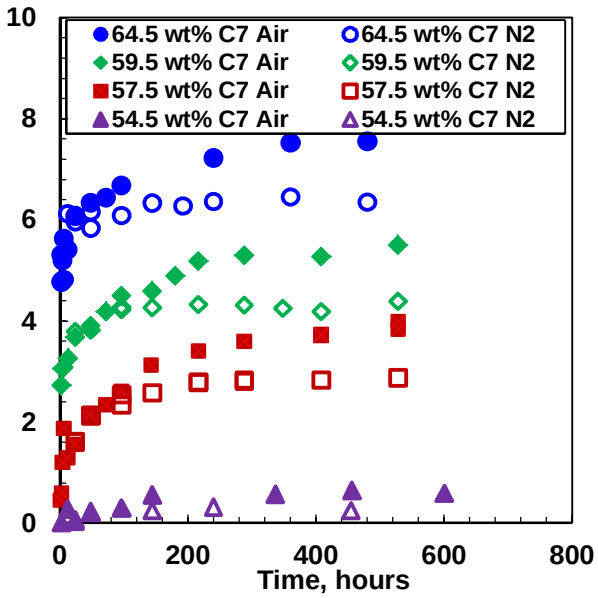

Figure 4.8: Comparison of asphaltene yields from n-heptane diluted WC_B2 bitumen over time in air and nitrogen at 23°C and 1 atm. Error bars in yield of ±0.61 wt% are not shown to avoid clutter.

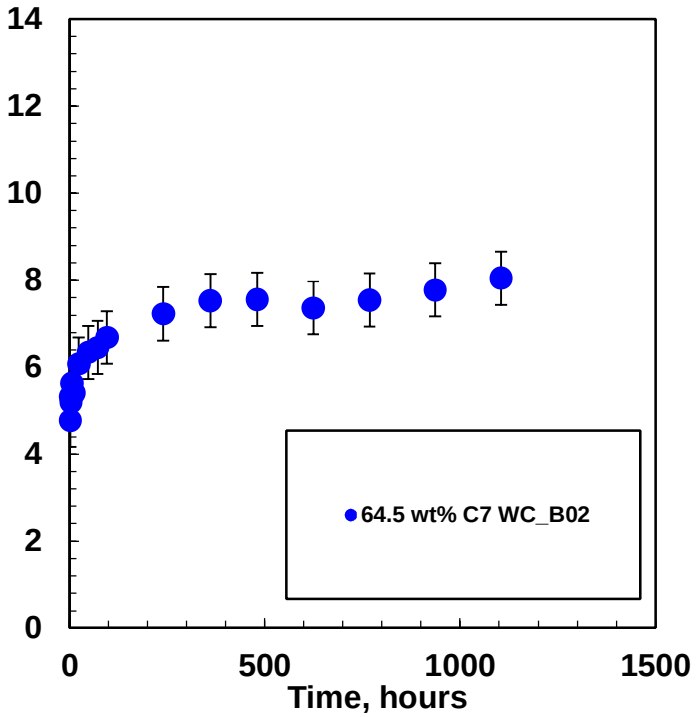

Figure 4.9: Asphaltene precipitation over longer run from WC_B2 bitumen diluted with *n*-heptane in air at 23°C and 1 atm.

The yields in nitrogen were fitted with the following expression:

$$Y = Y_{slow}\,(1-\exp\{-0.03t\}) + Y_{\text{fast}}\,(1-\exp\{-5t\}) \qquad (4.1)$$

where Y is the yield (w/w) and t is time in hours. The fitted data are presented in Figure 4.10. The first term in the rate expression represents the gradual increase in yield over time and the second term represents the rapid initial precipitation that is observed only when $Y > Y_{slow}$. Note, the rate constants will likely depends on the temperature, solvent, and possibly pressure and; therefore, the values used in Equation 4.1 are only valid for *n*-heptane at ambient conditions. The correlation fits the yield data with an AARD of 3.6%.

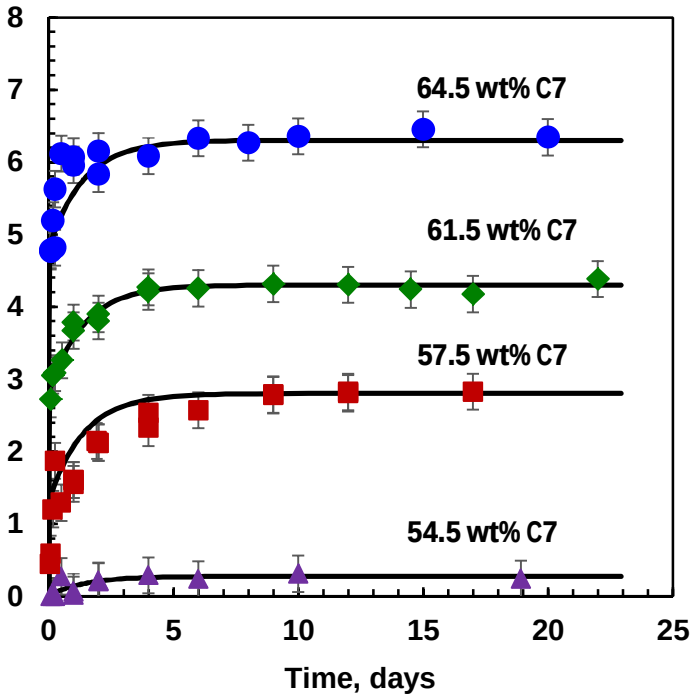

Figure 4.10: Measured and fitted asphaltene yields over time from *n*-heptane diluted WC_B_B02 bitumen in a nitrogen atmosphere at 23°C and 1 atm.

4.3 Asphaltene Onset and Yield in *n*-Pentane Diluted Bitumen

A preliminary investigation of asphaltene precipitation in *n*-pentane diluted bitumen was carried out. Yields for n-pentane diluted WC_B2 bitumen could not be measured because there was insufficient sample. Instead, yields were measured for WC_B3 bitumen. However, the onset of precipitation in WC-B3 bitumen could not be determined because there were too many non-asphaltene particulates to clearly observe the onset and insufficient time to filter the bitumen.

The onset of asphaltene precipitation from WC_B2 bitumen diluted with *n*-pentane as the precipitant was determined microscopically, Figure 4.11, to be 49.0 ± 0.5. As expected, because

pentane is a poorer solvent for asphaltenes than heptane, the onset was significantly lower than the onset of 56.5 ±0.5wt% determined in *n*-heptane. The transition from haze to clearly defined particles with flocculation was significantly faster in *n*-pentane than in *n*-heptane. Figure 4.2 shows that at one minute, no particles were present but by 2 minutes, significant flocculation was already apparent. It appears that the transition from haze to well-defined particles is virtually instantaneous in the poorer solvent.

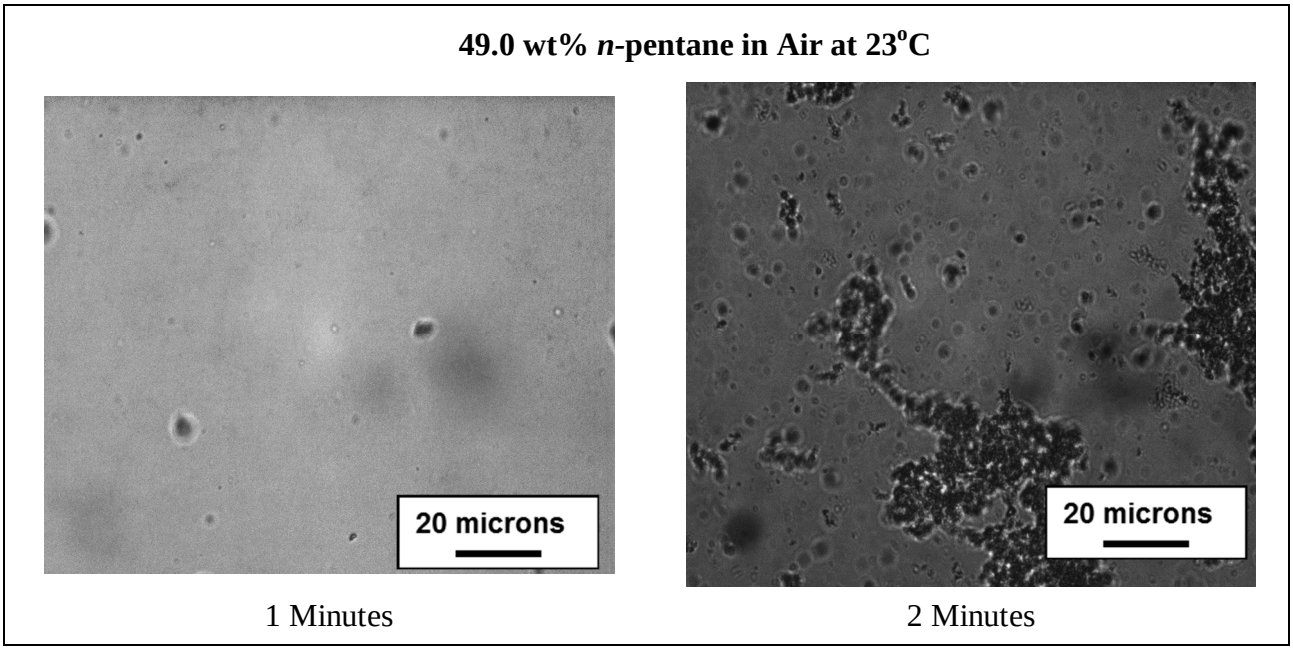

Figure 4.11: Micrographs showing the onset of asphaltene precipitation from *n*-pentane diluted WC_B2 bitumen at 49 wt% *n*-pentane in air at 23°C.

Figure 4.12 compares the gravimetric (WC_B3) and microscopic onsets (WC_B2) bitumen diluted with *n*-pentane. The data are scattered and do not show a clear trend over time. In addition, the data from the gravimetric measurement is not consistent with the microscopic method. The gravimetric method yields an onset of about 44 wt%, whereas the micrographs

results are 49 wt%. There are a number of possible explanations for the inconsistency of the onset measured from gravimetric versus the microscopic methods which are outlined below:

1. There is a possible error in the experimental measurements of yield data using *n*-pentane.
2. The microscopic onset is determined from WC_B2 bitumen, while the gravimetric yield measurements are obtained from WC_B3 bitumen. Therefore, the microscopic onset from *n*-pentane diluted with B03 bitumen may differ from the B02. However. WC_B2 and B03 bitumen diluted with *n*-heptane, yield similar onsets using the gravimetric method.

It is recommended to repeat the experiments with filtered bitumen to reduce the scatter and improve the consistency of the results. Note, the scatter has a large impact on onset determination but less impact on higher yield data.

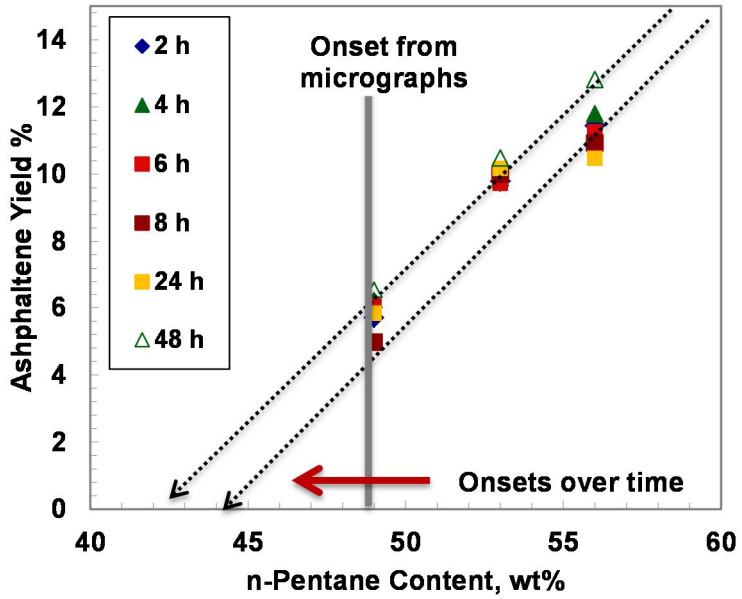

Figure 4.12: Comparison of gravimetric and microscopic precipitation onsets up to 48 hours in *n*-pentane diluted WC_B_B03 (Motahhari, 2013) bitumen in air at 23°C and 1 atm.

The kinetics of asphaltene precipitation in *n*-pentane diluted bitumen are rapid, Figure 4.13. Despite the scatter observed in the data, it appears that the precipitation kinetics is virtually instantaneous. The slight increase in yield over time may be an oxygen related artefact but more data are required for corroboration.

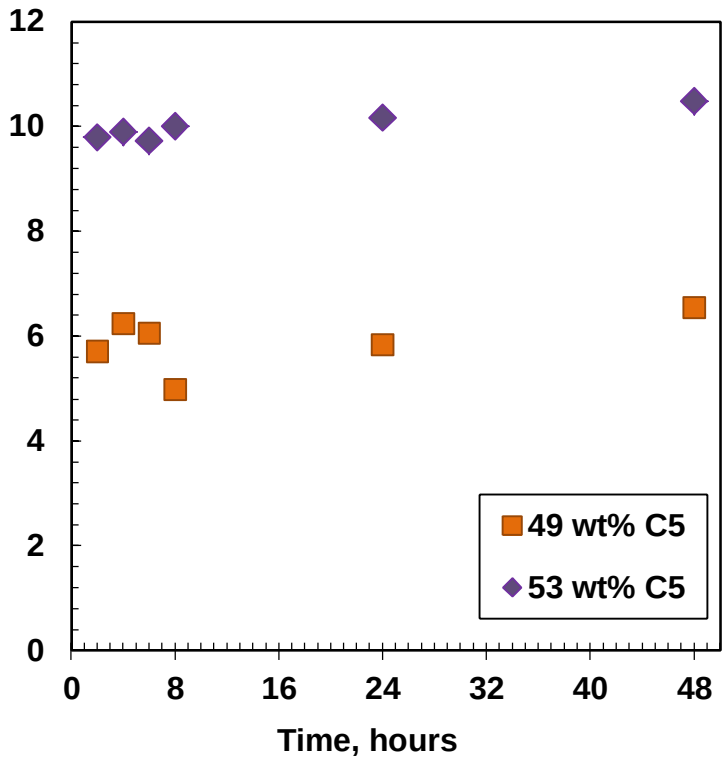

Figure 4.13: Asphaltene precipitation from WC_B_B03 bitumen (Motahhari, 2013) diluted with *n*-pentane in air at 23°C and 1 atm.

Implications of Results

It appears that after 48 hours, onset and yield data are affected by oxygen related artifacts. Considering that most industrial processes will be at anaerobic conditions, data collected after 48

hours in air may not be valid. The “real” kinetic appears to take place within 48 hours. Therefore, the relevant data can still be collected in air with negligible error.

One consequence of the observed kinetics is that the onsets determined within the first few hours do not represent a thermodynamic equilibrium. In this work, the initial onset in *n*-heptane was 57.5 wt% while the apparent equilibrium onset is 54.5 wt%. Hence, some care is required in choosing methods and data for particular asphaltene precipitation issues. For example, if the target is data for a thermodynamic model, then data should be collected after approximately 24 hours. Short term titration data, such as those often collected with near-IR and visual observations, will give misleading data for equilibrium models. On the other hand, if precipitation at process conditions and residence times is of interest, short term titrations are the appropriate choice. Equilibrium based models may give misleading results for short residence time processes.

CHAPTER FIVE: ASPHALTENE FLOCCULATION MODEL

This chapter describes the Smoluchowski population balance equation used to model asphaltene flocculation. First, the principles of the original model are shown and then the reaction terms developed by Rastegari (2004) and Daneshvar (2005) for this model are discussed. Fractal dimension is a key parameter in the model and in interpreting measured floc sizes and is described in detail. Finally, the algorithm used to solve the population balance equations is presented.

5.1 Smoluchowski Population Balance Equation for Asphaltene Flocculation Model

When particles in solution interact through molecular or colloidal forces and the convective forces of a moving fluid, they will collide unless electrostatically stabilized. If flocculation is reversible, collisions can result in flocculation, disintegration, or no net effect. Hence, the number of flocs and number of particles in a floc is determined from the number of collisions and the balance between the probabilities of flocculation and disintegration. The classical Smoluchowski population balance, modified to include disintegration (Hamedi Rad *et al.,* 2013; Daneshvar, 2005; Rastegari *et al.,* 2004; Rahmani *et al.,* 2004), is used to model the reversible flocculation and is given by:

$$\frac{dC_k}{dt} = \frac{1}{2}\sum_{i+j=k}\left(F_{i,j}C_iC_j - D_{i+j}C_{i+j}\right) - \sum_{j=1}^{N-k}\left(F_{k,j}C_kC_j - D_{k+j}C_{k+j}\right) \qquad (5.1)$$

$$k=1,2,3,\ldots,N$$

where the indices *i, j, k,* and *N* indicate the number of particles in the floc; $F_{i,j}$, and D_{i+j}, are the number of reactions (collisions) per unit volume per unit time that result in flocculation and disintegration, respectively. C_i and C_j are the concentrations of species, while *t* is the time (Rastegari *et al.,* 2004). This model describes the rate of change of concentration of *k*-fold aggregates, C_k, under the assumption of binary collisions. These derivates are integrated over finite time steps to update the calculated particle size distribution over time. The algorithm to perform these calculations is presented later.

5.2 Flocculation and Disintegration Reaction Terms

The two characteristic time scales which govern flocculation kinetics are the diffusion time and reaction time. Diffusion time (τ_{diff}) is the time it takes for two arbitrary particles to approach to the point of contact. Reaction time (τ_{reac}) is time it takes for two particles to flocculate when they are in mutual proximity. The kinetics of flocculation is described as diffusion-limited in instances where the diffusion time is greater than the reaction time. In this case, particles most likely flocculate on their first encounter with a neighbor particle and the kinetics are influence by local fluctuations in the concentration of the particles.

When the diffusion time is less than the reaction time, the kinetics is reaction-controlled and is limited by the relatively large reaction time. In this case, a particle may sample large volumes of its surrounding neighbors before flocculating and thus it effectively responds to the global concentration of other particles. In other words, particles may come within reaction range of each other numerous times before flocculation occurs. Reaction-limited flocculation is expected to be

the dominant mechanism in well-mixed experiments, like those used in this thesis, because stirring homogenizes the local concentration.

5.2.1 Flocculation Reaction Term

Based on reaction-limited flocculation theory, the reaction terms are dependent on the probability of bond formation upon collision of two clusters (Ball *et al.*, 1987). Rastegari *et al.* (2004) proposed the following reaction rate which is dependent on the reaction-limited flocculation reaction theory:

$$F_{i,j} = k'_f \left(\frac{M_j}{M_i + M_j} M_i^{1/D_f} + \frac{M_i}{M_i + M_j} M_j^{1/D_f} \right)^{\lambda} \tag{5.2}$$

where k'_f is the flocculation reaction constant scaled for mass, M_i is the mass of floc i, D_f is the fractal dimension of the floc, and λ is the flocculation reaction exponent which generally varies between 2 and 3. The mass of a floc is directly proportional to the number of particles in the floc; hence, Equation 5.2 can be expressed as follows (Daneshvar, 2005):

$$F_{i,j} = k_f \left(\frac{n_j}{n_i + n_j} n_i^{1/D_f} + \frac{n_i}{n_i + n_j} n_j^{1/D_f} \right)^{\lambda} \tag{5.3}$$

where k_f is the flocculation reaction constant scaled for the number of particles and n_i is the number of particles in floc i, These equations ignore the effect of three-cluster flocculation and were developed for low concentrations. Note that the flocculation reaction exponent decreases with a higher fractal dimension (more compact flocs) because more compact flocs interpenetrate less, which results in a less surface area of mutual contact (Rastegari, 2004).

5.2.2 Disintegration Reaction Term

The disintegration reaction term is expressed by a power law relationship to the particle diameter and is given by (Rastegari *et al.*, 2004; Daneshvar 2005):

$$D_{i+j} = k_d R_{i+j}^{\beta} = k_d \left(n_i^{1/D_f} + n_j^{1/D_f} \right)^{\beta} \quad \text{where} \quad R_{i+j} \approx R_i + R_j \tag{5.4}$$

where i and j represent the two flocs formed when a larger floc of $i+j$ breaks up, k_d is the disintegration reaction constant, R_i, R_j, are the radii of the flocs, and the disintegration reaction exponent β is a number from 0 to 3. The assumption that $R_{i+j} \approx R_i + R_j$ is only valid when $R_i >> R_j$ or vice versa. For simplicity, Equation 5.4 has been used for all floc sizes. Note, the second equality is obtained from the relationship between floc radius and fractal dimension which is below.

5.3 Fractal Dimension

Aggregates that are clusters of monomers can have fractal structures, meaning that parts of the objects are similar to the whole. This self-similar structure is characterized by fractal dimension which is the measure of how the aggregates fill the space (Gmachowski, 2014; Kinsner, 2005). Fractal dimension is a key parameter for the asphaltene flocculation model, not only because it appears in the reaction terms, but also because it is used to scale the measured floc diameters to the number of particles in the flocs.

Before introducing fractal dimension, first consider Euclidian dimensions. A mathematical description of dimension is based on how the "size" of an object behaves as the linear dimension increases. Consider a line segment as a one dimensional example. If the linear dimension of the

line segment is doubled, then based on the characteristic size, the length of the line has also doubled. In two dimensional objects such as a rectangle, if the linear dimensions are doubled, then the area increases by a factor of four. In three dimensional objects if the linear dimensions are doubled then the volume increases by a factor of eight. The relationship between dimension D, linear scaling R, and the resulting multiple increase in size or scaling factor, S_f, can be generalized as follows:

$$S_f = R^D \tag{5.5}$$

Classical Euclidean geometry explains objects in integer dimensions. However, many things in nature are described in non-integer dimensions, such as clouds, mountain ranges, and the stars in the sky. For example, a straight line has a dimension of one, but a fractal curve, depending on how much space it takes up as it curves and twists, has dimension between one and two. The term fractal is used to describe objects that cannot be described using normal Euclidean geometry. Fractals are characterized by a non-integer power law of dependence of the object length and Equation 5.5 can be generalized as follows:

$$S_f = R^{D_f} \tag{5.6}$$

Mass or number scaling as a method for characterizing the structure of flocs containing fine particles has received wide attention (Mullins and Sheu 1998). Figure 5.1 shows a floc of individual particles that can be enclosed in a spherical volume of diameter, d_m. The number of particles (or mass) within the floc can be related to the diameter of the floc as follows:

$$n_f \propto R^{Df} \tag{5.7}$$

where n_f is the number of individual particles in the floc. Here, the number of particles is equivalent to the scaling factor. Note, the mass and number fractal dimensions are the same regardless of whether the particles are monodispersed or polydispersed (Rastegari *et al.*, 2004). Any object that has a fractal structure has a mass fractal dimension between one and three. This is because the fractal dimension must be less than or equal to the dimension of the space in which the fractal exists, otherwise the space cannot contain the fractal.

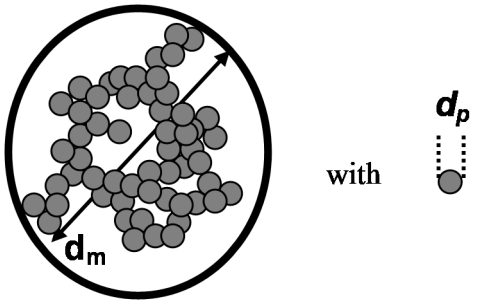

Figure 5.1: Schematic of a floc with fractal structure.

The number of particles in the floc scales to the floc diameter as follows:

$$n_f = \left(\frac{d_m}{d_p} \right)^{D_f} \tag{5.8}$$

where d_m is the spherical mean diameter of a floc, and d_p is the diameter of the individual particle. It follows from Equation 5.8 that the actual volume of the particles in the floc, V_{actual}, is given by:

$$V_{actual} = \frac{\pi}{6} \left(\frac{d_m}{d_p} \right)^{D_f} d_p^3 \tag{5.9}$$

The apparent volume occupied by the floc, as measured by a particle size analyzer, is given by:

$$V_{app} = \frac{\pi}{6} d_m^3 \tag{5.10}$$

Equations 5.9 and 5.10 will be used to interpret and model particle size distribution data for flocculating asphaltenes.

An interesting consequence of fractal mass scaling is that the density of the fractal object depends on its fractal dimension. The flocs become denser and more compact with increasing fractal dimensions, as shown in Table 5.1. One consequence of this dimensional relationship is that the fractal dimension can be estimated from the area projection of the floc. This is done by analyzing the micrographs of the flocs. The two dimensional fractal dimension, D_{f2}, can be determined from the perimeter and the surface area of the flocs as follows:

$$A = P^{2/D_{f2}} \tag{5.11}$$

where A is surface area and P is perimeter

Table 5.1: Mass fractal dimension of a floc.

Fractal Structure	# of individual Particles, n_f	Fractal Dimension, D_f	Volume actual/ Volume Measured $V_{actual}/V_{measured}$
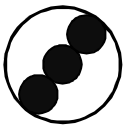	3	1.00	0.11
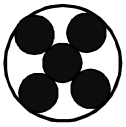	5	1.47	0.19
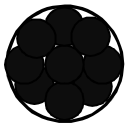	9	2.00	0.33
	1	3.00	1.00

5.4 Computer Flow Chart to Solve Population Balance Equation

There is no analytical solution to the population balance with both flocculation and disintegration reaction terms. Therefore, the Explicit Euler method numerical method is employed to obtain the particle size distribution as a function of time using Matlab^{TM} (Matlab^{TM}, 2014). The algorithm used to calculate the distribution of particles per floc is provided in Figure 5.5.

The inputs to the model are the initial particle size distribution, the fractal dimension (D_f), the coefficients (k_f and k_s) and exponents (λ and β) for the two reaction terms, and the upper limit for the number of particles per floc (N). The values of λ and β were set to the midpoint of their permitted intervals, 2.5 and 1.5, and were not adjusted. The effect of adjusting λ and β is similar to changing the k_f/k_s ratios. Hence, the model has three adjustable parameters, k_f , k_s, and D_f. An initial time step of 0.01 is also specified. The time step associated with Euler method is set to ensure that total number of primary asphaltene particles remains constant during asphaltene flocculation. The numerical error from too large a time step results in an error in total concentration of individual particles.

In diluted bitumen systems, the largest floc could contain up to 1,200,000 individual particles at a fractal dimension of 2.33, therefore the number of calculations required to perform a population balance of individual particles becomes exhaustive for a practical numerical solution. To reduce the computational time, the population balance is based on clusters of particles instead of individual particles. A cluster of size 841 particles with mean diameter of 18 microns was chosen to obtain simulation times less than 4 hours. The floc sizes ranged from 18 microns (1 cluster of 841 individual particles) to 396 microns (566 clusters and a total of 11,28,833 individual particles). In other words, the distribution of flocs was divided into 1344 bins so that the i^{th} bin contains i clusters of 841xi individual particles. The equations used to find the bin sizes, the number of bins, and the numbers of asphaltene primary particles of the bins are all presented in Appendix B.

At each iteration, the reaction terms are calculated from Equations 5.3 and 5.4 and the change in concentration of each floc size is determined from Equation 5.1. The concentrations are then updated using Euler's method:

$$C_k^{[n+1]} = C_k^{[n]} + \frac{\Delta C_k}{\Delta t}^{[n]} \tag{5.12}$$

where superscript [n] indicates the n^{th} time step. Once the distribution is updated, a material balance check is performed as follows:

$$MB_{err} = \left(\sum_{k=1}^{N} kC_k \right)^{[n]} - \left(\sum_{k=1}^{N} kC_k \right)^{[n-1]} \tag{5.13}$$

where MB_{err} is the material balance error at each time step. If the material balance error exceeds a 0.05 a smaller time step is selected and the iteration is repeated. When specified times are reached, the concentration and apparent volume distribution of the flocs over time is printed.

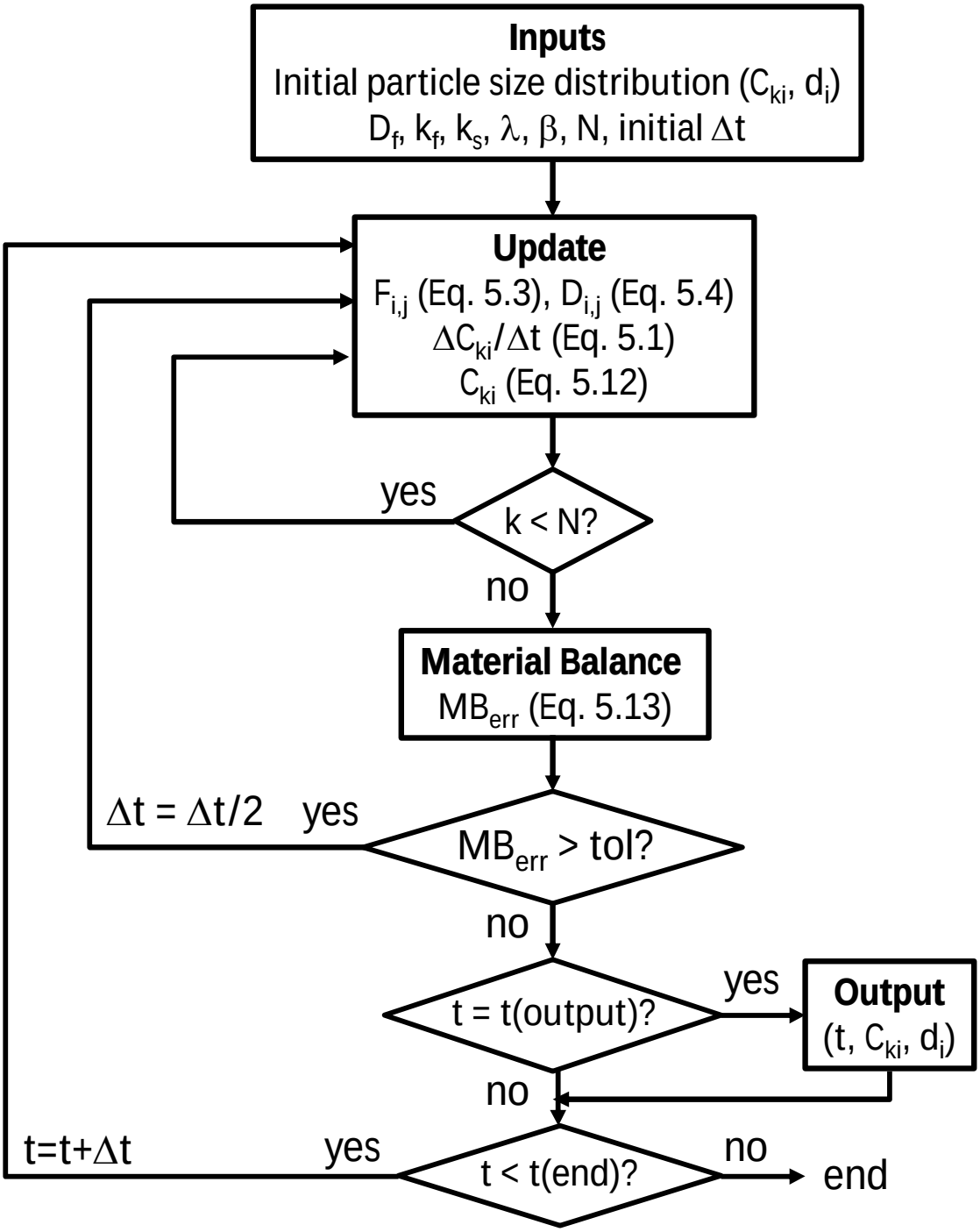

Figure 5.2: The algorithm used to calculate the distribution of particles per floc.

CHAPTER SIX: : ASPHALTENE FLOCCULATION RESULTS

This chapter presents the data collected to investigate the kinetics of asphaltene flocculation. The initial objective of this work was to investigate the kinetics of asphaltene flocculation near the onset of precipitation. However, after conducting several experiments, it became apparent that the particle size analyzer could not detect the particle size distribution near the onset. Therefore, data were collected at several dilutions above the onset. The flocculation model presented in Chapter 5 was fitted to the data and the suitability of the model to predict the behaviour near the onset of precipitation was assessed.

The approaches taken to determine the detection limit of the particle size analyzer are presented. The effects of the solvent content, mixing scheme, and shear rate on the behaviour of the kinetics of asphaltene flocculation are discussed. The fractal structure and determination of the fractal dimension are described. Finally, model tuning and predictions for flocculation near the onset are presented.

6.1 Asphaltene Flocculation Measurements

6.1.1 Processing of Flocculation Data

A typical example of an asphaltene flocculation measurement is given in Figure 6.1. This figure shows the measured asphaltene floc number and volume frequency distributions for 87.5 wt% *n*-heptane in bitumen, using a two-stage mixing method with mixing speed of 195 rpm, and temperature of 23°C for 5 minutes and 30 minutes. The number distribution, Figure 6.1 a, is

required for modeling. The volume distribution, Figure 6.1 b, illustrates more clearly how the mass of the asphaltenes is distributed in the solution. In this example, the floc sizes range from 2 to 300 μm. In general, the shape of the distribution does not change significantly with time and similar distributions were observed at all of the conditions examined above the onset of asphaltene precipitation. Therefore, it was possible to use an average value, such as the volume mean diameter, when comparing flocculation at different conditions.

Figure 6.2 show the volume mean diameter and total number of flocs or agglomerates counted per second for the frequency distribution presented in Figure 6.1. Note, the number count per second does not provide an accurate particle count, but is useful for relative comparisons. The initial size distribution of the flocs depends on the heptane content as well as the mixing scheme used to combine the heptane and bitumen. The size distribution evolves over time until a steady state condition is achieved. In this case, a relatively small number of relatively large flocs are broken into smaller fragments. After approximately ten minutes, the volume mean diameter and number counts per second become constant indicating that steady state has been reached. As will be shown later, the steady state condition can be altered with a change in mixing speed. The evolution towards a steady state condition and dependence on shear rate is consistent with reversible asphaltene flocculation. Hence, for modeling purposes, flocculation must be combined with disintegration.

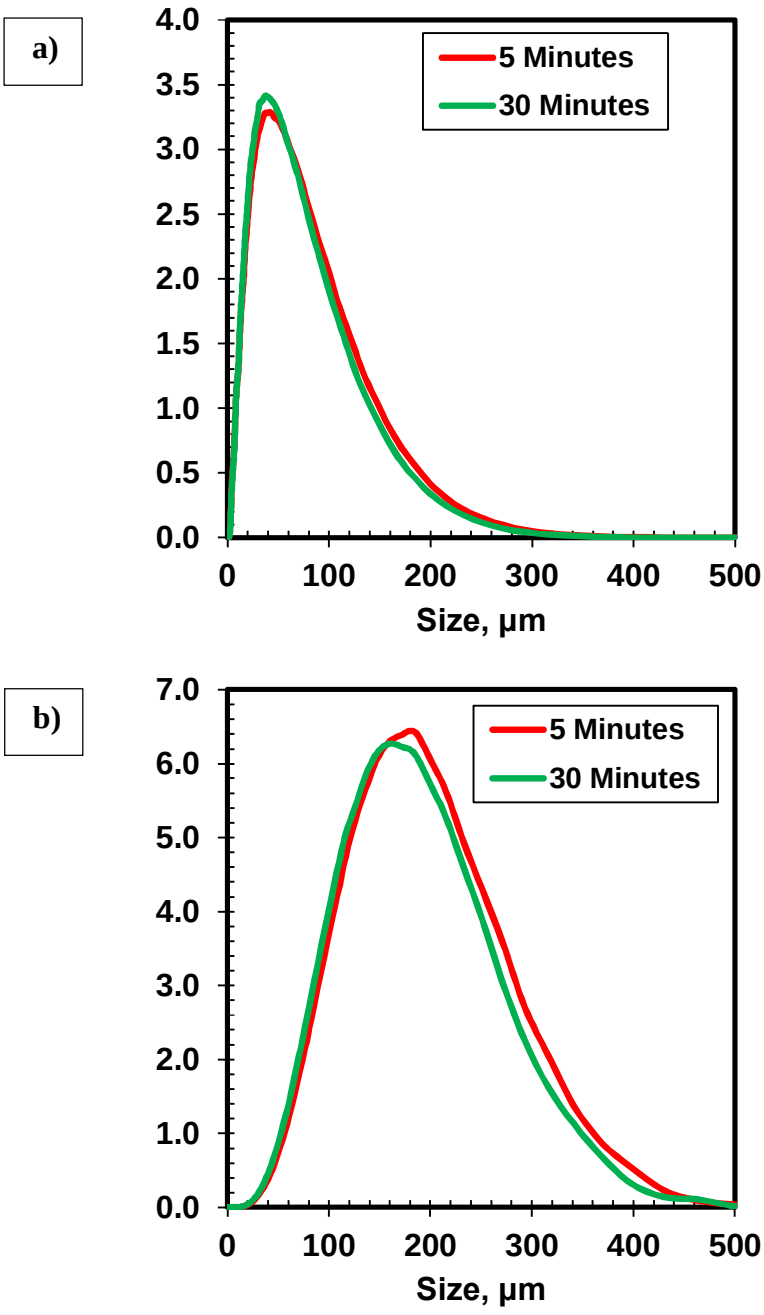

Figure 6.1: Measured asphaltene floc number (a) and volume frequency (b) distributions after 5 and 30 minutes for 87.5 wt% *n*-heptane diluted bitumen using two-stage mixing method at 195 rpm and 23°C.

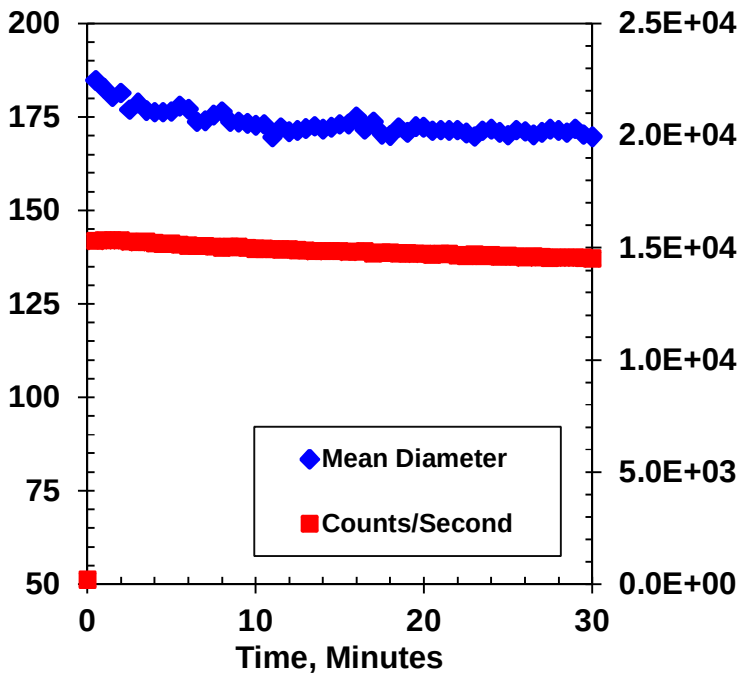

Figure 6.2: Volume mean diameter and number count of asphaltene flocculation over time from 87.5 wt% *n*-heptane diluted bitumen using the two-stage mixing method at a mixing speed of 195 rpm, and 23°C.

6.1.2 Flocculation Data near the Onset of Asphaltene Precipitation

As discussed in Chapter 4, the onset of asphaltene precipitation from *n*-heptane diluted bitumen was found to be 57.5 wt% *n*-heptane. Therefore, the particle size analyzer was first tested for a series of diluted bitumen samples with *n*-heptane contents from 54.5 to 95.5 wt%. First, consider the volume mean diameter and particle count for the samples at 61.5 and 65.0 wt% *n*-heptane, Figure 6.3. In both cases, the particle count is very low, 2 to 4 counts per second in contrast with a count of approximately 150,000 in the example shown in Figure 6.2. The volume mean diameter is 10 to 40 μm and shows no pattern over time. The low particle count and scattered mean diameter data suggest that noise has obscured any signal.

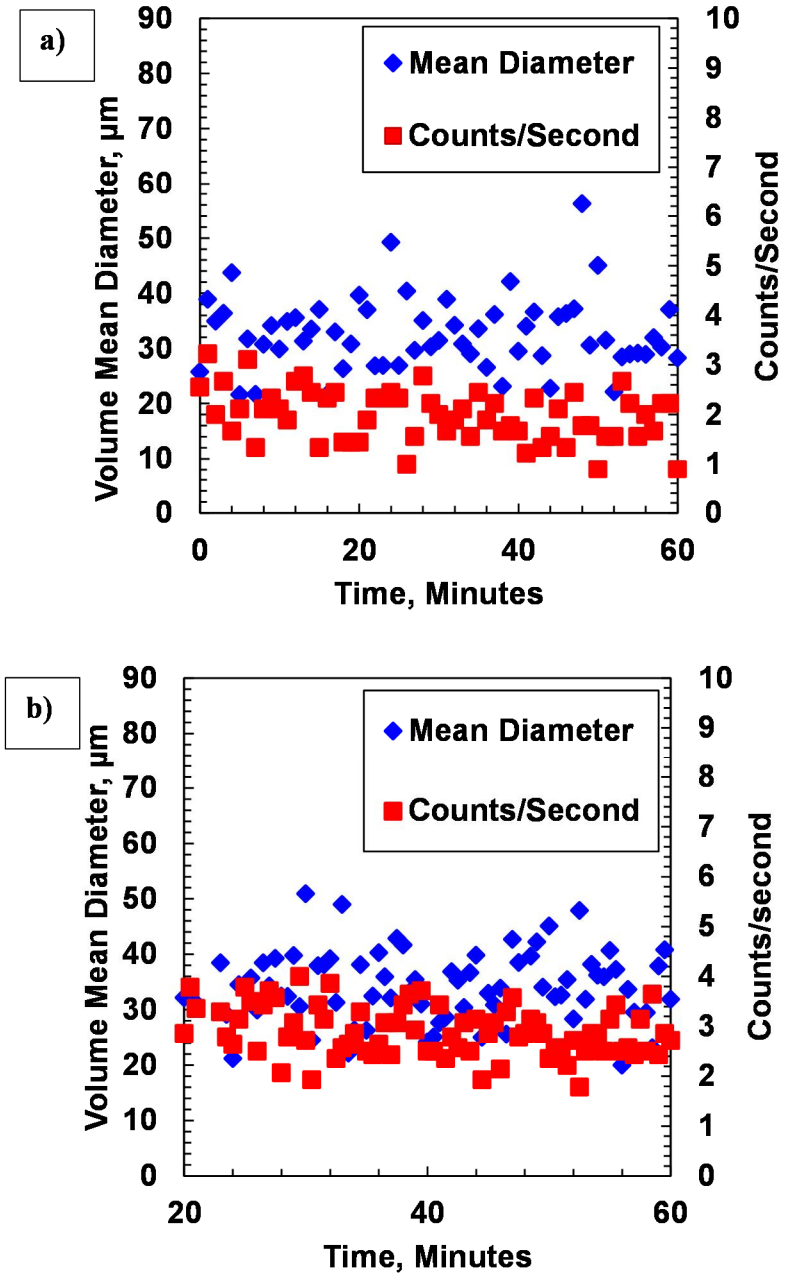

Figure 6.3: Kinetics of asphaltene flocculation at low dilutions of a) 61.5 wt% and b) 65 wt% *n*-heptane using two-stage mixing method at 195 rpm, and 23°C.

Now consider higher dilutions. Figure 6.4 compares the volume frequency distributions after 60 minutes at *n*-heptane contents ranging from 62.5 to 93.5 wt%. At 87.0, and 93.5 wt% *n*-heptane, a smooth approximately log normal is observed. As the *n*-heptane content decreases, spikes appear in the volume frequency distribution. The spikes suggest that noise has entered the signal. The question arises: at what *n*-heptane content does the error become significant?

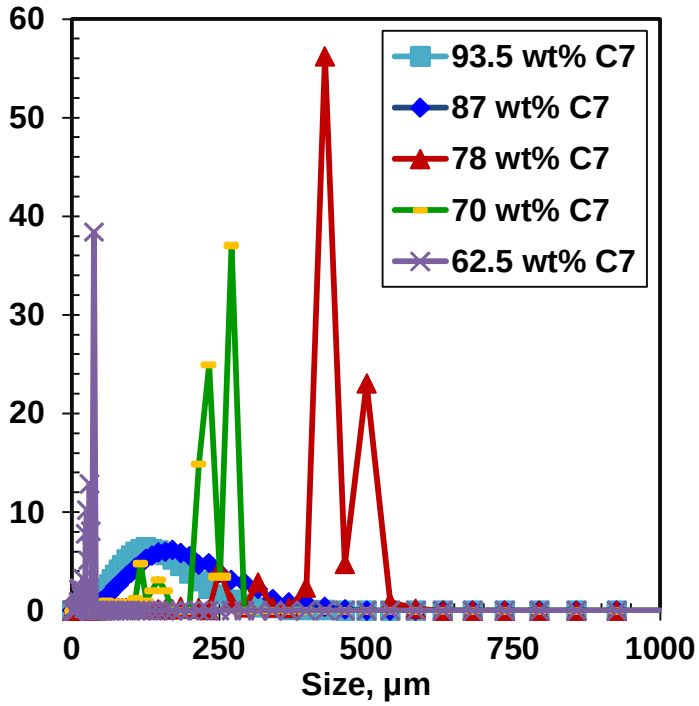

Figure 6.4: Measured volume frequency distribution for low and high *n*-heptane (C7) diluted bitumen after 60 minutes using two-stage mixing method at 195 rpm, and 23°C.

The changes in the diameter distribution and number counts with dilution provide a clue. The population balance model in Chapter 5 indicates that both the floc number count and the volume mean diameter are expected to correlate to the number concentration of the individual asphaltene particles. Hence, data that do not correlate with these trends are suspect. The mass concentrations of individual particles were calculated from the known yields at each dilution. The number

concentration of individual particles is expected to be proportional to the mass concentration assuming that the average particle diameter is insensitive to the *n*-heptane content. Figure 6.5 shows that the number concentration of individual particles increases from the onset to approximately 75 wt% *n*-heptane as more asphaltenes precipitate but then decreases at higher *n*-heptane concentrations as the effect of dilution dominates any increase in precipitation. Figure 6.5 a shows that the number count trend only matches the particle concentration trend above 87 wt% *n*-heptane. Figure 6.5 b shows that the volume mean diameter trend matches the particle concentration trend at and above 78 wt% *n*-heptane. Recall that the distributions at 78 wt% n-heptane were spiky and not log-normal. Therefore, only the data above 78 wt% the data were considered acceptable for analysis.

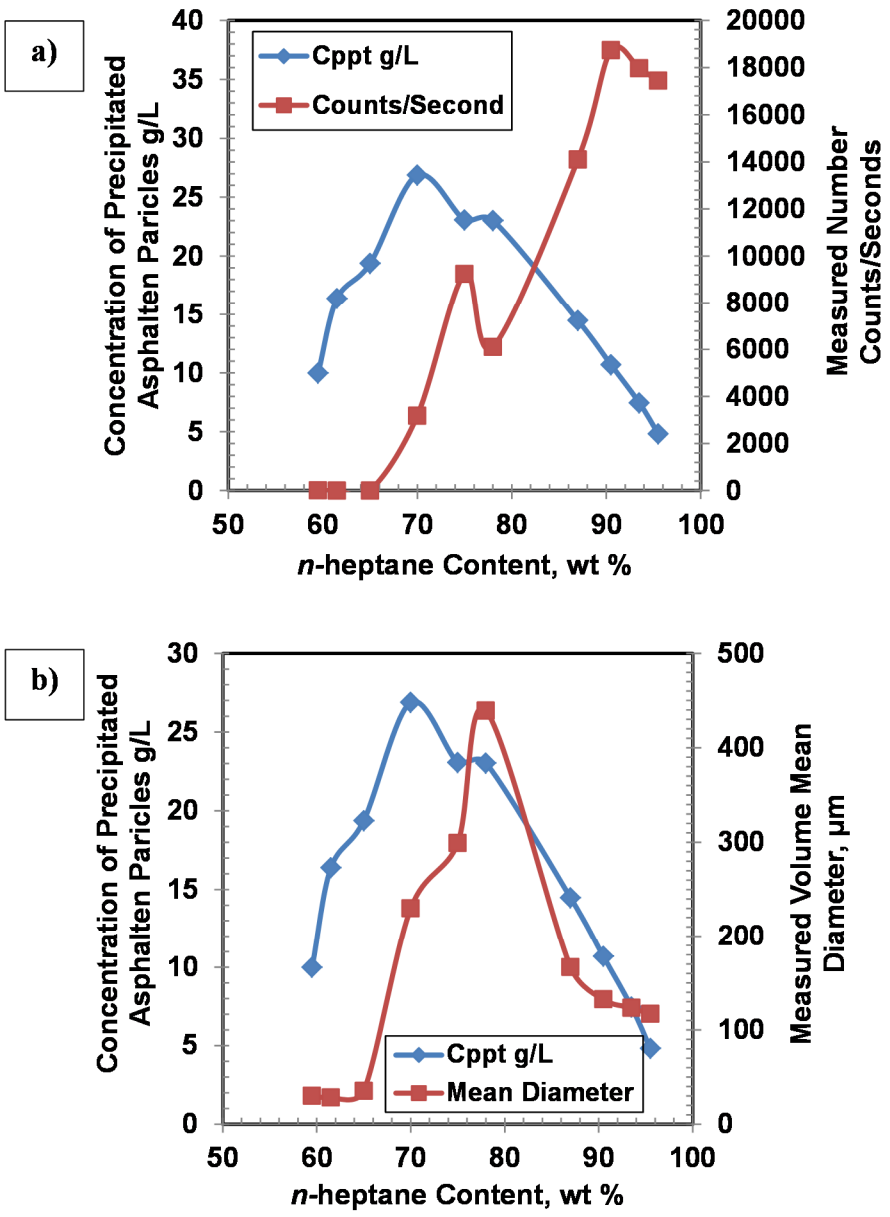

Figure 6.5: Comparison of measured number count (a) and measured volume mean diameter (b) with concentration of precipitated asphaltenes based on the yield data for 24 hours presented in Chapter 4 at 23^{o}C.

Possible reasons for the loss of signal at low dilution are: a low particle concentration, deposition, and sedimentation and opacity of the fluid. Since the mixtures were well stirred and

no sediment was observed during the experiments, sedimentation is ruled out. At first glance the most obvious explanation is a low particle count which must decrease near the onset as shown in Figure 6.5 a. However, the calculated particle concentrations at 61.5 and 95.5 wt% n-heptane are similar and yet the distribution could only be measured at the high dilution. Therefore, the problem at low dilution is not too few individual particles.

It is possible that there is much more significant flocculation at the low dilution resulting in a small number of very large flocs. To address this question, samples were taken from the 61.5 and 87.5 wt% *n*-heptane solutions and examined with an optical microscope, Figure 6.6. The micrographs confirm that there are a significant number of visible particles at both dilutions. The flocs are somewhat larger at higher dilutions but there are no other significant differences. Therefore, the detection problem at low dilution is not related to the particle count.

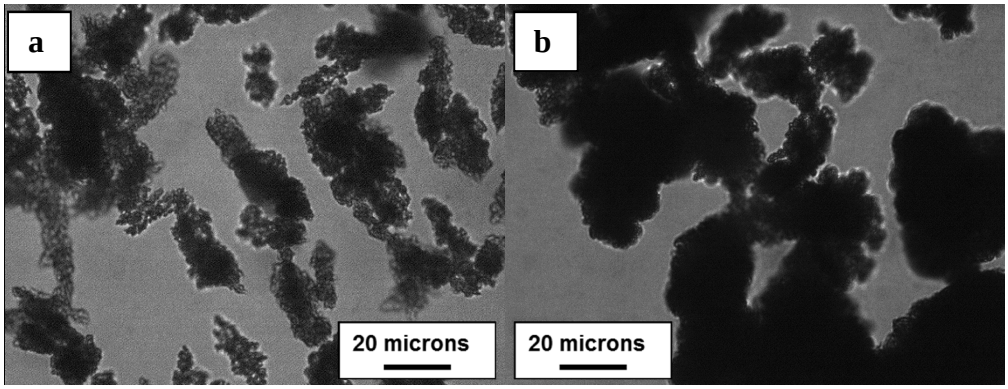

Figure 6.6: Micrographs showing a high volume of visible particles at both a) 61.5 and b) 87.5 wt% *n*-heptane at 23°C.

An examination of the 61.5 wt% data over longer times, as long as 1000 hours, revealed that deposition can be an issue. Figure 6.7 shows that the particle count and mean diameter suddenly

increased after approximately 200 hours. This sudden change is inconsistent with all other measurements of asphaltene flocculation. Therefore, the experiment was repeated but, this time, after a hundred hours, the beaker was removed and the probe from the analyzer was examined. Chunks of agglomerated asphaltene particles were observed on the probe window and the impeller. It appears that at low dilutions the asphaltenes stick to the impellers. This material may occasionally detach and cause a random spike in the measured distributions. The asphaltenes may also stick to the probe window causing a more systematic error.

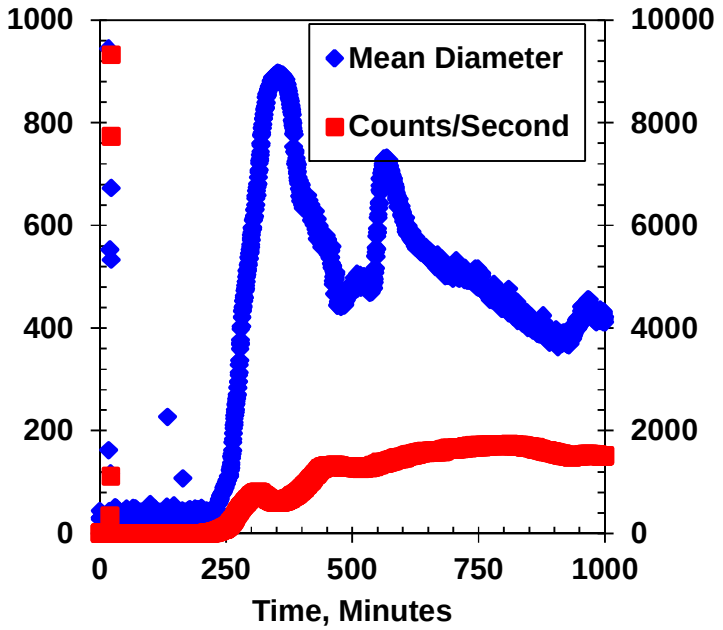

Figure 6.7: Volume mean diameter and particle count measurements at longer time for 61.5 wt% *n*-heptane, using two-stage mixing method at 195 rpm, and 23^{o}C.

Deposition happens at the onset and can explain the random spikes in the volume frequency distributions at low dilution; however, it does not explain the lack of a signal at early time intervals. The most likely explanation for this occurrence is the opacity of the fluid. The effect of

opacity of the fluid was tested by diluting the bitumen with toluene at a 1:1 mass ratio of toluene to bitumen and then adding *n*-heptane. If opacity is a factor, a clear signal should be obtained at lower *n*-heptane content. Figure 6.8 shows the number counts and volume mean diameters for mixtures with 64.5 and 70 wt% *n*-heptane. No meaningful signal was obtained at 64.5 wt% but the data at 70 wt% *n*-heptane appear to be valid. In other words, dilution with toluene allowed data to be collected as low as 70 wt% *n*-heptane compared with above 78 wt% without toluene. Hence, it appears that both the opacity of the fluid and the stickiness of the asphaltene particles result in an unreliable measurement at low dilution. For unadulterated bitumen, only measurements above 78.0 wt% *n*-heptane were evaluated further.

Note the onset of asphaltene precipitation will occur at higher *n*-heptane dilution when toluene is present. Toluene addition also allowed for measurement of the particle size distributions at lower *n*-heptane contents. Therefore, for future work, it is recommended to investigate near onset kinetics in toluene diluted bitumen.

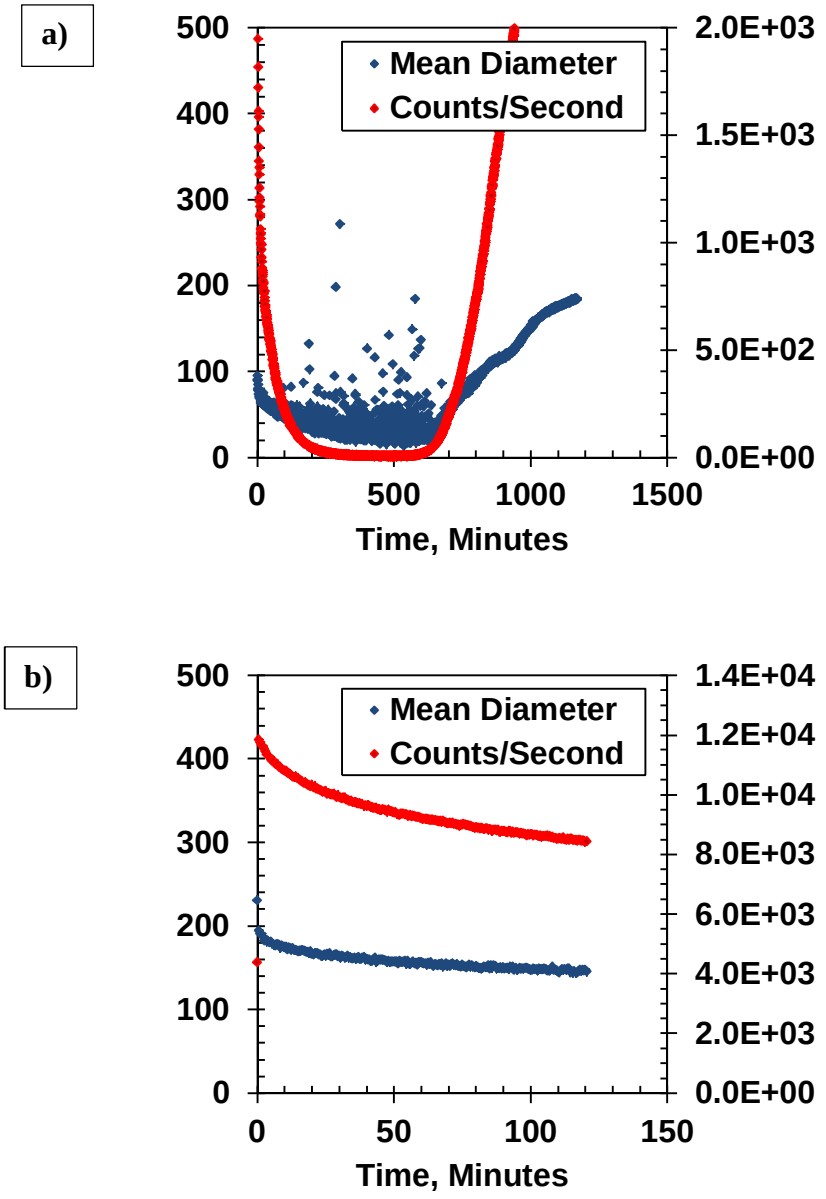

Figure 6.8: Volume mean diameter and particle count measurements at longer time for a) 64.5 wt% *n*-heptane and b) 70 wt% *n*-heptane in bitumen diluted with toluene at a 1:1 mass ratio (two-stage mixing method at 195 rpm, and 23^{o}C). Note: the two plots are not on the same scale.

6.1.3 Flocculation Data at High Dilution

In this section, the effects of dilution, type of mixing scheme, and shear rate on the kinetics of asphaltene flocculation are discussed in detail. Some of the data collected in this thesis are compared to the Daneshvar's work (2005).

Effect of Heptane Content

Figure 6.9 shows how the volume mean diameters and particle counts evolve over time for the experiments conducted at *n*-heptane contents from 85.5 to 95.5 wt% using the two-stage mixing method for mixing speed 195 rpm at 23^{o}C. The initial condition after adding the *n*-heptane is a relatively low number of relatively large flocs. Over time, the number of flocs increase and their mean diameter decreases. Several processes may be occurring simultaneously. First, precipitation continues for several hours as discussed in Chapter 4. Hence, the number or size of the primary particles increases over time. Most precipitation occurs in the first few minutes and the dramatic increase in particle count over the first 10 minutes likely includes the effect of increased precipitation. Second, flocculation and disaggregation take place until a steady state condition occurs. Third, some compaction of the flocs may occur during flocculation. The latter two processes are discussed later in the modeling section. Note, at 93.5 wt% *n*-heptane, the initial number count and volume mean diameter are lower than expected compared with the other cases. The reason for the different is not clear; it is possible that the initial distributions are more sensitive than expected to the procedure when adding the final batch of *n*-heptane such as the time taken to pour in the *n*-heptane and the exact timing for starting the mixer.

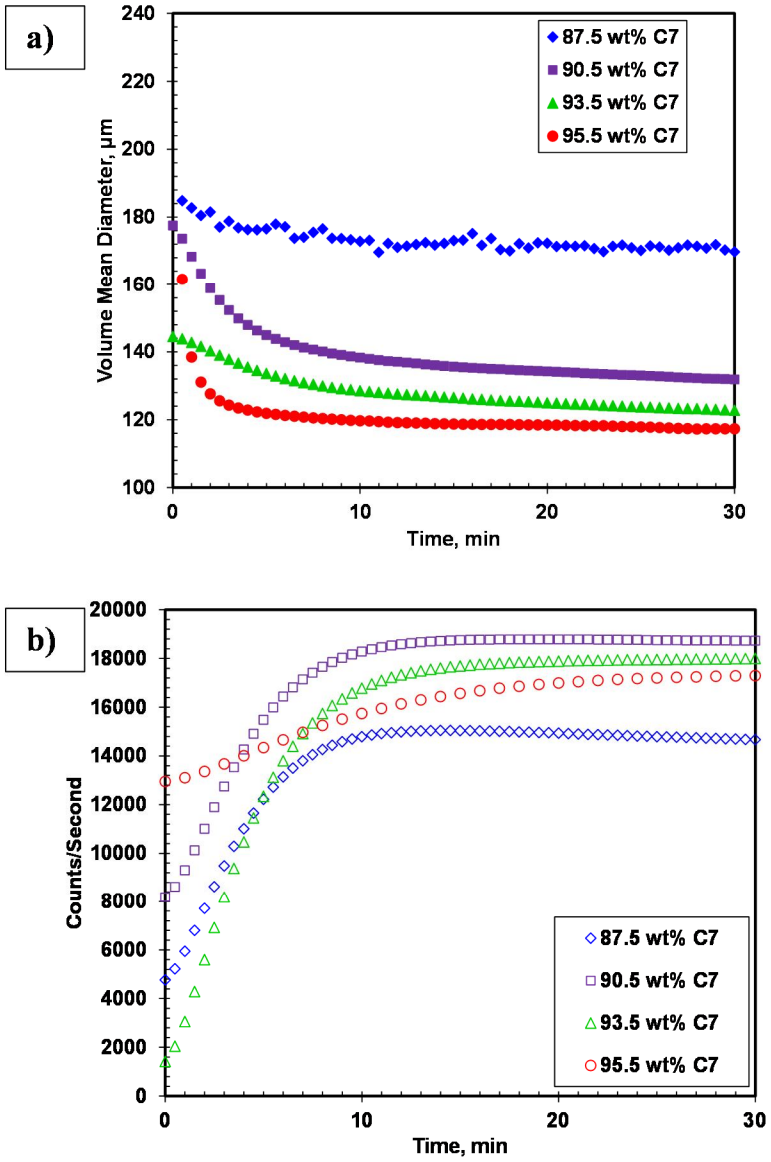

Figure 6.9: Kinetics of asphaltene flocculation for various *n*-heptane contents: (a) on the volume mean diameter and (b) the number count rate for two-stage mixing with a mixing speed of 195 rpm, 23°C.

Dilution can have opposing effects on the size and number of flocs. First, there are less individual particles at higher dilutions and both the average size and the total number of flocs will decrease if all else remains the same. In addition, higher heptane contents are expected to

increase the attractive forces between asphaltene particles which will promote greater flocculation and larger and therefore fewer flocs. On the other hand, the particles may be stickier at low dilution which would promote flocculation versus disaggregation. This effect would lead to fewer, larger flocs at lower dilutions.

Figure 6.10 compares the volume mean diameter if the same solutions after 30 minutes of mixing. At these dilutions, the volume mean diameter decreases as the *n*-heptane content increases. Daneshvar (2005) also observed a similar trend for the change in volume mean diameter with an increase in *n*-heptane content. The decrease in the volume diameter with greater dilution correlates with the decrease in individual particle concentrations that was shown in Figure 6.5.

Figure 6.10 also shows that measured number rate increases as the *n*-heptane content increases from 87.5 to 90.5 wt% and then decreases slightly at *n*-heptane content above 90.5wt%. In other words, the trend in the number of flocs does not exactly correlate with the trend in individual particle concentration. This discrepancy suggests that the flocculation and disaggregation rates do also depend on the solvent composition; that is, on the heptane content. These effects will be examined in more detail in the modeling section.

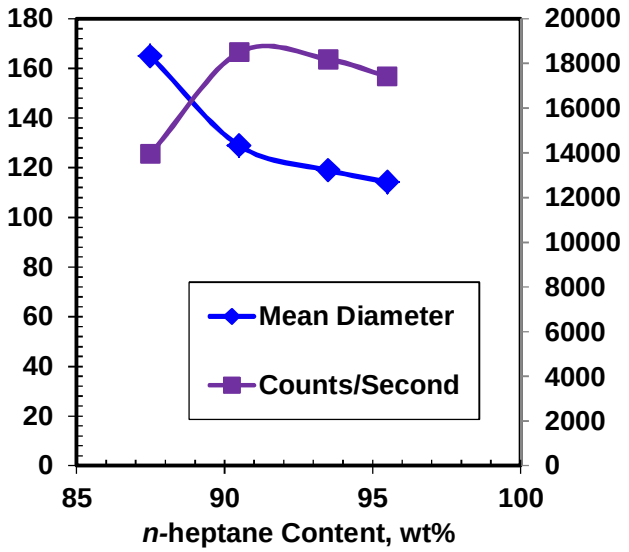

Figure 6.10: Effect of *n*-heptane content on the volume mean diameter and the number count rate after 30 minutes in the two-stage mixing method at 195 rpm, and 23°C.

Effect of Mixing Scheme

As discussed in Chapter 3, two different mixing schemes were employed to induce asphaltene flocculation. For one-stage mixing, all the diluent was added to the bitumen all at once and then the stirrer was turned on and the particle size measurement started. One-stage mixing is more representative of the industrial process. For two-stage mixing, the bitumen was premixed with solvent to a solvent content below the onset of asphaltene precipitation, but sufficient to reduce the viscosity to allow for rapid mixing (50 wt% *n*-heptane), and then the remainder of the diluent was added all at once to reach the final desired concentration of *n*-heptane. Two-stage mixing reduces the potential for artefacts related to poor mixing and therefore provides a better measure of the "true" flocculation kinetics.

The volume mean diameter and the number count rate for one-stage and two-stage mixing schemes for the dilutions of 87.5 and 90.5 wt% *n*-heptane are presented in Figure 6.11. As shown, one-stage mixing results in higher volume mean diameter both initially and at steady state. The steady state is also reached quite slowly, approximately after twenty minutes, whereas in two-stage mixing steady state is reached more rapidly, approximately after five minutes, as shown in Figure 6.12.

A possible explanation for the high initial volume mean diameter in one-stage mixing is the bitumen is not well mixed with the solvent. Therefore, the particle size analyzer is measuring both regions of unmixed fluid as well as asphaltene flocs. This difference would be expected to disappear over time as the solution becomes well mixed. The dramatic reduction in volume mean diameter over the first 10 minutes and the slower approach to steady state with the one stage mixing method are consistent with this explanation.

There are a number of possible explanations for the higher steady state volume mean diameters with one-stage versus two-stage mixing and they are outlined below:

1. The total number of asphaltene particles at a given dilution may depend on the mixing scheme. High local concentrations of solvent could force a higher than expected amount of precipitation. Asphaltene particles are difficult to redissolve once precipitated and there is a hysteresis between precipitation and redissolution (Beck *et al.*, 2005). Therefore, a larger number of individual particles would persist throughout the experiment. High local concentrations are more likely with one-stage mixing.

2. The size of the individual particles may differ with different mixing conditions. If their size differs, then the amount of particles will also differ for the same amount of precipitation. The steady state number and size of the flocs depends on both the size and number of individual particles.
3. The viscosity and solvent content of the local medium may affect how compact the flocs become leading to different fractal dimension and volume mean diameter. However, this effect would like disappear with time unless some aspects of flocculation are irreversible; for example, if particles begin to fuse over time.
4. The run times of 80 minutes may have been too short to reach steady state.

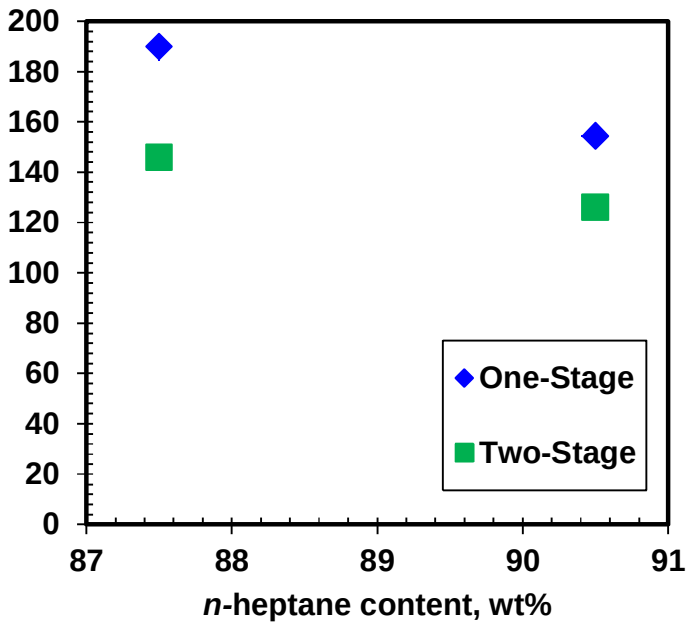

Figure 6.11: Effect of mixing scheme on the steady state volume mean diameter of asphaltene flocs after 30 minutes at 195 rpm and 23°C.

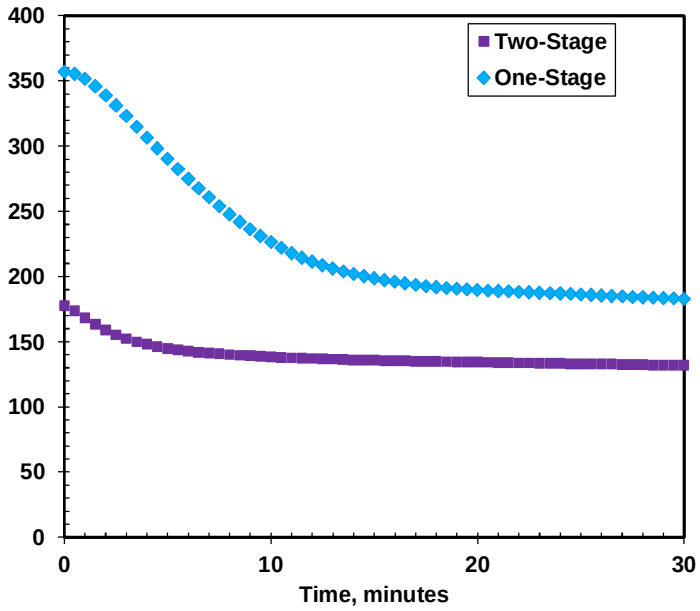

Figure 6.12: Effects of mixing scheme on the kinetics of asphaltene flocculation for 90.5 wt% *n*-heptane, at 195 rpm and 23°C.

Effect of Shear Rate

As discussed in Chapter 3, three different mixing speeds of 195, 275, and 330 rpm were used to study the effect of shear rate on the volume mean diameter and particle counts for 87.5 wt% *n*-heptane. Figure 6.13 shows the steady state volume mean diameter and number count rate versus mixing speed. The steady state volume mean diameter decreases with mixing speed while the number count remains increases slightly from 195 to 275 rpm mixing speeds and remains constant above 275 rpm.

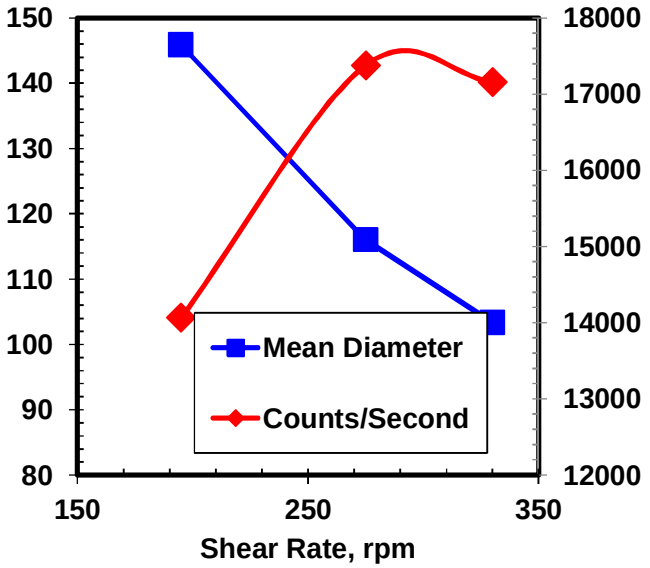

Figure 6.13: Effect of shear rate (mixing rate) on the steady state volume mean diameter and number count rate for 87.5 wt% *n*-heptane using two-stage mixing scheme at 23°C.

It appears that, overall, an increase in shear leads to restructuring of the flocs to become smaller and denser; that is; higher shear increases shattering over aggregation. However from 275 to 330 rpm, despite the decrease in the volume mean diameter with an increase in shear, the number count stays approximately constant. Rastegari *et al.*, (2004) and Daneshvar (2005) reported similar results observing constant number count at higher dilution ratios. This observation suggests that the asphaltene flocs may have different structures at different shear rates; that is, the fractal dimension of the asphaltene flocs is shear dependent.

6.2 Asphaltene Aggregate Fractal Dimension

The fractal dimension is a required input for the modeling approach used in this thesis. Daneshvar (2005) determined a lower limit of the fractal dimension based on the total volume occupied by the flocs as a function of the fractal dimension. In this study, fractal dimension is estimated using Daneshvar's approach coupled with image analysis of micrographs of settled flocs.

Daneshvar's approach begins with the relationship of the total volume of a distribution of flocs to their fractal dimension given by:

$$V_{total} = N_f \frac{\pi}{6} \sum_{i=1}^{N_f} f_i d_i^3 \tag{6.1}$$

where N_f is the total number of asphaltene flocs in mixture, f_i is the number frequency of the i^{th} floc, d_i is the measured diameter of the i^{th} floc. The total number of flocs can be determined from the mass of precipitated asphaltenes, m_A, as follows:

$$N_f = \frac{m_A}{\sum f_i m_i} \tag{6.2}$$

where m_i is the mass of the i^{th} floc. The mass of the i^{th} floc is given by:

$$m_i = \frac{\pi}{6} n_f d_p^3 \rho_A = \frac{\pi}{6} \left(\frac{d_i}{d_p} \right)^{D_f} d_p^3 \rho \tag{6.3}$$

where d_p is the diameter of an individual asphaltene, ρ_A is the asphaltene density of 1.2 g/cm³ (Yarranton and Masliyah, 1996), and D_f is the fractal dimension,. Therefore, the total number of flocs is given by:

$$N_f = \frac{m_A}{\frac{\pi}{6} d_P^{3-D_f} \rho_A \sum_i^{N_f} f_i d_i^{D_f}} \tag{6.4}$$

Equation 6.4 is substituted into Equation 6.1 to obtain:

$$V_{total} = \frac{m_A \sum_{i=1}^{N_f} f_i \left(\frac{d_i}{d_p} \right)^3}{\rho_A \sum_{i-1}^{D_f} f_i \left(\frac{d_i}{d_p} \right)^{D_f}} \tag{6.5}$$

The mass of precipitated asphaltenes and sediment volume fraction is known; therefore, the fractal dimension can be determined experimentally assuming that settling does not alter the fractal dimension of the flocs. Note, an inherent assumption when using fractal dimension is that the fractal dimension is independent of the floc size. Visual observation of settled asphaltenes at high dilutions indicates that the flocculated asphaltenes occupy no more than 25 to 35% of the solution volume. The average fractal dimension was calculated to be 2.3 ± 0.15.

The calculated fractal dimension was also determined using a microscopic technique. The two dimensional fractal dimension, D_{f2}, can be determined from the perimeter and the surface area of the flocs as follows and as shown in Figure 6.14:

$$A = P^{2/D_{f2}} \tag{6.6}$$

where A is surface area and P is perimeter. The measured areas and perimeters for 34 flocs are plotted on log-log coordinates, Figure 6.15, and a fractal dimension of 2.33 ±0.24 was found from the slope (D_f = 2/slope). Despite the assumptions that the two dimension fractal dimension is the same as the three dimensional fractal dimension and that settling has not altered the fractal dimension, the microscopic and sediment volume methods are in excellent agreement.

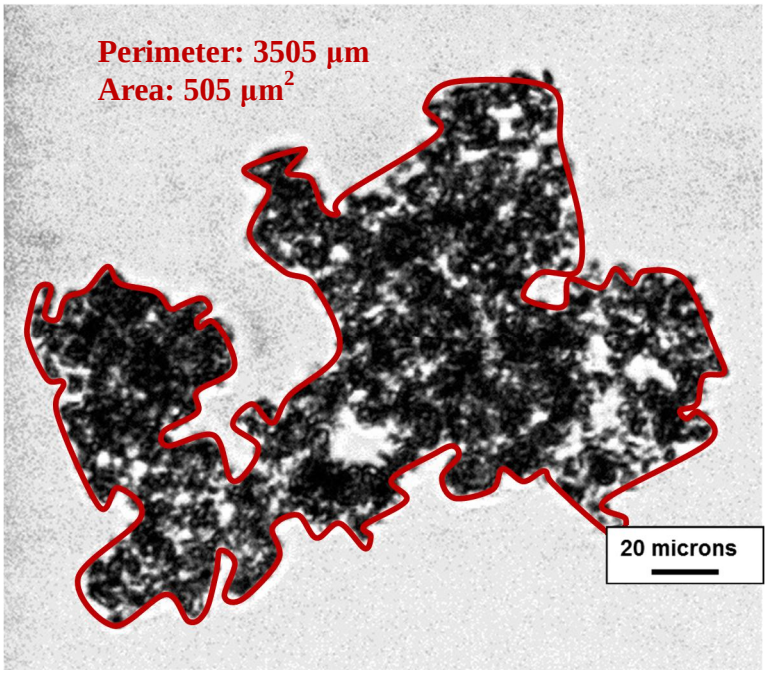

Figure 6.14: Micrograph of floc showing the area and perimeter used to determine the fractal dimension in 87.5 wt% *n*-heptane in bitumen at 23°C

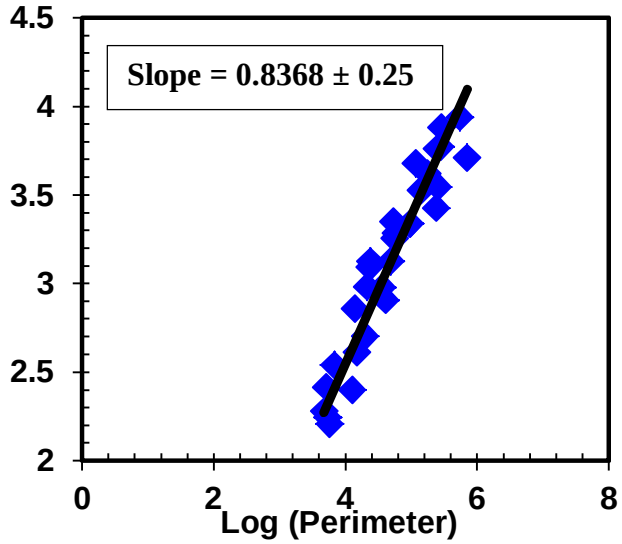

Figure 6.15: Determination of perimeter-based asphaltene aggregates fractal dimension from image analysis of flocs from 87.5 wt% *n*-heptane in bitumen at 23°C.

Note, the asphaltene fractal dimension may depend on the solvent type and content, which can affect the primary particle size and interparticle forces, as well as on shear rate. The fractal dimension could also change over time if the flocs become more or less compact over prolonged mixing. Figure 6.16 shows that the fractal dimension based on sediment volume decreases linearly with increasing *n*-heptane content and the trend was fitted with the following expression:

$$D_f = -0.028 w_H + 4.84 \quad (6.7)$$

where w_H is the mass fraction of *n*-heptane. The flocculation model will be evaluated with a constant fractal dimension of 2.33 and with the linear function of *n*-heptane content from Figure 6.16. It is assumed that the fractal dimension is constant for all flocs at all times and shear conditions.

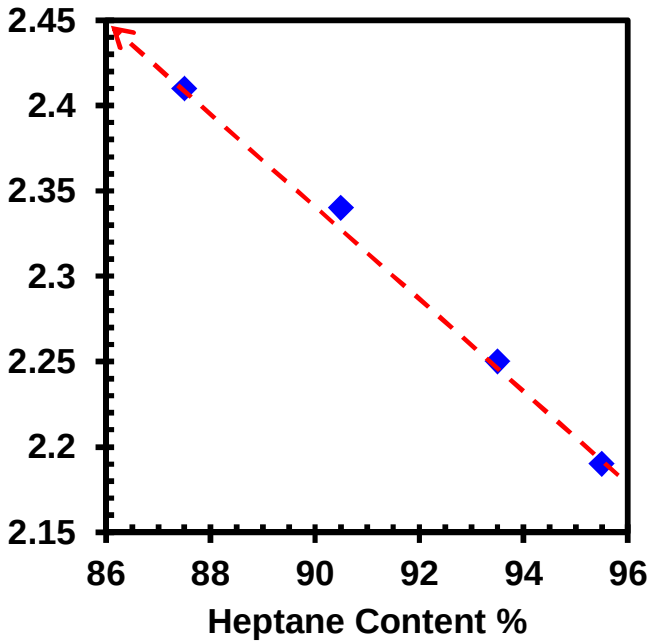

Figure 6.16: Fractal dimension determined based on sediment volume of 25% for dilutions of 87.5 to 95.5 wt% diluted in *n*-heptane.

6.3 Modeling of Asphaltene Flocculation

The flocculation data presented in section 6.1 is modeled using the population balance model as presented in Chapter 5. The effects of heptane content, shear rate, and mixing scheme on the model parameters will be discussed. The prediction of the kinetics near the onset of precipitation is assessed. Finally, a sensitivity analysis is performed on input parameters of the model.

6.3.1 Model Input

The inputs in the model are as followed: the initial floc size distribution obtained from the particle size analyzer at time zero, the fractal dimension of the flocs D_f, the reaction constants k_f and k_s, and the reaction exponents β and λ. The reaction exponents, β and λ, were set to the midpoint of their permitted intervals 1.5 and 2.5 respectively. Initially, the fractal dimension D_f was set to 2.33 and then with Equation 6.7, as discussed in Section 6.2. In the model, the reaction constants k_f and k_s will serve as the primary parameters utilized to match the experimental data.

As discussed in Chapter 5, the number of calculations required to perform a population balance of individual particles becomes exhaustive for a practical numerical solution. Hence, to reduce the computational time, the population balance equation was solved based on clusters of particles. A cluster of size of 841 particles (18 μm) was chosen to obtain simulation time less than 3 hours. The floc size ranged from 18 μm to 396 μm. Therefore, the distribution of flocs was divided into 1344 bins.

The initial particle size distribution was set to the first measured number size distribution which is approximately one minute after the initiation of flocculation. The distribution was converted to the distribution of bins. First, the floc diameters corresponding to the bin boundaries were calculated. Then, the number of flocs within these boundaries was determined using linear regression. The initial measured cumulative number frequency and the converted bin number frequency are compared in Figure 6.17. The initial bin cumulative number frequency distribution is an exact match to the initial cumulative number frequency with the following exceptions. By its definition, the model initial bin distribution cannot capture flocs less than 18 μm or flocs greater than 396 μm. The choice of the minimum floc size will be investigated further in Section 6.3.4.

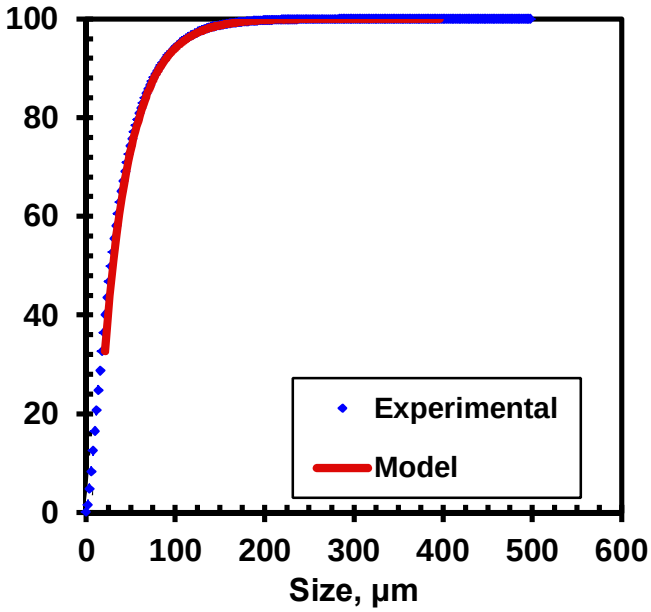

Figure 6.17: Comparison between measured and the converted initial bin cumulative number frequency for 87.5 wt% n-heptane using two-stage mixing method at 195 rpm, and 23°C.

6.3.2 Model Fitting – Constant D_f

To illustrate the modeling procedure, consider the case of 87.5 wt% *n*-heptane diluted bitumen using the two-stage mixing method and a mixing speed of 195 rpm at 23°C. First, the ratio of flocculation to disintegration reaction constants was adjusted to fit the steady state volume mean diameter. Then, the magnitude of both k_f and k_s were adjusted to match the kinetics of the flocculation (shape of the curve). The ratio and magnitude were then fine-tuned to obtain the final match as shown in Figure 6.18. The fitted model parameters are presented in Table 6.1. The model fit the experimental data with AARD of 1.1%.

Table 6.1: Parameters employed in each step to match the experimental volume mean diameter.

Parameter	Value
D_f	2.33
λ	2.5
β	1.5
k_f	3.11×10^{-15}
k_s	0.75×10^{-7}
k_f/k_s	4.15×10^{-8}

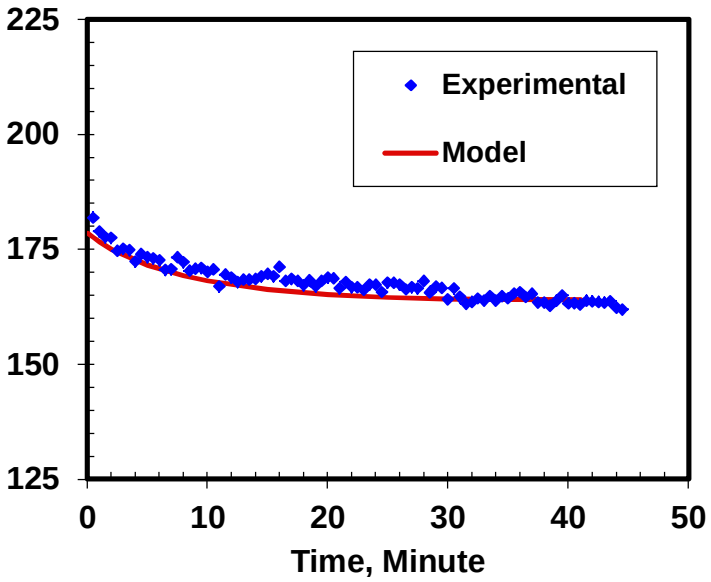

Figure 6.18: The fitted and experimental volume mean diameter for 87.5 wt% n-heptane using two-stage mixing method at 195 rpm, and 23^{o}C.

The model is able to capture the dynamics of volume mean diameter with time. However, at time zero, the model volume mean diameter doesn't quite match the experimental volume mean diameter. It was found that the volume mean diameter is sensitive to truncation of the particle number counts. After measurements, the experimental data are exported from the particle size analyzer software to excel. It appears that during this process the number frequency distribution is truncated by the software therefore the volume mean diameter used in the model are slightly lower than used in the software.

The results of the model and the experimental cumulative volume frequency distribution for the base case after 10 and 30 minutes are shown in Figure 6.19. The size intervals in the measured and predicted distributions are not the same; therefore, the cumulative size distributions are compared. It appears that the model underestimates the proportion of small flocs; this deviation

is partly attributed to the choice of lower limit cluster size of 18 μm in diameter. The effect of the minimum floc size on the predicted volume frequency is discussed in the sensitivity analysis, Section 6.3.4. The functional form chosen for the reaction kernals, Equation 5.3 and 5.4, may also cause the deviation.

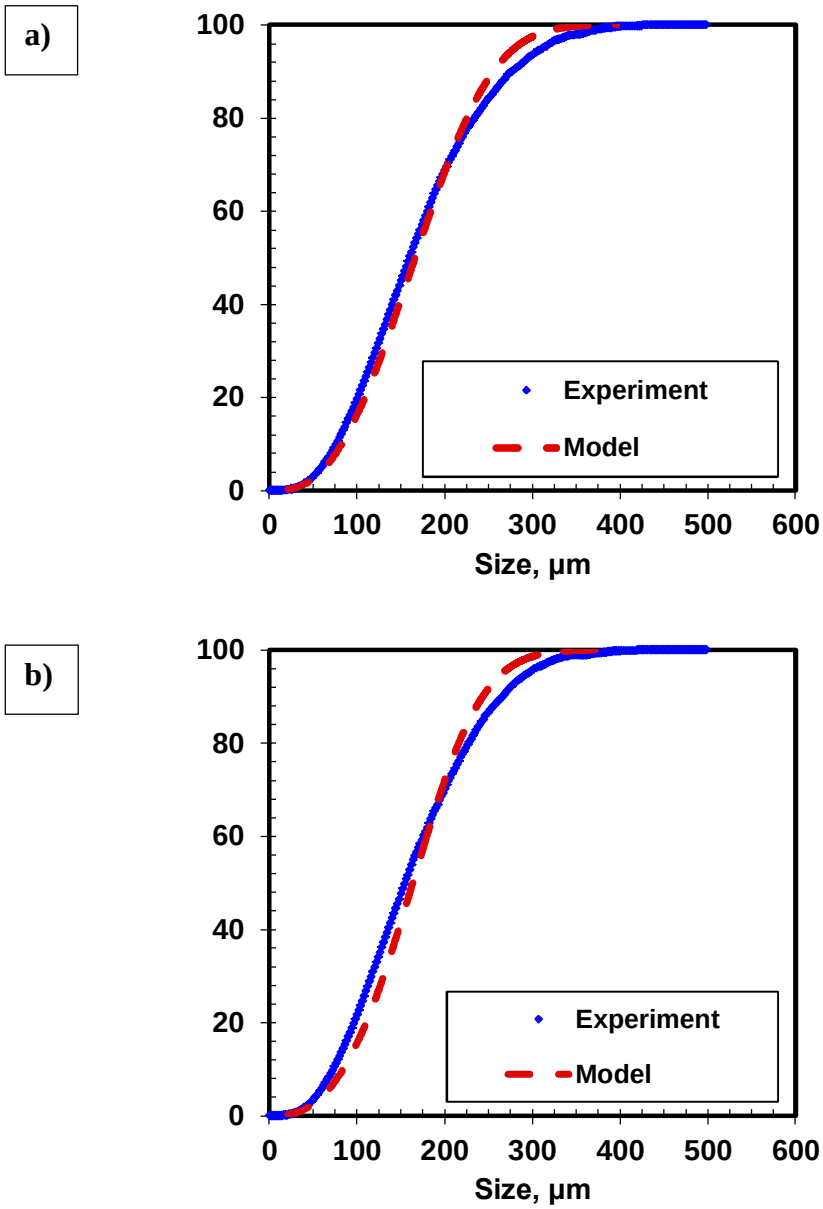

Figure 6.19: Predicted and experimental cumulative volume frequencies for the case study after: a) 10 minutes and b) 30 minutes.

6.3.3 Correlation of Model Parameters to n-Heptane Content – Constant D_f

As previously noted, the particle size analyzer could not detect the particle size distribution in unadulterated bitumen near the onset condition. Therefore, an attempt was made to extrapolate the model to estimate flocculation rates approaching the onset condition. To extrapolate the model, correlations of the model parameters must be developed. The first step is to fit the model to the data at different dilutions. The second step is to find a correlation of the fitted parameters to the *n*-heptane content, shear rate, and other parameters as required.

Step 1: Data Fitting

The data for each experimental condition were fitted as described in Section 6.3.2. The value of D_f, λ, and β were taken from Table 6.1 and only k_s and k_f/k_s ratio were adjusted. Figure 6.20 shows the fitted model (Case 1) for 87.5 to 95.5 wt% *n*-heptane diluted bitumen using the two-stage mixing method for the mixing speed of 195 rpm at 23^{o}C. The fitted model parameters are provided in Table 6.2. The model fit the experimental data with AARD of 1.1%.

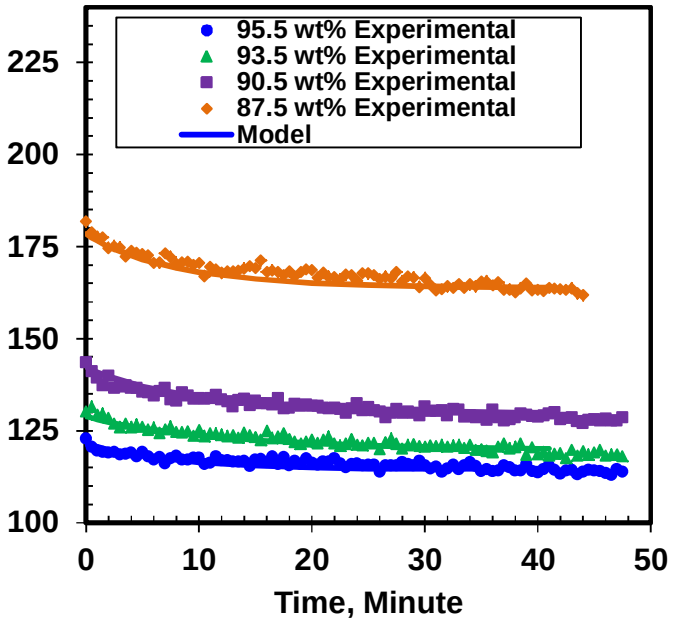

Figure 6.20: Case 1 model fitted to data for 87.5-95.5 wt% *n*-heptane diluted bitumen using the two-stage mixing method and a mixing speed of 195 rpm at 23°C**.**

Table 6.2: Fitted model parameters (Case 1) for n-heptane diluted bitumen with two-stage mixing method and a mixing speed of 195 rpm at 23°C.

Parameter	87 wt% C7	90.5 wt% C7	93.5 wt% C7	95.5 wt% C7
k_s	$0.75\ 10^{-7}$	$1.13\ 10^{-7}$	$1.02\ 10^{-7}$	$1.60\ 10^{-7}$
k_f/k_s	$4.15\ 10^{-8}$	$2.48\ 10^{-8}$	$2.90\ 10^{-8}$	$3.67\ 10^{-8}$

Step 2: Develop Correlation for Model Parameters

The value of k_s was similar for all dilutions, Table 6.2. Therefore, the k_s was set to a constant value of $1.13\ 10^{-7}$. Then, the model was fitted to the data by manipulating the ratio of k_f/k_s to match the steady state volume mean diameter (Case 2), Figure 6.21. The constant k_s model

matched the experimental data with AARD of 1.4%. There was little change in the fitted k_f/k_s values as shown in Figure 6.22.

There was more variation in the k_f/k_s values than the k_s values. Nonetheless, an attempt was made to model the data with a constant k_f/k_s value of $3.00\ 10^{-8}$ (Case 3). The constant k_f/k_s model fit the 90.5 to 95.5 wt% data with an AARD of 1.3%; however, it did not fit the 87.5 wt% data well, Figure 6.23. Instead, an average k_f/k_s value of $3.00\ 10^{-8}$ was used for *n*-heptane contents at or above 90.5 wt% n-heptane and the previously fitted value of $4.25\ 10^{-8}$at 87.5 wt% was used at that dilution (Case 4). In other words, it was assumed that from the onset of precipitation, the k_f/k_s value decreases with increasing *n*-heptane content but approaches an asymptote at approximately 90.5 wt% *n*-heptane. The Case 4 model fit the 87.5 to 95.5 wt% data with an AARD of 1.3%, Figure 6.24.

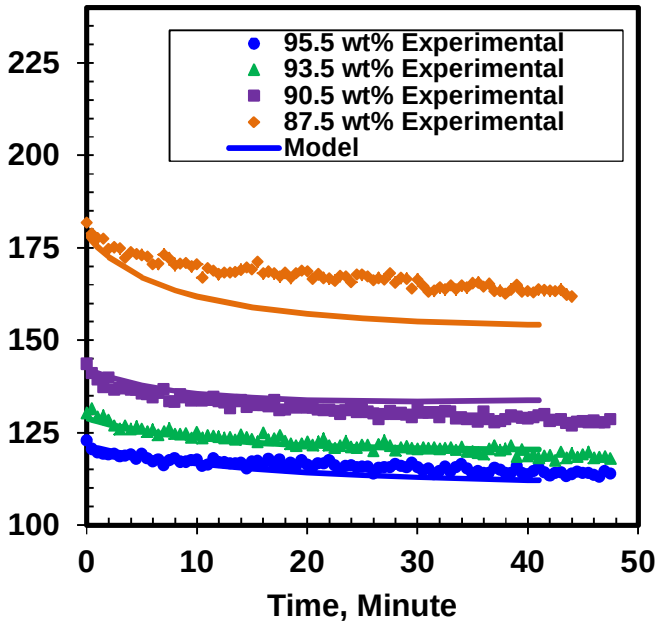

Figure 6.23: Case 3 (constant k_f/k_s ratio and k_s) model results for 87.5 to 95.5 wt% *n*-heptane diluted bitumen using the two-stage mixing method and mixing speed of 195 rpm at 23°C.

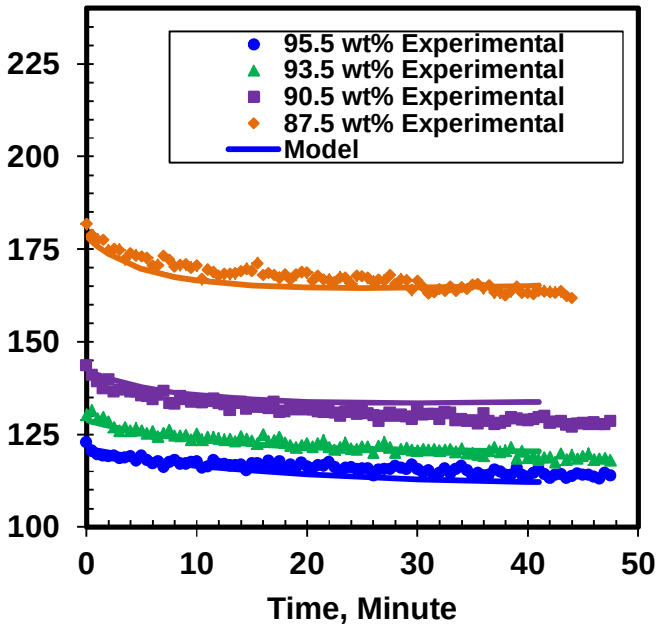

Figure 6.24: Case 4 (correlated k_f/k_s ratio and constant k_s) model results for 87.5 to 95.5 wt% *n*-heptane diluted bitumen using the two-stage mixing method and mixing speed of 195 rpm at 23°C.

The trend in the k_f/k_s ratios with *n*-heptane content is not conducive to finding a correlation to extrapolate to lower dilutions with confidence. Therefore, particle size distribution data from Daneshvar (2005) for Athabasca bitumen were also modeled using the Case 4 approach and compared with the Case 4 results for the WC_B02 bitumen used in this thesis, Figure 6.25. The same trends were observed for the Athabasca bitumen. The k_f/k_s ratio is constant at a value of 3.05 10^{-8} dilutions above 90 wt% n-heptane and increases at lower dilutions. The constant k_f/k_s values are within experimental error of each other.

Unfortunately, there are still insufficient data to determine the trend at lower dilutions and only a simple linear trend is examined here. A trendline with a slope of -4.2 10^{-09} 1/wt% for WC_B02 and -1.5 10^{-09} 1/wt% for Athabasca bitumen can be used to fit the k_f/k_s ratios at lower heptane content. The difference is significant. As an illustration, slopes from -6.7 10^{-09} to -1.7 10^{-09} 1/wt% were used to extrapolate the ratio for the WC_B02 at 87.5 wt% n-heptane, Figure 6.26 a. The model predictions using the extrapolated ratios are shown in Figure 6.26 b. The extrapolated volume mean diameters range from 160 to 175 μm. The uncertainty in the extrapolation will only increase at lower dilutions. It appears that data collected at high dilutions cannot be extrapolated with any confidence to the onset condition.

a)

b)

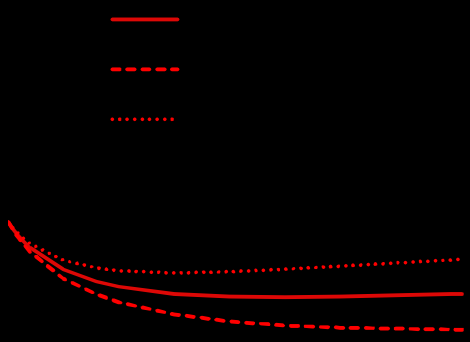

6.3.4 Model Fitting –D_f as Function of n-Heptane Content

The model was refitted following the same procedure described in Section 6.3.2 but using Equation 6.7 for the fractal dimension. The value of k_s was again set to a constant value of 1.13 10^{-7} and the model was fitted to the data by adjusting the ratio of k_f/k_s to match the steady state volume mean diameter. The model fit the 87.5 to 95.5 wt% data with an AARD of 1.9%, Figure 6.27. The fitted k_f/k_s values are shown in Figure 6.28.

The trend of the k_f/k_s ratios with *n*-heptane content now follows an exponential relationship. Extrapolation of the exponential relationship to the onset condition is still questionable. For example, the predicted k_f/k_s ratio at the onset composition of 57.5 wt% *n*-heptane is 7.0 10^{-5}, 900 times greater than the highest fitted value. Furthermore, the predicted shape for the volume frequency distribution curve becomes less accurate, Figure 6.29. Therefore, the constant fractal dimension model was used to examine the effect of shear rate and for the sensitivity analysis.

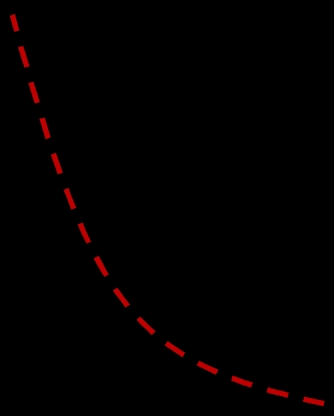

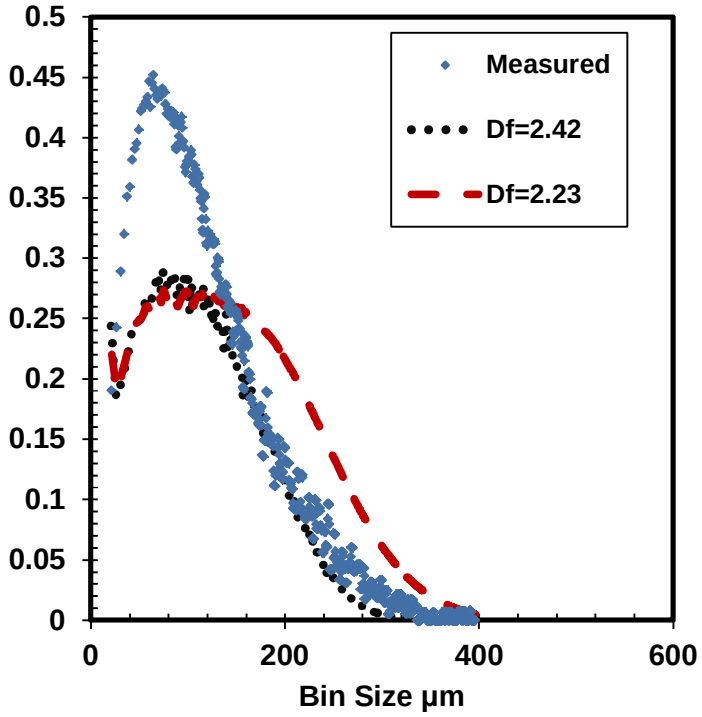

Figure 6.29: Effect of adjusting D_f on the volume frequency distribution for 87.5 wt% *n*-heptane diluted bitumen using the two-stage mixing method and a mixing speed of 195 rpm at 23°C.

6.3.5 Effect of Shear Conditions – Constant D_f

This section investigates the effects of shear rate on the k_f/k_s ratio at various heptane contents. Shear rates and Reynolds numbers were reported in Table 3.2. Figure 6.30 a plots the k_f/k_s ratio versus the Reynolds number (Re) at each dilution ratio and mixing speed. Figure 6.30 b shows that the same trends are observed for both Athabasca and WC_B02 bitumen. The k_f/k_s ratio appears to decrease with increasing Reynolds number up to a Reynolds number of 12000 above which the ratio becomes constant. In general, increasing shear is expected to increase shattering rates relative to flocculation rates.

For mixing vessels, Re < 10 corresponds to laminar flow, while Re > 10000 corresponds to turbulent flow (McCabe *et al.,* 2005; Nere *et al.,* 2003). The transition region lies between Re of 1000 and 10000. Figure 6.30 a shows that the transition to a constant value appears to correlate to the transition to fully turbulent flow. The plateau in turbulent regime indicates that, once turbulence is established, increasing the mixing speed does not alter the local shear conditions experienced by the particles.

There is an outlier at 95.5wt% n-heptane and the reason for the outlier is unknown. It is possible that increasing *n*-heptane content increases the attractive forces between the particles and therefore increases the flocculation rate. The increase in attractive forces would oppose the shear effect.

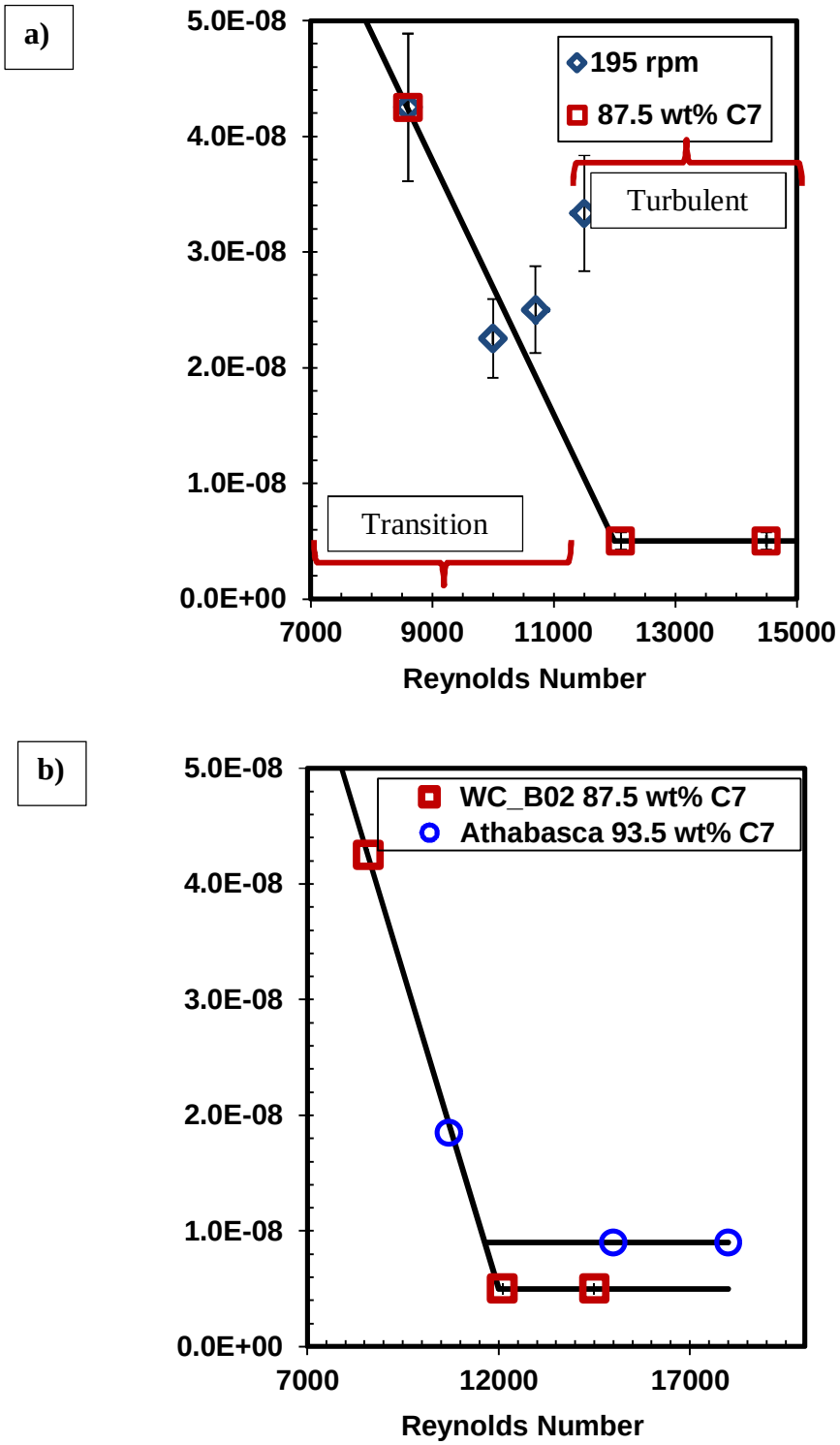

Figure 6.30: Summary of k_f/k_s ratio for a) 87.5-95.5 wt% at 195 rpm and 87.5 wt% at different shear, b) comparison of two bitumen, WC_B02 and Athabasca.

6.3.6 Sensitivity to Model Parameters – Constant D_f

The effect of the input parameters k_s, β, λ, and D_f as well as the bin size distribution on the predicted volume mean diameter are presented. The sensitivities were performed on the 87.5 wt% *n*-heptane in bitumen using the two-stage mixing method and mixing speed of 195 rpm at 23°C case. The base input parameters for this case were provided in Table 6.1. The following sensitivities were examined: k_sx2 and k_s/2, β ±0.1, λ ±0.1, and D_f ±0.12.

Disintegration Constant, k_s

The effect of adjusting disintegration reaction constant, k_s, on the predicted steady state condition is similar to adjusting the k_f/k_s ratio, Figure 6.31. However, the magnitude of k_s also affects the kinetics of flocculation (the shape of the curves in Figure 6.31 a). As expected, increasing k_s by factor of two decreases the volume mean diameter and increases the floc number count. Increasing k_s also leads to a more rapid approach to the steady state although it is difficult to see in Figure 6.31 because the difference between the initial and steady state condition is also a factor. Figure 6.32 shows that the volume frequency distributions are broader for higher volume mean diameters but there is no other significant change in their shape.

Reaction Kernel Exponents, β and λ

The effects of adjusting β and λ were similar to that of changing the k_f/k_s ratio, as shown in Figure 6.33 to 6.34. Therefore, there is likely little advantage in further tuning the model fits using the reaction exponents.

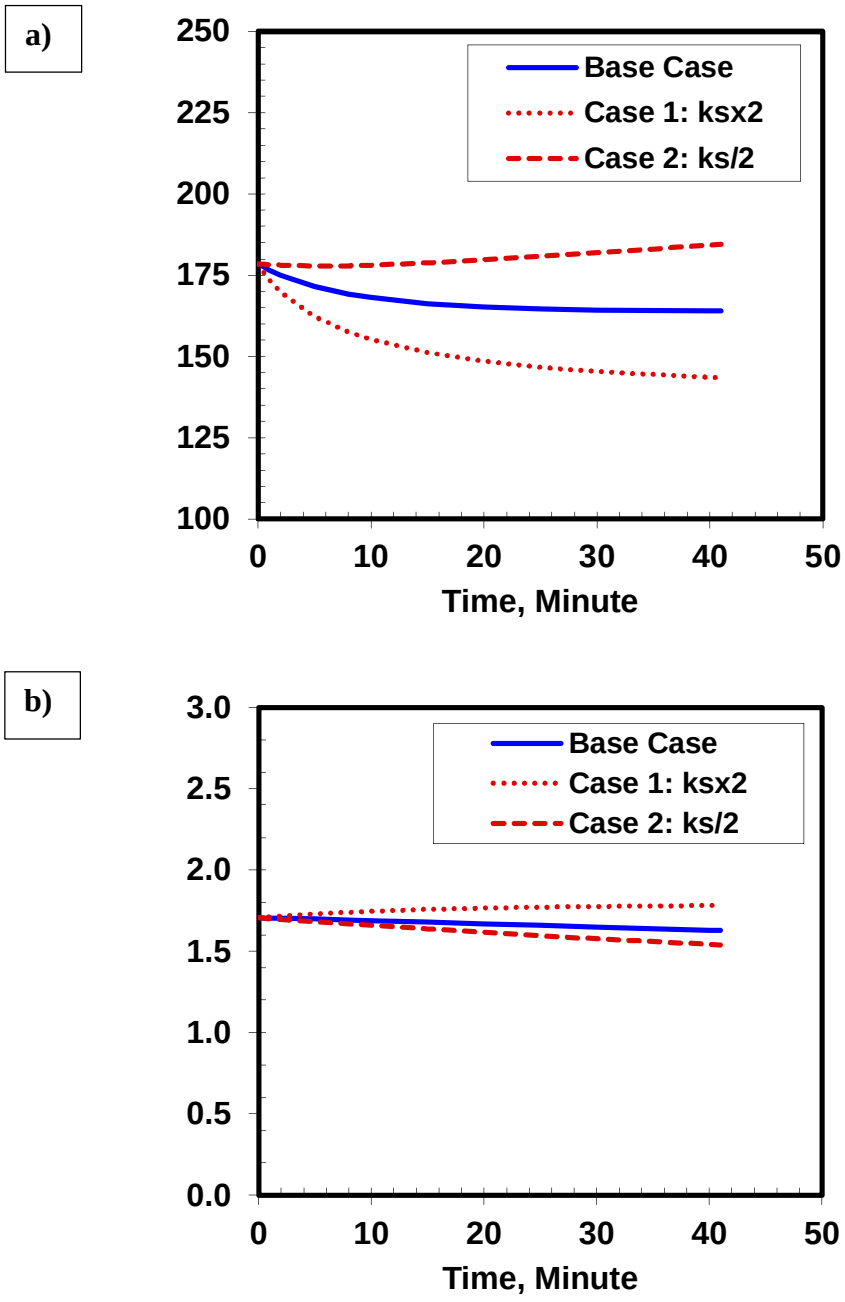

Figure 6.31: Effect of k_s on the predicted a) volume mean diameter and b) number counts.

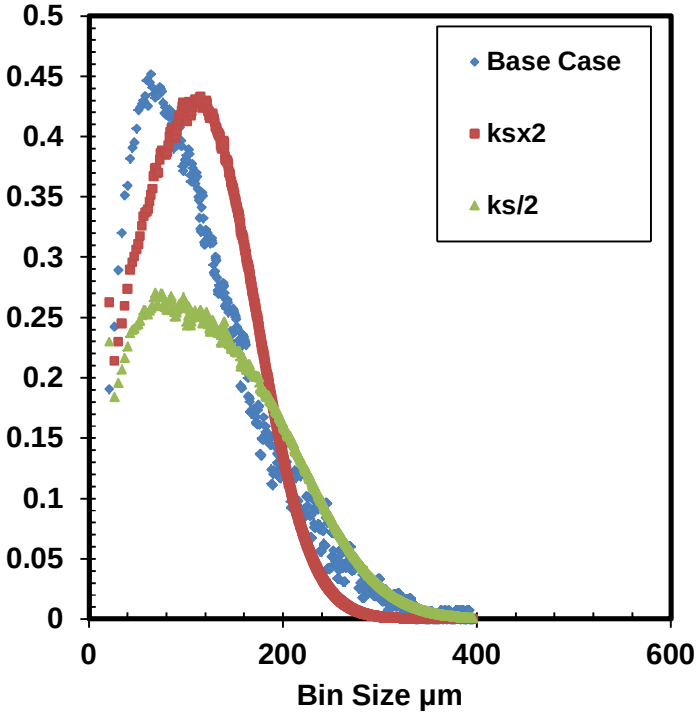

Figure 6.32: Effect of adjusting a) k_s and b) β on the volume frequency distribution.

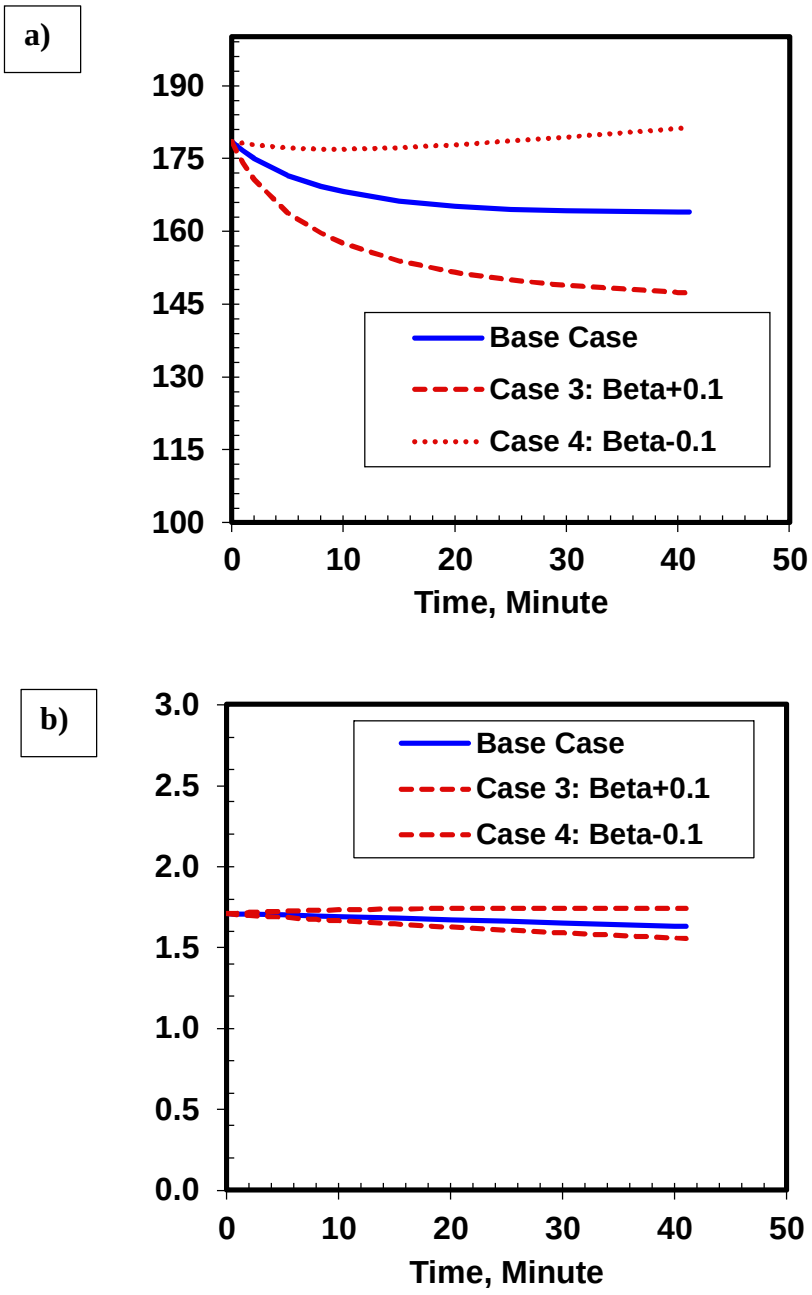

Figure 6.33: Effect of disintegration reaction exponent on the predicted a) volume mean diameter and b) number counts**.**

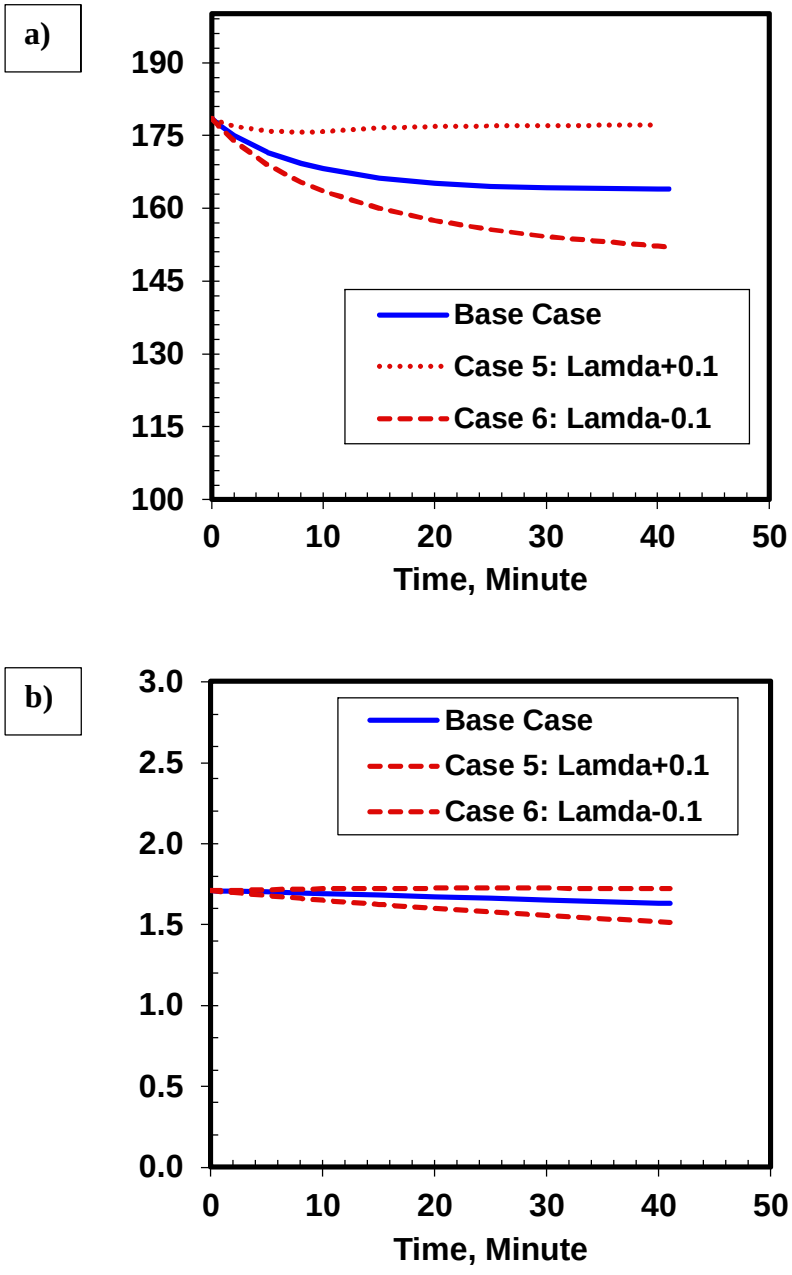

Figure 6.34: Effect of flocculation reaction exponent on the predicted a) volume mean diameter and b) number counts.

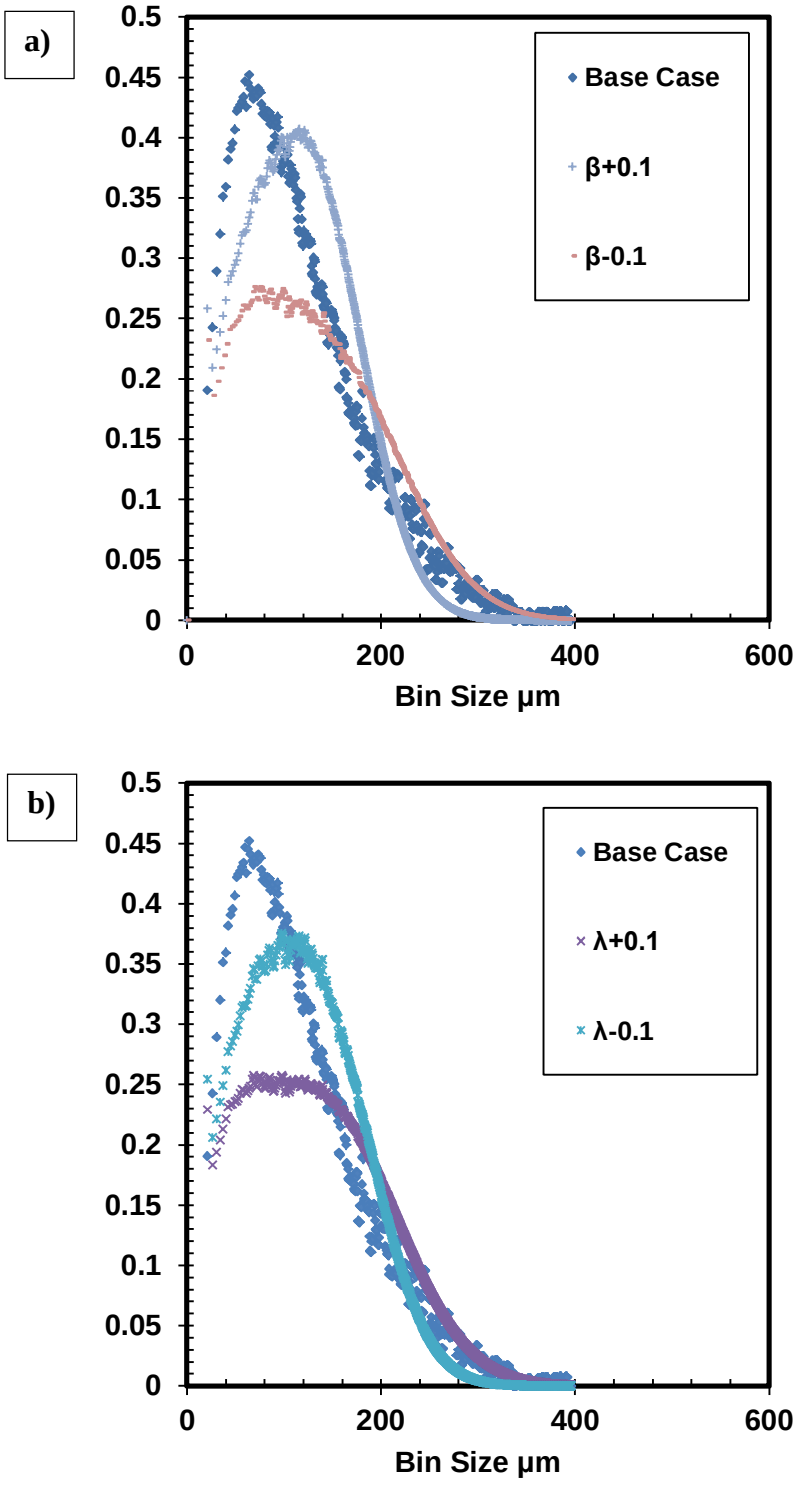

Figure 6.35: Effect of adjusting a) β and b) λ on the volume frequency distribution.

Fractal Dimension, D_f

The fractal dimension can potentially have a large impact on the model predictions. However, the fractal dimension can be constrained to a small range. Recall, that the sediment volume of the settled flocs is very sensitive to fractal dimension. For example, an increase of the fractal dimension, D_f, from 2.33 to 2.45 decreases the sediment volume from 35% to 25%. Therefore, the sensitivity analysis was restricted to ±0.12. As expected, decreasing the fractal dimension increases the number and size of the flocs, Figure 6.36. As noted previously, changing the fractal dimension significantly alters the shape of the distributions, Figure 6.37. At lower fractal dimension, the same number of particles gives a larger floc volume and the distribution tends to become broad and flat. At higher fractal dimension, there are fewer but more compact flocs giving a narrower distribution.

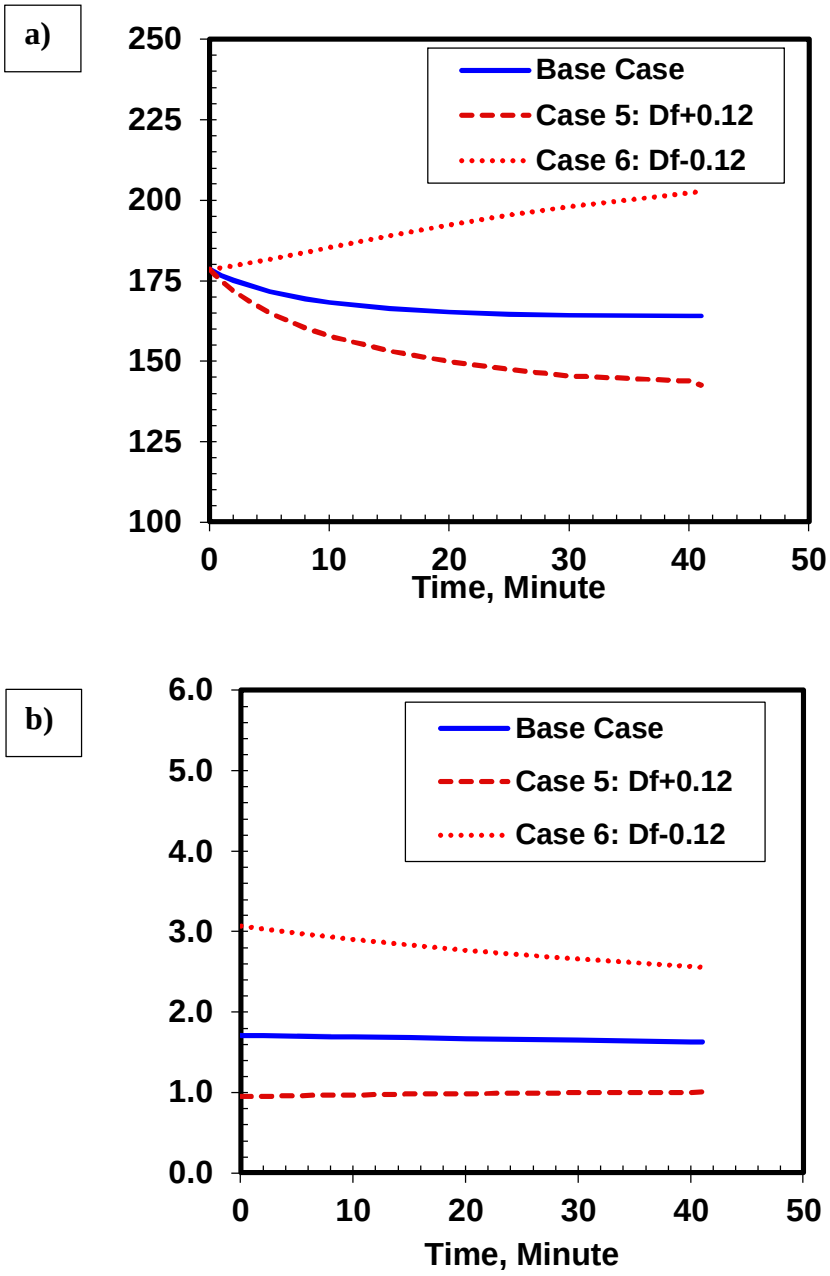

Figure 6.36: Effect of fractal dimension on the predicted a) volume mean diameter and b) number counts.

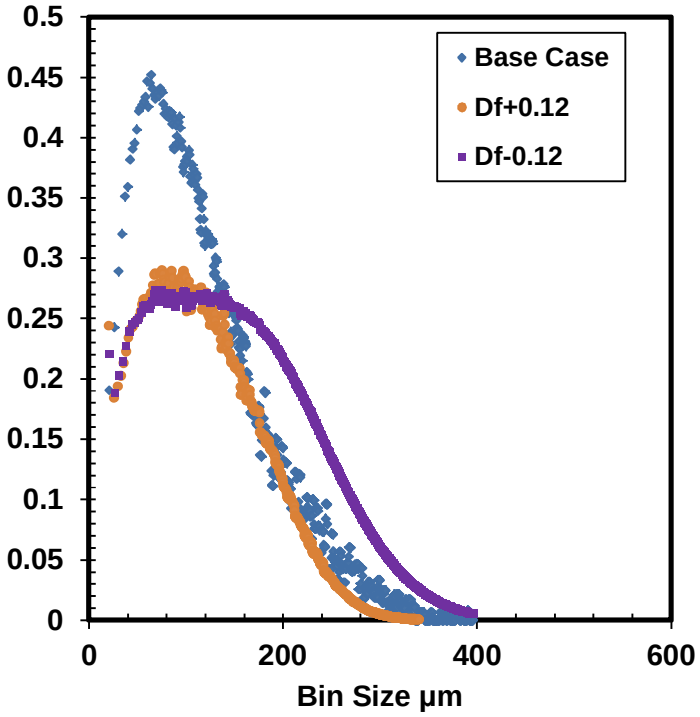

Figure 6.37: Effect of adjusting D_f on the volume frequency distribution.

Minimum Cluster Size

Originally the model was run based on the choice of lower limit cluster size of 18 µm in diameter. The data was fitted again with a lower limit cluster size of 9 µm in diameter. The k_f/k_s ratio was increased from 4.15 10^{-8} to 2.50 10^{-7} to fit the data, Figure 6.38 a. Figure 6.38 b shows that reducing the lower limit in cluster size has little effect on the predicted volume mean frequency distribution. It appears reducing the minimum cluster size will not provide a better prediction of the exact shape of the volume frequency distribution. Therefore, it is recommended to model the data with a different flocculation and disintegration reaction equations in order to have a better prediction of the shape of the volume frequency distribution.

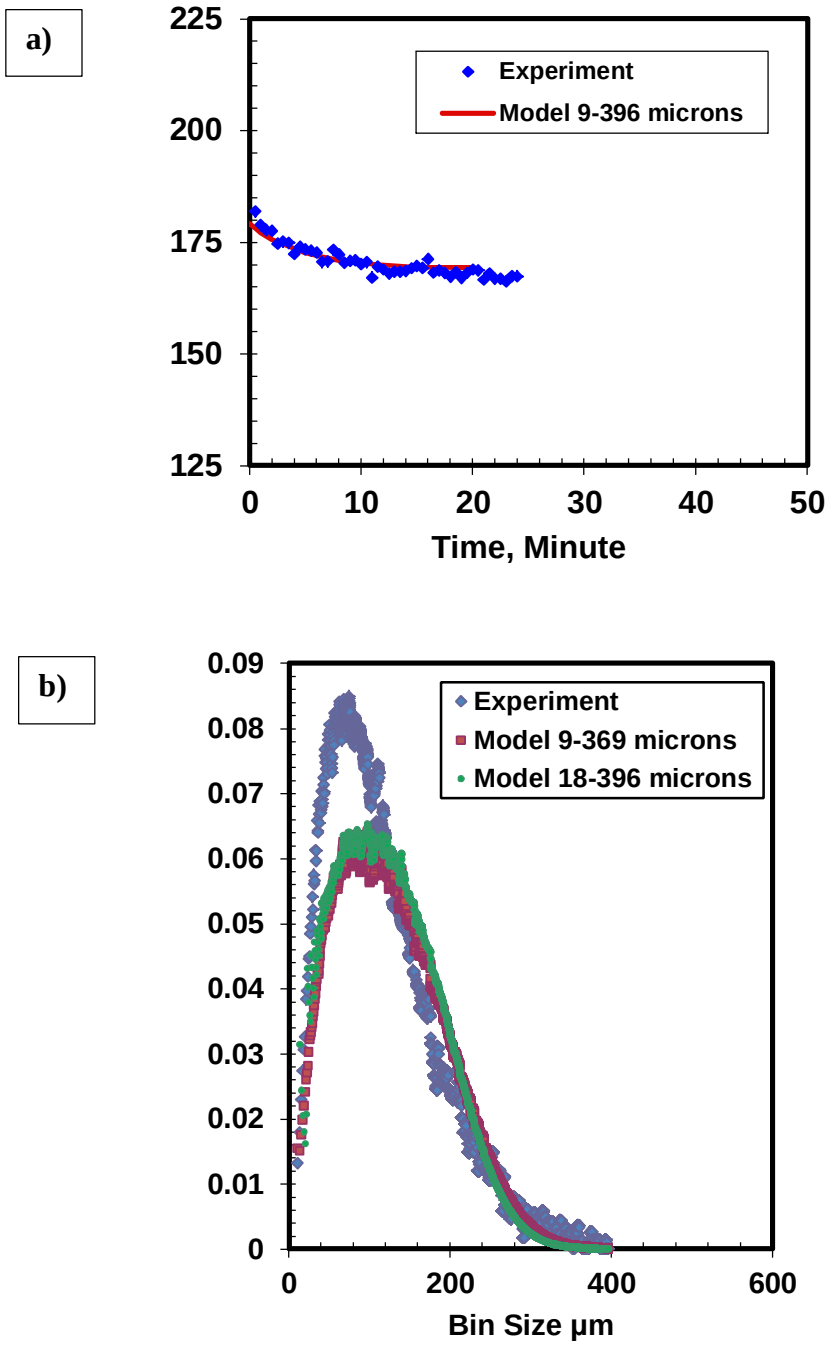

Figure 6.38: Effect of lower limit cluster size on a) volume mean diameter, and b) volume mean diameter distributions.

6.3.7 Summary

While asphaltene flocculation could not be measured near the onset conditions, data were collected and modeled at higher dilutions. The main parameters controlling asphaltene flocculation appear to be the particle concentration, the ratio of flocculation versus shattering rates, and the fractal dimension of the flocs. In general, flocculation decreases at higher dilutions because the particle concentration decreases. The driving force for flocculation (flocculation versus shattering rate) appears to increase with increasing *n*-heptane content. The fractal dimension decreases with increasing *n*-heptane content, leading to larger floc sizes for the same number of particles. While the above trends could be extrapolated to near the onset condition, the change in the parameter values is too great to have confidence in the extrapolation.

The effect of shear rate appears to be correlated to the Reynolds number. In transitional flow, flocculation decreases as the Reynolds number increases. However, in turbulent flow, flocculation becomes insensitive to changes in the Reynolds number. It appears that increasing the mixing speed in turbulent conditions does not alter the local conditions encountered by the flocs.

CHAPTER SEVEN: CONCLUSIONS AND RECOMMENDATIONS

The principal objectives of this thesis were to: 1) assess the role of oxygen in asphaltene precipitation kinetics; 2) determine the kinetics of asphaltene precipitation from diluted bitumen near the onset of precipitation, and; 3) investigate the kinetics of asphaltene flocculation near the onset of precipitation. The main conclusions and recommendations from this work are summarized below.

7.1 Conclusions

1. The onset determined from the gravimetric method was found to be in a good agreement with microscopic observations. In air, the onset of asphaltene precipitation migrates to lower solvent content over months and perhaps years, consistent with the observations of Maqbool *et al.* (2009). In nitrogen, the onset of precipitation followed the same trends as in air for the first 48 hours, but then became invariant over time.

2. Yields in air and nitrogen atmospheres were similar for the first 24 hours, but deviated after 48 hours. The yields in air increase gradually over time over months while the yields in nitrogen became invariant after 48 hours.

3. The long-term changes in onset and yield observed in air appear to be caused by oxidation or oxygen-catalyzed polymerization. Hence, the yields in nitrogen must be used to determine the kinetics of asphaltene precipitation in non-aerobic conditions. The shift

in onset and over the first 48 hours is not an oxygen related artifact, and is consistent with a nucleation and growth process before reaching equilibrium. Asphaltene precipitation kinetics follow a first order reaction model.

4. The particle size analyzer could not detect the particle size distribution in unadulterated bitumen near the onset. The opacity and the stickiness of asphaltene particles resulted in unreliable measurements at low dilutions. Therefore, data was collected at dilutions well above the onset.

5. The method used to dilute bitumen with *n*-heptane can significantly change the asphaltene floc size distribution and volume mean diameter. The one-stage mixing method resulted in higher volume mean diameter both initially and at steady state. The steady state is also reached quite slowly, whereas in two-stage mixing steady state is reached more rapidly. Two-stage mixing reduces the potential for artifacts related to poor mixing and therefore provides a better measure of the "true" flocculation kinetics.

6. For two-stage mixing, the asphaltene volume mean diameter decreases as the *n*-heptane content increases. The decrease in the volume diameter with greater dilution correlates with the decrease in individual particle concentrations.

7. An increase in the shear rate results in a decrease in the asphaltene volume mean diameter, while the total number of asphaltene flocs in the mixture remained relatively constant. This observation indicates that asphaltene flocs likely become more compact at

higher shear rates. Rastegari *et al.* (2004) and Daneshvar (2005) also reported that the volume mean diameter decreases as the shear rate increases for the solutions of asphaltene in the mixture of *n*-heptane and toluene.

8. The fractal dimension of the flocs was determined from the volume of a known mass of asphaltene sediment and from image analysis of micrographs of settled flocs. The results from both of these methods were consistent with an average fractal dimension of 2.3 ±0.1.

9. The flocculation model was fitted the data at different dilutions. The main parameters governing flocculation were the particle concentration, the fractal dimension, and the magnitude and ratio of the flocculation and shattering rates, k_f/k_s. A constant value of the shattering rate was sufficient to fit the data. Both the fractal dimension and the reaction rate ratio could be correlated to the mass fraction of *n*-heptane. However, a long extrapolation with a significant a change in parameter values is required to estimate the behavior near the onset condition. Hence, the flocculation rates near the onset conditions cannot be determined from the available data with any confidence.

10. The effect of shear rate on the k_f/k_s ratio at various heptane contents was investigated for two different bitumen samples. The k_f/k_s ratio appears to decrease with increasing Reynolds number up to 12000, above which the ratio becomes constant. The decrease in the ratio corresponds to the transition zone, while the plateau corresponds to the establishment of a turbulent zone.

7.2 Recommendations For Future Study

1. The thermodynamic onset was determined gravimetrically in a nitrogen atmosphere. It is recommended to verify the thermodynamic onset with the microscopic techniques in nitrogen atmosphere.

2. The onset of precipitation could not be determined in diluted WC-B03 bitumen with *n*-pentane due to the existence of non-asphaltene particulates that obscured the onset. In addition, the data from the gravimetric measurement was not consistent with the microscopic method. Therefore, it is recommended to repeat the experiments with filtered bitumen to reduce the scatter and improve the consistency of the results.

3. The onset of asphaltene precipitation occurs at higher *n*-heptane dilution when toluene is present, allowing particle size distributions to be measured at lower *n*-heptane contents. Therefore, for future work, it is recommended to investigate near onset kinetics in toluene-diluted bitumen.

4. The population balance equation was derived assuming that only binary or two cluster interactions are significant. This assumption is applicable only in dilute solutions. In highly concentrated solutions more than two flocs can interact or flocculate at the same time. Hence, it may be necessary to employ a new population balance equation including those interaction terms.

5. The correlation established based on the trend in the k_f/k_s ratios with *n*-heptane content was associated with high levels of uncertainty, largely due to the lack of data at lower dilutions. Data collected at lower dilutions (for example in toluene diluted bitumen) could be modeled to increase the level of confidence in the correlation.

6. The fractal dimension was assumed to be the same for all floc sizes and to remain constant over time in the model. Considering a variable fractal dimension might improve the performance of model.

7. For the commercial oil sand paraffinic froth treatment process, it is desirable to model the flocculation of asphaltenes, solid particulates, and water droplets. It is recommended to collect flocculation data for bitumen with emulsified water and solids using similar procedures as described in this thesis. It is also recommended to measure floc sizes and settling rates in a microscopic visualization cell. With this data, it may be possible to extend the flocculation model to the commercial system.

4 REFERENCES

Agrawal, P., Schoeggl, F.F., Satyro, M.A., Taylor, S.D., Yarranton, H.W., 2012. Measurement and modeling of the phase behavior of solvent diluted bitumens. Fluid Phase Equilibria 334, 51–64.

Agrawala, M., Yarranton, H.W., 2001. An asphaltene association model analogous to linear polymerization. Ind. Eng. Chem. Res. 40, 4664–4672.

Angle, C.W., Long, Y., Hamza, H., Lue, L., 2006. Precipitation of asphaltenes from solvent-diluted heavy oil and thermodynamic properties of solvent-diluted heavy oil solutions. Fuel 85, 492–506. doi:10.1016/j.fuel.2005.08.009

Atkins, F.J., MacFadyen, A.J., 2008. A Resource Whose Time Has Come? The Alberta Oil Sands as an Economic Resource. Energy J. 29, 77–98.

Barrett, P., Glennon, B., 1999. In-line FBRM Monitoring of Particle Size in Dilute Agitated Suspensions. Part. Part. Syst. Charact. 16, 207–211.

Beck, J., Svrcek, W.Y., Yarranton, H.W., 2005. Hysteresis in Asphaltene Precipitation and Redissolution. Energy Fuels 19, 944–947. doi:10.1021/ef049707n

Brawn, 2003. PRINCIPLES OF FLUID MIXING.

Browarzik, D., Laux, H., Rahimian, I., 1999a. Asphaltene flocculation in crude oil systems. Fluid Phase Equilibria 154, 285–300. doi:10.1016/S0378-3812(98)00434-8

Browarzik, D., Laux, H., Rahimian, I., 1999b. Asphaltene flocculation in crude oil systems. Fluid Phase Equilibria 154, 285–300. doi:10.1016/S0378-3812(98)00434-8

Buckley, J.S., 1999. Predicting the Onset of Asphaltene Precipitation from Refractive Index Measurements. Energy Fuels 13, 328–332. doi:10.1021/ef980201c

Burke, N., Hobbs, R., Kashou, S., 1990. Measurement and Modeling of Asphaltene Precipitation (includes associated paper 23831). J. Pet. Technol. 42. doi:10.2118/18273-PA

Castillo, J., Gutierrez, H., Ranaudo, M., Villarroel, O., 2010. Measurement of the Refractive Index of Crude Oil and Asphaltene Solutions: Onset Flocculation Determination. Energy Fuels 24, 492–495. doi:10.1021/ef900861d

Clark, K.A., Pasternack, D.S., 1932. Hot Water Seperation of Bitumen from Alberta Bituminous Sand. Ind. Eng. Chem. 24, 1410–1416.

Daneshvar, S., 2005. Asphaltene Flocculation in Diluted Bitumen Systems (MSc.). University of Calgary, Calgary.

De Clercq, B., Lant, P.A., Vanrolleghem, P.A., 2004. Focused beam reflectance technique for in situ particle sizing in wastewater treatment settling tanks. J. Chem. Technol. Biotechnol. 79, 610–618.

Elimelech, M., Jia, X., Gregory, J., Williams, R., 1998. Particle deposition & aggregation: measurement, modelling and simulation. Butterworth-Heinemann.

Eyssautier, J., Levitz, P., Espinat, D., Jestin, J., Gummel, J., Grillo, I., Barré, L., 2011. Insight into asphaltene nanoaggregate structure inferred by small angle neutron and X-ray scattering. J. Phys. Chem. B 115, 6827–6837.

Family, F., Meakin, P., Deutch, J.M., 1986. Kinetics of coagulation with fragmentation: scaling behavior and fluctuations. Phys. Rev. Lett. 57, 727.

Fenistein, D., Barré, L., Broseta, D., Espinat, D., Livet, A., Roux, J.-N., Scarsella, M., 1998. Viscosimetric and neutron scattering study of asphaltene aggregates in mixed toluene/heptane solvents. Langmuir 14, 1013–1020.

Ferworn, K.A., Svrcek, W.Y., Mehrotra, A.K., 1993. Measurement of asphaltene particle size distributions in crude oils diluted with n-heptane. Ind. Eng. Chem. Res. 32, 955–959. doi:10.1021/ie00017a026

Gmachowski, L., n.d. Hydrodynamic Properties of Aggregates with Complex Structure.

Hamedi Rad, M., Tavakolian, M., Najafi, I., Ghazanfari, M.H., Taghikhani, V., Amani, M., 2013. Modeling the kinetics of asphaltene flocculation in toluene–pentane systems for the case of sonicated crude oils. Sci. Iran. 20, 611–616. doi:10.1016/j.scient.2012.12.018

Headen, T.F., Boek, E.S., Stellbrink, J., Scheven, U.M., 2009. Small angle neutron scattering (SANS and V-SANS) study of asphaltene aggregates in crude oil. Langmuir ACS J. Surf. Colloids 25, 422–428. doi:10.1021/la802118m

Heath, A.R., Fawell, P.D., Bahri, P.A., Swift, J.D., 2002. Estimating average particle size by focused beam reflectance measurement (FBRM). Part. Part. Syst. Charact. 19, 84–95.

Higashitani, K., Okuhara, K., Hatade, S., 1992. Effects of magnetic fields on stability of nonmagnetic ultrafine colloidal particles. J. Colloid Interface Sci. 152, 125–131. doi:10.1016/0021-9797(92)90013-C

Hirschberg, A., DeJong, L.N.J., Schipper, B.A., Meijer, J.G., 1984. Influence of temperature and pressure on asphaltene flocculation. Soc. Pet. Eng. J. 24, 283–293.

Hoepfner, M.P., Vilas Bôas Fávero, C., Haji-Akbari, N., Fogler, H.S., 2013. The Fractal Aggregation of Asphaltenes. Langmuir.

Hu, Y.-F., Guo, T.-M., 2001. Effect of temperature and molecular weight of n-alkane precipitants on asphaltene precipitation. Fluid Phase Equilibria 192, 13–25. doi:10.1016/S0378-3812(01)00619-7

Kempkes, M., Eggers, J., Mazzotti, M., 2008. Measurement of particle size and shape by FBRM and in situ microscopy. Chem. Eng. Sci. 63, 4656–4675.

Kim, S.T., Boudh-Hir, M.-E., Mansoori, G.A., 1990. The Role of Asphaltene in Wettability Reversal . Society of Petroleum Engineers. doi:10.2118/20700-MS

Kinsner, W., 2005. A unified approach to fractal dimensions, in: Cognitive Informatics, 2005.(ICCI 2005). Fourth IEEE Conference on. IEEE, pp. 58–72.

Kotlyar, L.S., Sparks, B.D., Woods, J.R., Raymond, S., Le Page, Y., Shelfantook, W., 1998. Distribution and types of solids associated with bitumen. Pet. Sci. Technol. 16, 1–19.

Kraiwattanawong, K., Fogler, H.S., Gharfeh, S.G., Singh, P., Thomason, W.H., Chavadej, S., 2007. Thermodynamic solubility models to predict asphaltene instability in live crude oils. Energy Fuels 21, 1248–1255.

Kraiwattanawong, K., Fogler, H.S., Gharfeh, S.G., Singh, P., Thomason, W.H., Chavadej, S., 2009. Effect of asphaltene dispersants on aggregate size distribution and growth. Energy Fuels 23, 1575–1582.

Mangold, M., 2012. Use of a Kalman filter to reconstruct particle size distributions from FBRM measurements. Chem. Eng. Sci. 70, 99–108. doi:10.1016/j.ces.2011.05.052

Maqbool, T., Balgoa, A.T., Fogler, H.S., 2009. Revisiting asphaltene precipitation from crude oils: A case of neglected kinetic effects. Energy Fuels 23, 3681–3686.

Maqbool, T., Raha, S., Hoepfner, M.P., Fogler, H.S., 2011. Modeling the aggregation of asphaltene nanoaggregates in crude oil- precipitant systems. Energy Fuels 25, 1585–1596.

Mason, T.G., Lin, M.Y., 2003. Time-resolved small angle neutron scattering measurements of asphaltene nanoparticle aggregation kinetics in incompatible crude oil mixtures. J. Chem. Phys. 119, 565.

McCabe, W.L., Smith, J., Harriott, P., 2005. Unit Operations of Chemical Engineering. McGraw-Hill Education.

Mousavi-Dehghani, S.., Riazi, M.., Vafaie-Sefti, M., Mansoori, G.., 2004. An analysis of methods for determination of onsets of asphaltene phase separations. J. Pet. Sci. Eng. 42, 145–156. doi:10.1016/j.petrol.2003.12.007

Mullins, O.C., Sabbah, H., Eyssautier, J., Pomerantz, A.E., Barré, L., Andrews, A.B., Ruiz-Morales, Y., Mostowfi, F., McFarlane, R., Goual, L., Lepkowicz, R., Cooper, T., Orbulescu, J., Leblanc, R.M., Edwards, J., Zare, R.N., 2012. Advances in Asphaltene Science and the Yen–Mullins Model. Energy Fuels 26, 3986–4003. doi:10.1021/ef300185p

Mullins, O.C., Sheu, E.Y., 1998. Structures and dynamics of asphaltenes. Springer.

Najafi, I., Mousavi, S.M.R., Ghazanfari, M.H., Ghotbi, C., Ramazani, A., Kharrat, R., Amani, M., 2011. Quantifying the Role of Ultrasonic Wave Radiation on Kinetics of Asphaltene Aggregation in a Toluene–Pentane Mixture. Pet. Sci. Technol. 29, 966–974. doi:10.1080/10916460903394144

Nere, N.K., Patwardhan, A.W., Joshi, J.B., 2003. Liquid-phase mixing in stirred vessels: turbulent flow regime. Ind. Eng. Chem. Res. 42, 2661–2698.

Nielsen, B.B., Svrcek, W.Y., Mehrotra, A.K., 1994. Effects of temperature and pressure on asphaltene particle size distributions in crude oils diluted with n-pentane. Ind. Eng. Chem. Res. 33, 1324–1330.

Rahmani, N.H.G., Dabros, T., Masliyah, J.H., 2004. Evolution of asphaltene floc size distribution in organic solvents under shear. Chem. Eng. Sci. 59, 685–697. doi:10.1016/j.ces.2003.10.017

Rahmani, N.H.G., Dabros, T., Masliyah, J.H., 2005. Fractal structure of asphaltene aggregates. J. Colloid Interface Sci. 285, 599–608. doi:10.1016/j.jcis.2004.11.068

Rastegari, K., Svrcek, W.Y., Yarranton, H.W., 2004. Kinetics of Asphaltene Flocculation. Ind. Eng. Chem. Res. 43, 6861–6870. doi:10.1021/ie049594v

Romanova, U.G., Valinasab, M., Stasiuk, E.N., Yarranton, H.W., Schramm, L.L., Shelfantook, W.E., 2006. The effect of oil sands bitumen extraction conditions on froth treatment performance. J. Can. Pet. Technol. 45, 36–45.

Sanford, E.C., Seyer, F.A., 1979. PROCESSIBILITY OF ATHABASCA TAR SAND USING A BATCH EXTRACTION UNIT-ROLE OF NAOH. CIM Bull. 72, 164–169.

Saryazdi, F., Motahhari, H., Schoeggl, F.F., Taylor, S.D., Yarranton, H.W., 2013. Density of Hydrocarbon Mixtures and Bitumen Diluted with Solvents and Dissolved Gases. Energy Fuels 27, 3666–3678. doi:10.1021/ef400330j

Sathe, D., Sawant, K., Mondkar, H., Naik, T., Deshpande, M., 2010. Monitoring temperature effect on the polymorphic transformation of acitretin using FBRM- Lasentec. Org. Process Res. Dev. 14, 1373–1378.

Savvidis, T.G., Fenistein, D., Barré, L., Behar, E., 2001. Aggregated structure of flocculated asphaltenes. AIChE J. 47, 206–211.

Sheu, E., Long, Y., Hamza, H., 2007. Asphaltene Self-Association and Precipitation in Solvents—AC Conductivity Measurements, in: Mullins, O.C., Sheu, E.Y., Hammami, A., Marshall, A.G. (Eds.), Asphaltenes, Heavy Oils, and Petroleomics. Springer New York, pp. 259–277.

Speight, J.G., 2006. The Chemistry and Technology of Petroleum, Fourth Edition. CRC Press.

Taylor, W.F., Frankenfeld, J.W., 1978. Deposit Formation from Deoxygenated Hydrocarbons. 3. Effects of Trace Nitrogen and Oxygen Compounds. Ind. Eng. Chem. Prod. Res. Dev. 17, 86–90.

The MathWorks, Inc. Matlab Version 2014 a, " Matlab User's Mannual" Calgary, Canada 2014.

Uhl, V.W., Gray, J.B., 1986. Mixing: theory and practice. Volume III.

Wattana, P., Wojciechowski, D.J., Bolaños, G., Fogler, H.S., 2003. Study of Asphaltene Precipitation Using Refractive Index Measurement. Pet. Sci. Technol. 21, 591–613. doi:10.1081/LFT-120018541

Welt, J., Lee, W., Krambeck, F.J., 1977. Catalyst attrition and deactivation in fluid catalytic cracking system. Chem. Eng. Sci. 32, 1211–1218.

Wiehe, I.A., Yarranton, H.W., Akbarzadeh, K., Rahimi, P.M., Teclemariam, A., 2005. The paradox of asphaltene precipitation with normal paraffins. Energy Fuels 19, 1261–1267.

Wilson, D.I., Watkinson, A.P., 1996. A study of autoxidation reaction fouling in heat exchangers. Can. J. Chem. Eng. 74, 236–246.

Wu, J., Graham, L.J., Noui Mehidi, N., 2006. Estimation of agitator flow shear rate. AIChE J. 52, 2323–2332. doi:10.1002/aic.10857

Yarranton, H.W., 2005. Asphaltene Self-Association. J. Dispers. Sci. Technol. 26, 5–8. doi:10.1081/DIS-200040234

Yarranton, H.W., Alboudwarej, H., Jakher, R., 2000. Investigation of Asphaltene Association with Vapor Pressure Osmometry and Interfacial Tension Measurements. Ind. Eng. Chem. Res. 39, 2916–2924. doi:10.1021/ie000073r

Yen, T.F., Chilingarian, G.V., 2000. Asphaltenes and Asphalts, 2. Elsevier.

Yen, T.F., Erdman, J.G., Pollack, S.S., 1961. Investigation of the structure of petroleum asphaltenes by X-ray diffraction. Anal. Chem. 33, 1587–1594.

Zhang, R., Khalizov, A., Wang, L., Hu, M., Xu, W., 2011. Nucleation and growth of nanoparticles in the atmosphere. Chem. Rev. 112, 1957–2011.

APPENDIX A: AVERAGE ABSOLUTE RELATIVE DEVIATION

The repeatability analysis for the asphaltene precipitation measurements are shown in Chapter 4. The mean, μ, is given by:

$$\mu = \frac{\sum_{i=1}^{n} y_i}{n} \tag{A.1}$$

Where y_i is the experimental measured value and n is the number of measurements or repeats. The sample variance, *s*, was calculated based on the variance for all of the measurements and is given by:

$$s = \sqrt{\frac{\sum_{i=1}^{n} (y_i - \mu)^2}{m-1}} \tag{A.2}$$

Where m is the number of variances determined for the measurement. The variance of the property measurements is then estimated using a chi-square distribution as follows:

$$\sigma = \sqrt{\frac{\lambda^2 s^2}{(n-1)}} \tag{A.3}$$

Where λ^2 is the Chi-square variable (from statistical tables) and s^2 is the population standard deviation. The 90% confidence interval for any measurement is determined as 1.645 σ.

The Average Absolute Relative Deviation (AARD) between the predicted y_i^* and experimentally measured values y_i are expressed by Equation A.4:

$$dev = y_i^* - y_i \tag{A.4}$$

The Average Absolute Deviation or AAD is given by Equation A.5:

$$AAD = \frac{1}{n} \sum_{1}^{n} |y_i^* - y_i| \tag{A.5}$$

and the Absolute Average Relative Deviation is given by:

$$AARD = \frac{1}{n}\sum_{1}^{n}\left|\frac{y_i^* - y_i}{y_i}\right| \quad \text{(A.6)}$$

APPENDIX B: ASPHALTENE BINS

In this appendix the equations used to calculate the asphaltene bins in the model are presented. As argued in Chapter 5 and 6, to have a reasonably short simulation time only the asphaltene bins with sizes approximately between 18 and 396 microns were considered. Those bins are assumed to consist of certain number of asphaltene primary particles with a size of d_p. Also, it is necessary to keep the same total number of asphaltene primary particles upon any agglomeration between different bins or fragmentation of one bin to a set of smaller bins or clusters. Hence, the following approach was employed:

1- The number of asphaltene primary particles in the biggest asphaltene bin n_2 was computed as shown by Equation B.1:

$$\boldsymbol{n}_2 = \left(\frac{396}{\boldsymbol{d}_p} \right)^{\boldsymbol{D}_f} \tag{B.1}$$

where d_p is the size of an asphaltene primary particle, and D_f is the asphaltene fractal dimension.

2- Similarly, the number of asphaltene primary particles in the smallest asphaltene bin n_{min} was calculated as depicted by Equation B.2:

$$\boldsymbol{n}_1 = \left(\frac{18}{\boldsymbol{d}_p} \right)^{\boldsymbol{D}_f} \tag{B.2}$$

3- n_1 and n_2 calculated using Equations B.1 and B.2 can be non-integer numbers while the number of asphaltene individual particles could not be non-integer so that Equations B.3 to B.6 should be employed to compute the number of bins with the sizes between approximately 18 and 396 microns:

$$\boldsymbol{ratio} = \frac{\mathrm{Int}(\boldsymbol{n}_2)}{\mathrm{Int}(\boldsymbol{n}_1)} \tag{B.3}$$

$$\boldsymbol{n}_{\min} = \mathrm{Int}(\boldsymbol{n}_1) \tag{B.4}$$

$$\boldsymbol{n}_{\mathrm{bin}} = \mathrm{Int}(\boldsymbol{ratio}) + 1 \tag{B.5}$$

$$\boldsymbol{n}_{\max} = \boldsymbol{n}_{\mathrm{bin}} * \boldsymbol{n}_{\min} \tag{B.6}$$

where n_{max}, n_{min}, and n_{bin} are the number of asphaltene individual particles in the biggest and smallest bins, and number of asphaltene bins with the sizes between approximately 18 and 396 microns, respectively. The Int function truncates the real numbers n_1 and n_2 to closest but smaller integer numbers than n_1 and n_2. Hence, there will be $i = 1$ to n_{bin} bins and each one will be equivalent to i clusters containing n_{min} number of asphaltene individual particles. The size of i^{th} bins can be simply calculated using Equation B.7:

$$\boldsymbol{d}_{\boldsymbol{m}} = \boldsymbol{d}_{\boldsymbol{p}} . \left(\boldsymbol{i} * \boldsymbol{n}_{\min}\right)^{1/\boldsymbol{D}_f} \tag{B.7}$$